



THE HONG KONG
POLYTECHNIC UNIVERSITY

香港理工大學

Pao Yue-kong Library

包玉剛圖書館

Copyright Undertaking

This thesis is protected by copyright, with all rights reserved.

By reading and using the thesis, the reader understands and agrees to the following terms:

1. The reader will abide by the rules and legal ordinances governing copyright regarding the use of the thesis.
2. The reader will use the thesis for the purpose of research or private study only and not for distribution or further reproduction or any other purpose.
3. The reader agrees to indemnify and hold the University harmless from and against any loss, damage, cost, liability or expenses arising from copyright infringement or unauthorized usage.

IMPORTANT

If you have reasons to believe that any materials in this thesis are deemed not suitable to be distributed in this form, or a copyright owner having difficulty with the material being included in our database, please contact lbsys@polyu.edu.hk providing details. The Library will look into your claim and consider taking remedial action upon receipt of the written requests.

**STUDY OF TWO DIMENSIONAL
MATERIALS AND ITS NONLINEAR
OPTICAL APPLICATIONS**

LONG HUI

Ph.D

The Hong Kong Polytechnic University

2017

The Hong Kong Polytechnic University

Department of Applied Physics

**STUDY OF TWO DIMENSIONAL
MATERIALS AND ITS NONLINEAR
OPTICAL APPLICATIONS**

LONG Hui

A thesis submitted in partial fulfillment of the
requirements for the degree of Doctor of Philosophy

July 2016

CERTIFICATE OF ORIGINALITY

I hereby declare that this thesis is my own work and that, to the best of my knowledge and belief, it reproduces no material previously published or written nor material which has been accepted for the award of any other degree or diploma, except where due acknowledgement has been made in the text.

_____ (Signed)

Hui Long (Name of student)

ABSTRACT

Nonlinear optical (NLO) materials have drawn much attention in the past decades because of the potential applications for protecting delicate optical instruments and human eyes from intense laser beam. A good optical limiter should provide high linear transmission at low power of incident but high non-linear absorption at high power. Two-dimensional transition metal dichalcogenide (TMD) nanosheet *e.g.* MoS₂, WS₂, MoSe₂, WSe₂, show great promise for laser photonic applications for their unique properties, such as high layer optical absorption, broad optical band response, large surface area, high mechanical strength, high inplane charge mobility. These 2D materials have strong optical limiting properties for high power near infrared laser. In this study, the nonlinear optical absorption properties of the MoS₂ in liquid N-methyl-2-pyrrolidone (NMP) and solid state matrix Polymethyl Methacrylate (PMMA) have been studied and compared. Also, a simple but effective ultrasonic exfoliation has been used to separate the WS₂ nanosheets into different layer number and size through controlling centrifugation rotation speed. Additionally, the optical limiting property of WS₂ sheet incorporated into PMMA show a close dependence on both size and thickness. Due to the edge and quantum confinement effect, WS₂ quantum dots exhibit the lowest onset threshold (F_{ON}) and optical limiting threshold (F_{OL}) among all the samples, which are comparable to the lowest threshold achieved in the graphene based materials.

Firstly, MoS₂ powder in suitable size is prepared by hydrothermal process and few-layer MoS₂ nanosheets are prepared using simple ultrasonic exfoliation method. Then MoS₂ nanosheets are homogeneously incorporated into solid state matrix

(PMMA) to test its NLO property. Z-scan results of MoS₂/PMMA composite bulk with 0.016 mg/cm³ MoS₂ nanosheets demonstrate the low NLO F_{ON}, 0.01 and 0.04 J/cm², F_{OL}, 0.4 and 1.3 J/cm², low optical limiting differential transmittance (T_C), 2% and 3% and high two-phonon absorption coefficient (β), 70 and 55 cm GW⁻¹ for the nanosecond laser operating at 532 nm and 1064 nm, respectively.

Secondly, the morphology of few layers MoS₂ nanosheet in NMP solution under laser illumination with wavelength of 532 and 1064 nm with various laser energy densities have been analysed. Also, the nonlinear optical limiting properties of the MoS₂ nanosheet in liquid NMP and solid PMMA have been studied and their results are compared. It shows that the nonlinear optical absorption properties of MoS₂ in NMP disappeared but without changes in MoS₂/PMMA composites after laser illumination. The significant changes in NMP caused by the oxidization of molybdenum disulfide (MoS₂) into molybdenum oxide (MoO₃). Due to its stronger absorption in visible range, 532 nm have stronger oxidization effect compared with 1064 nm as illumination wavelength. It confirms that the MoS₂ nanosheet is relatively much more stable within PMMA for preserving nonlinear absorption properties under high laser density illumination.

Thirdly, a series of different size and thickness WS₂ nanosheets are obtained through controlling centrifugation rotation speed effectively. Their surface morphology was characterized by Atomic Force Morphology. The successful size and thickness separation allows the research of thickness-dependent optical limiting properties of WS₂/PMMA composites. Results demonstrate that both NOL F_{ON} and F_{OL} of WS₂ under the excitation of nanosecond pulsed laser can be tuned over a wide range by controlling its size and thickness. The F_{ON} and F_{OL} show a rapid decline

with the decrease of size and thickness. The tunable NOL properties have been achieved through the control of size and thickness.

Finally, Ultra-small WS₂ quantum dots with diameter of 2.4 nanometer are fabricated by ultrasound method followed by high speed centrifugation up to 10000 rpm. Excellent NLO property of the WS₂ QD/ PMMA composite for the nanosecond pulsed laser at both 532 and 1064 nm has been measured. Results illustrate the lower F_{ON} , F_{OL} , and higher β with respect to higher concentration of embedded WS₂ quantum dots. The NOL performance exhibited in WS₂ QDs is comparable to the best result of graphene based materials reported so far, having very low F_{ON} (0.01 J/cm², 0.03 J/cm²) and F_{OL} (0.062 J/cm², 0.1 J/cm²) at 532 nm and 1064 nm respectively, which is attributed to the edge and quantum confinement effects.

In summary, two-dimensional materials MoS₂ WS₂ nanosheet embedded into solid state matrix PMMA have been studied systematically, and a series of related journal publications has been obtained. These results would advance and further promote the development of two dimensional materials and their optical applications.

List of publications

Journal Publications

1. **H. Long**, L. L. Tao, Chun Pang Chiu, C. Y. Tang, Kin Hung Fung, Yang Chai, Y. H. Tsang, “The WS₂ Quantum Dots: Preparation, Characterization and Its Optical Limiting Effect in PMMA”, *Nanotechnology*. vol. 27, p.414005, 2016. (Highlight)
2. **H. Long**, L. L. Tao, C. Y. Tang, H. Y. T, Q. W, Y. H. Tsang, “Effect of Laser Illumination on the Morphology and Optical Property of Few-Layer MoS₂ Nanosheet in NMP and PMMA”, *Journal of Materials Chemistry C*. vol. 4, p.678, 2016. (Inside Front Cover)
3. **H. Long**, L. L. Tao, C. Y. Tang, B. Zhou, Y. D. Zhao, L. H. Zeng, S. F. Yu, S. P. Lau, Y. Chai, Y. H. Tsang, “Tuning Nonlinear Optical Absorption Properties of WS₂ Nanosheets”, *Nanoscale*, vol. 7, p.17771, 2015.
4. L. L. Tao[#], **H. Long**[#], (Co- First Author) B. Zhou, S. F. Yu, D.S. P. Lau, Y. Chai, K. H. Fung, Y. H. Tsang, J. Q. Yao, D. G. Xu, “Preparation and Characterization of Few-Layer MoS₂ Nanosheets and Their Good Nonlinear Optical Responses in the PMMA Matrix”, *Nanoscale*, vol. 6, p. 9713, 2014..
5. Zeng. B, **Long.H**, “Three-Dimensional Porous Graphene-Co₃O₄ Nanocomposites for High Performance Photocatalysts”, *Applied Surface Science*, vol. 357, p. 439,

2015.

6. Zeng. B, **Long.H**, “Graphene Spheres-CuO Nanoflowers Composites for Use as a High Performance Photocatalyst”. *Nanotechnology and Nanomaterials* vol. 10, p. 5772, 2016.
7. C. Y. Tang, X. M. Zhang, Y. Chai, **H. Long**, L. Tao and Y. H. Tsang, “Controllable Parabolic Lensed Liquid-Core Optical Fiber by Using Electrostatic Force”, *Opt. Express*, vol. 22, p. 20948, 2014.
8. Y. Zhao, Z. Liu, T. Sun, L. Zhang, W. Jie, X. Wang, **H. Long**, et al, “Mass Transport Mechanism of Cu Species at the Metal/Dielectric Interfaces with a Graphene Barrier”, *ACS nano*, vol. 8, p. 122601, 2014.
9. C. S. Chen, S. Y. Cao, **H. Long**, G. P. Qian, Y. H. Tsang, L. Gong, W. W. Yu, Y. Xiao, “Highly Efficient Photocatalytic Performance of Graphene Oxide/TiO₂-Bi₂O₃ Hybrid Coating for Organic Dyes and NO Gas”, *Journal of Materials Science-Materials in Electronics*, vol. 26, p. 3385, 2015.
10. C. Y. Tang, Y. Chai, **H. Long**, L. Tao and Y. H. Tsang, “High-power Passively Mode-locked Nd: YVO₄ Laser Using SWCNT Saturable Absorber Fabricated by Dip Coating Method”, *Opt. Express*, vol. 23, p. 4880, 2015.
11. L. H. Zeng, C. Xie, L. Tao, **H. Long** and Y. H. Tsang, “Bilayer Graphene Based Surface Passivation Enhanced Nano Structured Self-Powered Near-Infrared Photodetector”, *Opt. Express*, vol. 23, p. 4839, 2015.

12. L. H. Zeng, L. L. Tao, C. Y. Tang, B. Zhou, **H. Long**, Y. H. Tsang, “High-Responsivity UV-Vis Photodetector Based on WS₂ Film Deposited by Magnetron Sputtering”, *Scientific Report*. vol. 6, p. 20343, 2016

Presentations in international conferences

1. **H. Long**, L. Tao, C. Y. Tang, L. H. Zeng, Y. H. Tsang, “Layer-Dependent Nonlinear Optical Response of WS₂ Nanosheet”, *European Materials Research Society (E-MRS 2015 Spring Meeting)*, May 11-15, Grand Palais, Lille, France. (Oral)
2. **H. Long**, L. Tao, Y. H. Tsang, “Effect of Laser Excitation on a Few-Layer MoS₂ Nanosheet in N-methyl Pyrrolidinone”, *2015 international conference for top and emerging materials scientists*, 19 July, 2015.
3. **H. Long**, L. Tao, S. N. Ma, C. Y. Tang, L. H. Zeng, Y. H. Tsang, “ Nonlinear Optical Properties of Two Dimensional Nanomaterials in Liquid and Solid State Matrix”, *2016 the three places well-known universities Physics doctoral academic innovation forum*, May 2016. (Poster)
4. L. Tao, **H. Long**, Y. Chai, K. H. Fung, and Y. H. Tsang, ‘Optical Non-Linear Absorption of Few Layer MoS₂’, *The 17th Conference of The physical society of Hong Kong*, 7 June, 2014.
5. Y. H. Tsang*, **H. Long**, Li L. Tao, B. Zhou, Chun Y. Tang, “The Potential of

Using Two-Dimensional Materials for Optical Limiting Applications”, *International conference on optical, optoelectronic and photonic materials and applications*, August 2014 in Leeds, UK.

6. Y. H. Tsang*, **H. Long**, L. Tao, Y. Chai, C. Y. Tang, L. H. Zeng, “Preliminary Study of Nonlinear Optical Response of Few-Layer WS₂”, *International Conference on Small Science*, December 8-11, Hong Kong, 2014.
7. L. Zeng, L. Tao, C. Tang, **H. Long**, and S. P. Lau, Y. H. Tsang*, “High Performance WS₂ Nano-film Photodetector”, *The 18th Conference of The physical society of Hong Kong*, 13 June, 2015.
8. C. Y. Tang, L. H. Zeng, **H. Long**, L. L. Tao, C. C. Huang, D. W. Hewak, Y. H. Tsang, "Study of TMDs Nanosheets Based Saturable Absorber Used for Q-switching and Mode Lock Laser System", *The EMN Bangkok Meeting 2015*, November 2015.

ACKNOWLEDGEMENTS

I would like to express my appreciation to my supervisor **Dr. Y. H. Tsang** and co-supervisor **Dr. C. L. Mak**, for their excellent guidance and constant encouragement throughout the period of my Ph.D study. Their high requirement and inspired discussions greatly contribute to improving the quality of my doctoral research.

I would also like to thank Prof. S. P. Lau, Prof. S. F. Yu, Prof. J. H. Hao, Dr. K. H. Fung and Dr. Y. Chai for their assistance on my doctoral research.

I appreciate Prof. Q.Wen from Shen Zhen University, Prof. C.S. Chen from Changsha University of science and technology, Prof. B. Zeng from Hunan University of Arts and Science for their helpful discussions and encouragement on my research.

I would like to give my thanks to my research group members Dr. L. L. Tao, Miss. S. N. Ma, Dr. B. Zhou, Dr. Q. Zheng, Mr. C. Y. Tang, Mr. L. H. Zeng, Mr. C. P. Chiu, Mr. Y. Chen, and Mr. X. Y. Wang for their help for my research. Thanks are also due to my friends and colleagues Miss. S. Guo, Miss. L. Chen, Miss. Y. J. Zhu, Miss. X. W. Huang, Miss. F. R. Tan, Mr. Y. D. Zhao, Mr. S. H. Liu, Mr. Z. Y. Bao, Mr. T. H. Li, Mr. Q. M. Chen.

Finally, I would like to thank my parents for their support on my study and life.

TABLE OF CONTENTS

ABSTRACT	IV
LIST OF PUBLICATIONS	VII
ACKNOWLEDGEMENTS	XI
TABLE OF CONTENTS	XII
LIST OF FIGURE CAPTIONS	XVII
LIST OF TABLE CAPTIONS	XXVII
CHAPTER 1 Introduction	1
1.1 Two dimensional materials.....	1
1.1.1 Preparation of two-dimensional materials	3
1.1.2 Properties and characterizations of two-dimensional materials.....	10
1.1.3 Application of two-dimensional materials	13
1.2 Nonlinear optical property	21
1.3 Objectives and organizations of the thesis	24
CHAPTER 2 Two Dimensional Materials Characterization and Theoretical Analysis	28

2.1 Characterization	28
2.1.1 X-ray diffraction.....	29
2.1.2 Absorption and transmittance spectrum	30
2.1.3 Fourier transform infrared spectroscopy.....	31
2.1.4 Photoluminescence spectra	32
2.1.5 Raman spectrum.....	33
2.1.6 Atom force microscopy	34
2.1.7 Transmission Electron Microscopy.....	35
2.1.8 Scanning Electron Microscopy	36
2.1.9 Nonlinear optical properties	38
2.2 Theoretical calculations	39
2.2.1 Two photon absorption theory.....	39
2.2.2 The minimal enthalpy of mixing solution.....	44
 CHAPTER 3 MoS ₂ Nanosheet Preparation And MoS ₂ /PMMA Composite For Nonlinear Optical Application	 46
3.1 Introduction.....	46
3.2 Experimental section.....	50
3.3 Structure and morphology of MoS ₂ nanosheet	50

3.3.1 XRD, TEM and EDS of MoS ₂ nanosheet	51
3.3.2 AFM of MoS ₂ nanosheet.....	55
3.3.3 Raman and PL of MoS ₂ nanosheet.....	57
3.3.4 Absorption of MoS ₂ nanosheet and MoS ₂ /PMMA	59
3.4 Nonlinear optical property of MoS ₂ /PMMA composite	60
CHAPTER 4 Effect Of Laser Illumination On few-layer MoS ₂	
Nanosheet In NMP And PMMA	
4.1 Introduction.....	66
4.2 Experimental section.....	67
4.3 Effect of laser illumination of morphology change of MoS ₂ nanosheet in NMP	68
4.3.1 Color changing of prepared MoS ₂ suspension in NMP under laser illumination.....	69
4.3.2 Morphology and size change of MoS ₂ suspension in NMP before and after 532 nm laser illumination.....	70
4.3.3 Size change of MoS ₂ nanosheet after 1064 nm laser illumination.....	74
4.3.4 UV/Vis absorption spectrums before and after laser illumination	75
4.3.5 Photoluminescence spectrums before and after laser illumination ...	77

4.4 The difference of nonlinear optical property between MoS ₂ nanosheet in NMP and PMMA	78
4.5 Summary	81
CHAPTER 5 WS ₂ Nanosheet Preparation And WS ₂ /PMMA Composite For Nonlinear Optical Application	82
5.1 Introduction	82
5.2 Experimental procedures.....	84
5.3 Structures and morphology of WS ₂ nanosheet in NMP.....	84
5.3.1 Height profile of WS ₂ nanosheet.....	85
5.3.2 Thickness distribution of WS ₂ nanosheet.....	88
5.3.3 Size distribution of WS ₂ nanosheet.....	89
5.3.4 Raman spectra of WS ₂ nanosheet	90
5.3.5 Absorption spectra of WS ₂ nanosheet.....	91
5.4 Nonlinear optical absorption performance of WS ₂ /PMMA composites	93
5.5 Discussion	96
5.6 Summary	98
CHAPTER 6 WS ₂ Quantum Dots: Preparation, Characterization And Its Optical Limiting Effect In PMMA	99

6.1 Introduction	99
6.2 Experimental section	100
6.3 Preparation and the structure of WS ₂ quantum dots	101
6.3.1 The structure and morphology of the WS ₂ QD	102
6.3.2 Absorption and Photoluminescence spectrum of WS ₂ QD	105
6.4 Z-scan measurement of WS ₂ QD/PMMA composites	106
6.5 Summary	112
CHAPTER 7 Conclusions and Future Work	113
7.1 Conclusions	113
7.2 Future work	116
References	118

LIST OF FIGURE CAPTIONS

- Fig. 1.1 Electrochemical lithiation process for the fabrication of 2D nanosheets from the layered bulk material. 5
- Fig. 1.2 Schematic representation of liquid-phase exfoliation process of TMDs bulk materials in the absence (top-right) and presence (bottom-right) of surfactant molecules [19]..... 6
- Fig. 1.3 (a) Schematic illustration for the synthesis of MoS₂ layers by MoO₃ sulfurization. A layer of MoO₃ (~3.6 nm) was thermally evaporated on the sapphire substrate. The MoO₃ was then converted to a MoS₂ by a two-step thermal process. (b) MoS₂ layer grown on a sapphire wafer [25]. 9
- Fig. 1.4 (a) Schematic diagram of the CVD system used for the growth of WS₂. (b) Optical image of as-grown WS₂ on SiO₂ (300 nm)/ Si substrate. Inset shows a triangular monolayer WS₂. (c) SEM image of the sample fabricated by setup shown in Fig. 1.4 (a) [26]. 9
- Fig. 1.5 WS₂/MoS₂ heterostructures. (a) Optical image of a monolayer WS₂ /MoS₂ heterostructure. (b,c) Raman mapping at the 408 cm⁻¹ (MoS₂) and 421 cm⁻¹ (WS₂). (d,e) PL mapping at the 1.85 eV (MoS₂) and 2.01 eV (WS₂) [28]... 10

Fig. 1.6 The crystal structure of transition metal dichalcogenide.	11
Fig. 1.7 Characterization methods of two-dimensional materials. (a) (b) TEM of MoS ₂ . Inset is the digital image of MoS ₂ solution[30]; (c) AFM of exfoliated g-C ₃ N ₄ nanosheets and corresponding thickness analysis taken around the white line [31]; (d) Raman spectra of MoS ₂ nanosheet [32]......	13
Fig. 1.1.8 Nonlinear transmittance characteristics of sub-Gox/PC film. (a) plot of output versus input fluence (b) plot of transmittance versus input fluence for 3.5 ns pulses are 532 nm [34]......	14
Fig. 1.1.9 Tunable MoS ₂ Q-switched fiber laser. (a) cavity shematic, (b) output 74 kHz pulse train, (c) profile of single pulse, (d) various spectra at wavelengths within the continuous tuning range of 1030-1070 nm [41]......	15
Fig. 1.10 (a) The MoS ₂ /m-C nanosheet superstructure; (b) the capacities retention of the MoS ₂ /m-C nanosheet superstructure, MoS ₂ /graphene composites, exfoliated graphene, and the annealed MoS ₂ nanosheets at current densities from 200 to 6400 mA g ⁻¹ [50]......	17
Fig. 1.11 (a) Typical AFM image of exfoliated nanosheets of WS ₂ ; (b) Polarization	

curves of bulk and as-exfoliated WS₂ (as-deposited film of 1T phase, sub-monolayer as-exfoliated film, and 2H phase after annealing at 300 °C) along with those corresponding to Pt nanoparticles and bulk WS₂ powder for comparison [6]. 17

Fig. 1.12 Schematic structure and property of field effect transistor (FET) containing MoS₂ (a) schematic structure of FET; (b) room-temperature transfer characteristic for the FET with 10 mV applied bias voltage (V_{ds}) [14]. 18

Fig. 1.13 Schematic and energy diagrams of the fabricated device with structure graphene/PEDOT:PSS/P3HT:PCBM/LiF/Al [51]. 20

Fig. 1.14 (a) schematic structure of gas sensor; (b) real-time current response of the device exposed to NO with increasing concentration [52]. 21

Fig. 2.1 Digital images of the Rigaku automated multipurpose Smartlab X-ray diffractometer. 30

Fig. 2.2 Digital image of the Ultraviolet-visible spectrophotometer. 31

Fig. 2.3 Digital image of the Fourier transform infrared spectrophotometer. 32

Fig. 2.4 Digital image of the photoluminescence spectrophotometer. 33

Fig. 2.5 Digital image of the Raman spectrophotometer.	34
Fig. 2.6 Digital image of scanning probe microscope nanoscope IV.....	35
Fig. 2.7 Digital image of Transmission electron microscopy.....	36
Fig. 2.8 Digital image of Scanning electron microscopy.....	38
Fig. 2.9 Digital image of Nd:YAG laser system (a) and the experimental setup for Z-scan measurement (b).....	41
Fig. 2.10 Energy scheme of a two photon excitation up conversion process.	41
Fig. 2.11 Absorption spectra of graphene and its band gap structure [55].	42
Fig. 2.12 Absorption spectra of graphene oxide and its band gap structure, the absorption at 1064 nm refer to [56].....	43
Fig. 2.13 Absorption spectra of MoS ₂ nanosheet and its band gap structure, the absorption at 1064 nm refer to [57].....	43
Fig. 2.14 Absorption spectra of WS ₂ nanosheets and its band gap structure.....	44
Fig. 3.1 (a) XRD pattern, (b) TEM and (c) HRTEM images of as-prepared MoS ₂ . Inset of (a) is the digital photo of MoS ₂ powder. Inset of (c) is the SAED pattern of the MoS ₂ sheet. (d) SEM image of the commercial MoS ₂ bought	

from Aladdin-Reagent Company. Inset is the SEM image with lower magnification..... 53

Fig. 3.2.(a) Low-magnification TEM image of MoS₂ nanosheets obtained after ultrasonic exfoliation, inset shows the SAED pattern. (b) EDS spectrum of MoS₂ nanosheets. (c) HRTEM image showing layer information of the MoS₂ sheets. (d) HRTEM image indicating atomic structure of MoS₂, inset illustrates the schematic structure with yellow and purple balls corresponding to S and Mo atoms, respectively..... 54

Fig. 3.3 (a) 2D topographical and (b) 2D stepped height-type AFM images of few-layer MoS₂ nanosheets. (c) Height profiles of the sections marked in (b). (d) Interlayer separation dependence on the layer number. (e) Schematic diagram of monolayer and double layer MoS₂ on Si substrate. (L: the thickness of S-Mo-S layer; D: the distance from MoS₂ to the substrate; S: the separation between the S-Mo-S layers.)..... 56

Fig. 3.4 (a) Raman spectrum and (b) Photoluminescence spectrum of MoS₂ nanosheets obtained after ultrasonic exfoliation. Insets of (a) show the schematic of the vibration modes at 384 cm⁻¹ (left) and 410 cm⁻¹ (right). 58

Fig. 3.5 (a) Absorption spectrum of the few layer MoS₂ suspension in NMP. Inset shows the digital photo of such sample. (b) Absorption spectra of pure PMMA and MoS₂/PMMA composite bulks. Insets show the enlarged absorption within 400-700 nm region, and digital photos of MoS₂/PMMA (left) and PMMA (right)..... 59

Fig. 3.6 The output fluence dependence on the input fluence at 532 nm (a) and 1064 nm (b), respectively. Insets are the corresponding normalized transmittance dependence on the input fluence. The concentration of MoS₂ in MoS₂/PMMA-1 and MoS₂/PMMA-2 are 0.008 and 0.016 mg/cm³, respectively..... 62

Fig. 4.1 Digital photos of prepared MoS₂ suspension in NMP after 532 nm laser illumination with different laser energy densities. The illumination time is 30 minutes..... 69

Fig. 4.2 Digital photos of prepared MoS₂ suspension in NMP after 1064 nm laser illumination with different laser energy densities. The illumination time is 60 minutes..... 70

Fig. 4.3 TEM images of MoS₂ suspension in NMP before and after 532 nm laser

illumination under different energy densities, (a) before laser illumination;
(b) 0.05 J/cm²; (c) 0.10 J/cm²; (d) 0.16 J/cm²; (e) 0.28 J/cm²..... 71

Fig. 4.4 Size distributions of MoS₂ nanosheet in NMP before and after 532 nm laser illumination under different energy densities (a) before laser illumination; (b) 0.05 J/cm²; (c) 0.10 J/cm²; (d) 0.16 J/cm²; (e) the most frequent size distribution with different energy intensities of illumination laser. 72

Fig. 4.5 EDS spectrum of the sample before laser illumination (a); EDS spectrum (b) and SAED pattern (c) of MoS₂ nanosheet after laser density of 0.28 J/cm². Insets(a-b) show the enlarged EDS within the 2.15-2.60 keV region..... 73

Fig. 4.6 TEM images of MoS₂ suspension in NMP after 1064 nm laser illumination for 60 minutes under different laser energy intensities (a) 0.77 J/cm²; (b) 3.35 J/cm²; (c) 3.72 J/cm². 74

Fig. 4.7 Size distribution of corresponding samples MoS₂ suspension in NMP after 1064 nm laser illumination for 60 minutes under different laser energy intensities (a) 0.77 J/cm²; (b) 3.35 J/cm²; (c) 3.72 J/cm²; (d) the most frequent size distribution..... 75

Fig. 4.8 Normalized UV/Vis absorption spectrum of MoS₂ suspension in NMP after

laser illumination of 532 nm (a) and 1064 nm (b), respectively.	77
Fig. 4.9 Normalized photoluminescence spectrum of MoS ₂ suspension in NMP after laser illumination of 532 nm (a) and 1064 nm (b), respectively.	78
Fig. 4.10 (a) (b) normalized transmittance; (c) (d) transmittance of MoS ₂ suspension in NMP and (e) (f) transmittance of MoS ₂ /PMMA before and after the 532 nm and 1064 nm laser illumination, respectively.....	80
Fig. 5.1 Experimental procedures for fabricating WS ₂ nanosheets with different size and thickness distribution.....	85
Fig. 5.2 (a-d) AFM images of WS ₂ sheets exfoliated in NMP and subsequently separated under different centrifugation rates of 500, 1000, 5000, and 7000 rpm, respectively. For each WS ₂ sample, about 50 sites were sampled for size and thickness analysis.	86
Fig. 5.3 (a-d) AFM images of WS ₂ sheets exfoliated in NMP and subsequently separated under different centrifugation rates of 500, 1000, 5000, and 7000 rpm, respectively. For each WS ₂ sample, about 50 sites were sampled for size and thickness analysis.	86
Fig. 5.4 Randomly selected section height profiles of WS ₂ sheets exfoliated in NMP	

and subsequently separated under different centrifugation rates of a-500, b-1000, c-5000, and d-7000 rpm, respectively. The interlayer space of WS₂ is 0.62 nm. 87

Fig. 5.5 Thickness distribution of WS₂ sheets exfoliated in NMP and subsequently separated under different centrifugation rates of a-500, b-1000, c-5000, and d-7000 rpm, respectively. The interlayer space of WS₂ is 0.62 nm. 88

Fig. 5.6 Size distribution of WS₂ sheets exfoliated in NMP and subsequently separated under different centrifugation rates of a-500, b-1000, c-5000, and d-7000 rpm, respectively. 89

Fig. 5.7 Most frequent size and thickness of the four samples, L - Estimated layer number. 90

Fig. 5.8 (a) Raman spectra (b) The peak frequency of E_{2g1}, A_{1g} and their frequency difference. 91

Fig. 5.9 (a) Absorption spectra; (b) Peak positions of the characteristic peaks A and B, and ratios of absorption intensity at 532 nm to 1064 nm (I_{532}/I_{1064}) of WS₂ suspension in NMP selected at 500 rpm, 1000 rpm, 5000 rpm and 7000 rpm centrifugation rate, respectively. 92

Fig. 5.10 Digital photographs of prepared WS₂/PMMA composites, they are S500, S1000, S5000 and S7000 from the left to right, respectively..... 93

Fig. 5.11 Nonlinear optical absorption performance of WS₂/PMMA composites. (a) and (b) are the output influence dependence on input fluence, the red lines are the fitting curve according to the TPA model. (c) and (d) are the corresponding normalized transmittance dependence on the input fluence at 532 nm and 1064 nm..... 94

Fig. 6.1 TEM images of WS₂ nanosheet in ethanol and water mixture (a) and NMP suspension (b) sonicated by 15 h, respectively. 102

Fig. 6.2 TEM images of the WS₂ quantum dots (a); (b, c) HRTEM images; and corresponding selected area FFT image (d); diameter distribution of WS₂ quantum dots (e); EDS spectrum of WS₂ quantum dots (f). 103

LIST OF TABLE CAPTIONS

Table 1-1 Current library of 2D materials [5].	2
Table 1-2 About 40 different layered TMD compounds exist [29].	11
Table 3-1 Optical parameters of linear transmittance (T_L), Two-photon absorption (TPA) coefficient, NOL starting threshold (F_{ON}) and Optical limiting threshold (F_{OL}) threshold of MoS ₂ / PMMA composites (sample 1 and 2).	64
Table 4-1 Transmittance of MoS ₂ suspension in NMP and embedded into PMMA matrix before and after 532 nm, 1064 nm laser illumination, respectively.	81
Table 5-1 Optical parameters of linear transmittance (T_L), two-photon absorption (TPA) coefficient (β), NOA onset thresholds (F_{ON}) and optical limiting thresholds (F_{OL}) for various WS ₂ /PMMA composites.	96
Table 5-2 The absorption coefficient α (L g ⁻¹ cm ⁻¹) of different samples at 532 and 1064 nm, respectively.	98
Table 6-1 Optical parameters of linear transmittance (T_L), two-photon absorption	

coefficient (β), NOL onset thresholds (F_{ON}) and optical limiting thresholds (F_{OL}) for WS₂ QD/PMMA composites 109

Table 6-2 The nonlinear optical property onset thresholds (F_{ON}) and optical limiting thresholds (F_{OL}) of different materials for the nanosecond laser operating at 532 and 1064 nm, respectively. 111

CHAPTER 1

Introduction

1.1 Two dimensional materials

During the past years, two dimensional transition metal dichalcogenide materials have attracted substantial attention from the industry and research communities due to their diverse applications including catalysis, light harvesting, batteries, solid lubricants, solar cell and optical limiting device. Great progress has been achieved in various research fields, particularly in nonlinear optics (e.g., saturable absorber and optical limiting). In this Chapter, an overview of the research progress is discussed. The objectives and organization of this thesis are presented.

In the year 2004, Andre Geim and Konstantin Novoselov prepared the first two-dimensional graphene using the transparent scotch tape method and were awarded the Nobel Prize in Physics in 2010. The structure of graphene is very special at the atomic scale structure, the electron mobility is high. Generally, the thickness of a single layer two-dimensional materials is in the scale of several nanometres. The electron mobility of graphene is 100 times higher than that of silicon [1] and it has a very good structural stability at room temperature. Furthermore, electrons moving along the track of graphene will not experience scattering due to the absence of foreign atoms or lattice defects. Due to the unique structure, graphene has a wide range of applications, including touch screens, solar cells, energy storage devices,

mobile phones and high-speed computer chips, flexible electronics, intelligent clothing, folding displays, and even future space elevator [2-4]. The direction of modern material development is from single to composite material and from crystalline to amorphous materials, from bulk to two-dimensional, one-dimensional and even zero-dimensional materials.

For the above reasons, graphene has drawn great attention for its excellent electron conductivity, optical and mechanical properties. Its unique properties are mainly due to its single atomic layer thickness and two-dimensional topological structure. Inspired by those unique properties of 2D materials, many researchers have devoted efforts in other new two-dimensional materials fabrication and characterization, a great number of novel two-dimensional materials have been obtained as shown in Table.1.1 [5]. With the emergence of advanced preparation and characterization of nano technologies, single-layer and multi-layer graphite-like materials has been focused at for a lot of research works. Other types of graphene-like materials e.g. MoS₂, WS₂ and TiS₂ are also prepared and widely used in catalysis, optoelectronic devices, batteries and solid lubrication and other fields [6-8].

Table 1-1 Current library of 2D materials [5].

Graphene family	Graphene	hBN 'white graphene'	BCN	Fluorographene	Graphene oxide
2D chalcogenides	MoS ₂ , WS ₂ , MoSe ₂ , WSe ₂		Semiconducting dichalcogenides: MoTe ₂ , WTe ₂ , ZrS ₂ , ZrSe ₂ and so on	Metallic dichalcogenides: NbSe ₂ , NbS ₂ , TaS ₂ , TiS ₂ , NiSe ₂ and so on	
				Layered semiconductors: GaSe, GaTe, InSe, Bi ₂ Se ₃ and so on	
2D oxides	Micas, BSCCO	MoO ₃ , WO ₃	Perovskite-type: LaNb ₂ O ₇ , (Ca,Sr) ₂ Nb ₃ O ₁₀ , Bi ₄ Ti ₃ O ₁₂ , Ca ₂ Ta ₂ TiO ₁₀ and so on		Hydroxides: Ni(OH) ₂ , Eu(OH) ₂ and so on
	Layered Cu oxides	TiO ₂ , MnO ₂ , V ₂ O ₅ , TaO ₃ , RuO ₂ and so on			Others

1.1.1 Preparation of two-dimensional materials

Generally, two main categories of methods, top-down and bottom-up have been employed to prepare these novel two-dimensional materials. The top-down methods include mechanical cleavage method [9]. The micro-mechanical exfoliation method e.g. scotch tape method is currently the most mature technique for its simple operation and possible to produce mono layer sample. The obtained two-dimensional materials exhibit high electron mobility, and suitable for field effect transistor fabrication. However, the drawback of this method is low productivity and poor reproducibility; chemical Li-intercalation and exfoliation with n-butyllithium (BuLi), electrochemical Li- intercalation and exfoliation[10], can bring about the high production yield for broad application scope. The production method can be employed to fabricate 2D materials used for secondary battery and light emitting diode. However, the disadvantage is time-consuming and harsh preparation conditions and the prepared 2D materials will be aggregated after removing the lithium ion; liquid phase exfoliation by direct sonication in solvents [11] is a simple and effective method although its exfoliation efficiency is much lower than the former two methods and the yield of single layer 2D materials is very low; and laser thinning technique requires expensive processing tool and low production yields [12].

The bottom-up approaches methods include CVD growth, hydrothermal reaction. Bottom-up synthesis e.g. CVD produces high thermal stability, chemical stability and potential large area sample but it has disadvantages of high manufacturing cost, complex process control and well controlled furnace required. However, it is a method with great potential to achieve large-scale and high-quality

the production of two dimensional materials through continuously optimizing the preparation conditions and innovating design. In the following part, we will discuss four types of methods in details.

(1) Mechanical cleavage

The mechanical cleavage method is a traditional method to prepare 2D flakes. Micromechanical force cleavage is used to exfoliate transition metal dichalcogenide bulk materials by using adhesive tape, and it is found 3M scotch tape will be good to obtain a monolayer or multilayer two dimensional flakes containing tens to hundreds of crystal layers. In 1965, Frindt used tape to obtain several layers of molybdenum disulfide for the first time [13]. The principle is using the viscous adhesive tape to overcome weak van der Waals forces between the molecular layer to exfoliate 2D materials. With the development and improvement of technology, single layer or several layers 2D materials have been obtained through this tape peel method [14, 15]. This method neither requires complex preparation device nor large energy consumption, which is simple, effective, and low cost. Using this method, single layer 2D materials can be obtained with high electron mobility. However, the disadvantages of this method are very low production yield, difficult to produce large size sample (limited to a few microns in size) and poor reproducibility. Single-layer BN, MoS₂, NbSe₂ and Bi₂Sr₂CaCu₂O_x have been obtained by using mechanical cleavage and have been used for electronic device fabrication [16].

(2) Electrochemical Li-intercalation and exfoliation

The above mentioned mechanical cleavage method can produce high quality single-layer 2D nanomaterials, however its low production yield has hindered its

from practical applications. Especially, the preparation of thin film needs large quantities

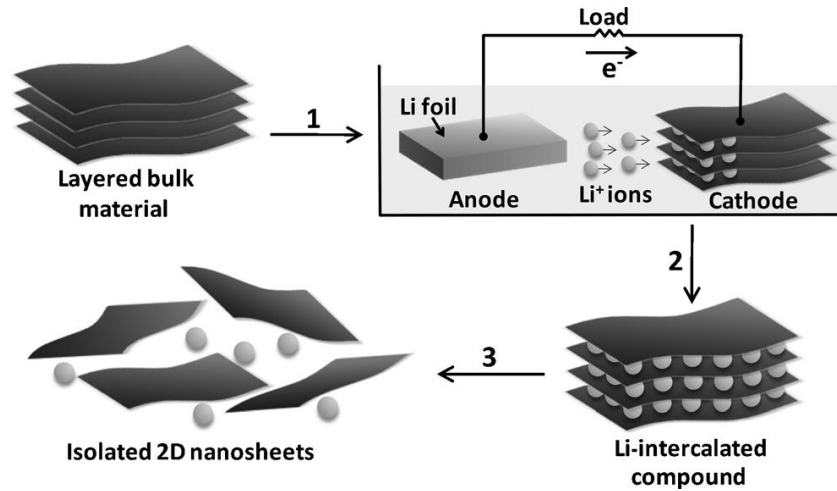


Fig. 1.1 Electrochemical lithiation process for the fabrication of 2D nanosheets from the layered bulk material.

2D nanomaterials with solution processability. Recently, zhang et al [10] developed an electrochemical Li-intercalation and exfoliation method to produce a large quantity of 2D materials, including BN, graphene nanosheet, MoS₂, WS₂, TiS₂, TaS₂, ZrS₂, NbSe₂, WSe₂, Sb₂Se₃ and Bi₂Te₃. For this method, the two dimensional transition metal dichalcogenides bulk materials is incorporated as a cathode and a lithium foil is used as an anode in a Li-ion battery setup. The basic principle is to use lithium-ion intercalation agent (such as butyl lithium, n-C₄H₉Li) embedded disulfide molybdenum powder, then form Li_xMoS₂ ($x \geq 1$) intercalation compound through intercalation compound with a protic solvent (typically water, which can also be acid or a low-boiling point alcohol) to produce large amount of hydrogen to enlarge the layer spacing between molybdenum sulfide, under vigorous agitation by sonication, thereby well-dispersed multilayer or a single layer molybdenum disulfide are

obtained as shown in Fig. 1.1. Although the process is relatively complicated, it can be used to exfoliate a wide range of 2D materials with good efficiency including molybdenum disulfide [17, 18]. The Li-intercalation process can be well-controlled by monitoring the discharge curve. The amount of inserted lithium can be optimized to avoid the insufficient Li-intercalation, leading to low-quantity of single-layer nanosheets, or too much Li-inserting, resulting in the structure decomposition of two-dimensional nanomaterials.

(3) Sonication in various solvents

Direct liquid ultrasonication exfoliation method is a new method which is developed recently. In 2011, the 2D nanomaterials have obtained through direct liquid exfoliation [19, 20] which is shown in Fig.1.2, such as MoS_2 , WS_2 , MoSe_2 ,

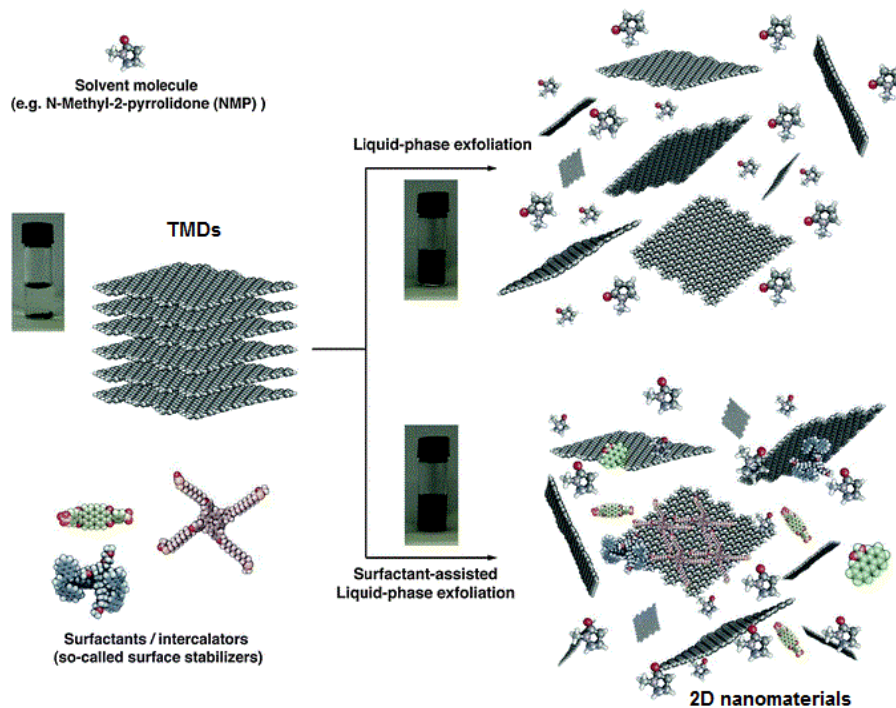


Fig. 1.2 Schematic representation of liquid-phase exfoliation process of TMDs bulk materials in the absence (top-right) and presence (bottom-right) of surfactant molecules [21].

NbSe₂, NiTe₂, MoTe₂, h-BN and Bi₂Te₃ [22]. Few layered MoS₂ nanosheet has been obtained through ultrasonication in N-methyl-2-pyrrolidone (NMP), followed by ultrasonication, appropriate centrifugation speed, then dried in vacuum. Liquid ultrasonic exfoliation process is carried out in liquid then supplemented by ultrasound, therefore, the ultrasound power is one of the critical parameter on the direct liquid ultrasonication exfoliation. Another significant condition is the suitable liquid organic solvent. A number of common solvents have been demonstrated for the effective and efficient exfoliation of layered materials by liquid exfoliation. The typical liquid organic solvents used for this application are N- methyl-2-pyrrolidone (NMP), N-ethyl-2-pyrrolidone (NVP), isopropanol (IPA), dimethyl sulfoxide (DMSO), dimethylformamide (DMF), etc. When the surface energy of the solvent matches with the layered material, the enthalpy for the exfoliation is minimized, then the transition metal dichalcogenides bulk materials can be exfoliated effectively and efficiently. As for MoS₂ and WS₂, solvents like N- methyl-2-pyrrolidone (NMP) will be suitable. These solvents has a surface energy of ~70 mJ m⁻², gave the best dispersity of exfoliated nanosheets [19, 22]. The mixture dispersions of the 2D nanomaterials can be made into hybrid dispersions or composites by mixing them with other types of functional materials. The molybdenum disulfide powder was put in an aqueous solution and added sodium cholate as a surfactant to inhibiting the aggregation of 2D nanomaterials, then followed by ultrasonication for 30 min and settling for 24 hours [23]. Then the suspension was centrifuged and the supernatant was removed. The collected suspension was dried under vacuum to obtain few-layered molybdenum disulfide nanosheets. Although the efficiency of direct liquid exfoliation is lower than electrochemical Li-intercalation and exfoliation

method, its simplicity, convenient and suitable for large-scale production have attracted great attention amount the researchers.

Although water and ethanol were previously demonstrated as poor solvents for the exfoliation of 2D materials, recently, the water-ethanol mixture is able to exfoliate and disperse 2D nanomaterials, due to the change of solubility of the solvent mixing. Zhang et al have proved that 45 vol% ethanol- water mixture can exfoliate MoS₂ into nano flakes, characterized by the UV-vis absorbance, the exfoliation efficiency is comparable to that in NMP solution[11]. Consider water and ethanol are low cost and common solvents, this method is one of the most convenient and economical ways to obtain the 2D nanomaterials solutions.

(4) Chemical vapor deposition

Chemical vapor deposition is a chemical process used to produce high quality, scalable size, controllable thickness and excellent electronic high performance 2D materials thin films and its fabricated electric device performance is comparable to the current nano- and micro- electronic fabrication processes [24]. Chemical vapor deposition is a process the gaseous substances chemical react on the solid surface and then produce solid deposits. The wafer scale deposition of MoS₂ layers have been obtained after direct sulfurization of as-deposited MoO₃ on the insulators as shown in Fig.1.3 [25].

The WS₂ monolayers flakes of fine triangular shape were grown after direct sulfurization of as-deposited WO₃ on SiO₂/Si substrates as illustrated in Fig.1.4 [26].

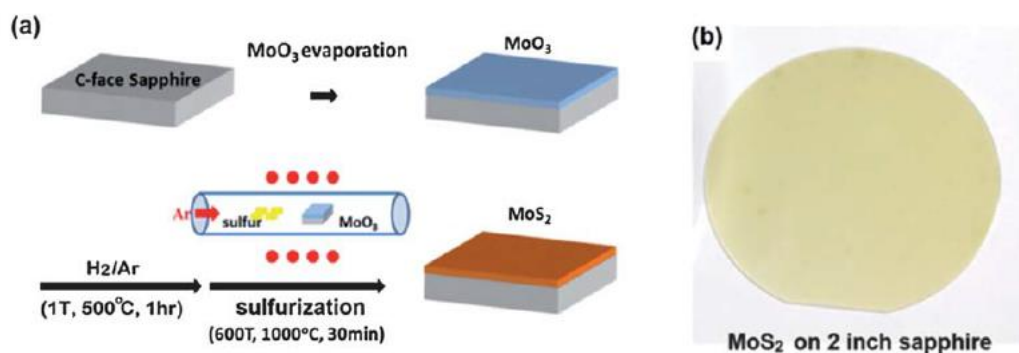


Fig. 1.3 (a) Schematic illustration for the synthesis of MoS_2 layers by MoO_3 sulfurization. A layer of MoO_3 (~3.6 nm) was thermally evaporated on the sapphire substrate. The MoO_3 was then converted to a MoS_2 by a two-step thermal process. (b) MoS_2 layer grown on a sapphire wafer [25].

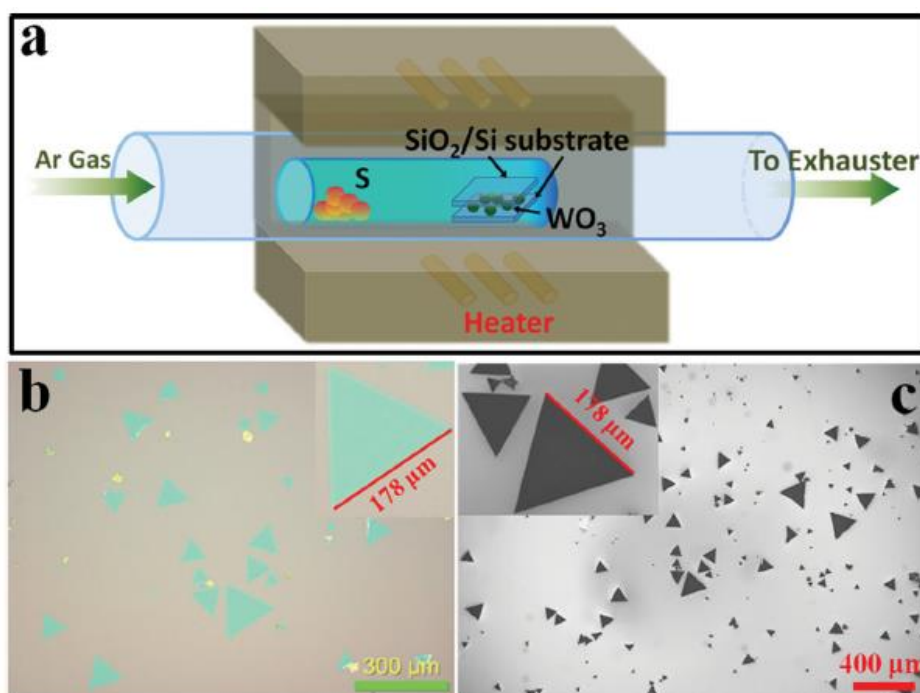


Fig. 1.4 (a) Schematic diagram of the CVD system used for the growth of WS_2 . (b) Optical image of as-grown WS_2 on SiO_2 (300 nm)/ Si substrate. Inset shows a triangular monolayer WS_2 . (c) SEM image of the sample fabricated by setup shown in Fig. 1.4 (a) [26].

The electrical devices based on the CVD-grown 2D nanomaterials show good electronic property, also with high On /Off ratios [27]. Furthermore, the direct formation of the WS_2/MoS_2 heterostructures shown in Fig. 1.5 offer a general route to prepare large-area TMDs tandem structures for fundamental study as well as some applications as catalyst or active redox centers [28].

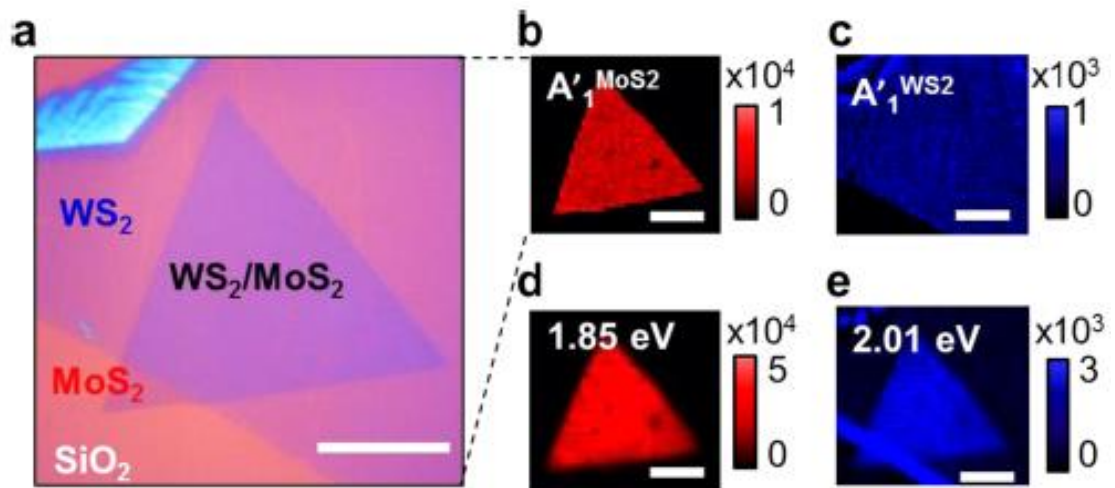


Fig. 1.5 WS_2/MoS_2 heterostructures. (a) Optical image of a monolayer WS_2/MoS_2 heterostructure. (b,c) Raman mapping at the 408 cm^{-1} (MoS_2) and 421 cm^{-1} (WS_2). (d,e) PL mapping at the 1.85 eV (MoS_2) and 2.01 eV (WS_2) [28].

1.1.2 Properties and characterizations of two-dimensional materials

Single-layered 2D TMDs- whose formula is MX_2 , where M is a transition metal of groups 4-10 and X is a chalcogen. As can be seen from Table.1-2, there are versatile chemistry above 40 kinds of TMDs [29]. This provides opportunities for fundamental research in various fields including catalysis, energy storage, sensing and electronic devices such as field-effect transistors. Transition metal chalcogen compound (TMDs) is a transition metal atom (including the group IV elements Ti,

Table 1-2 About 40 different layered TMD compounds exist [29].

MX_2 M = Transition metal X = Chalcogen																	
H																	He
Li	Be											B	C	N	O	F	Ne
Na	Mg	3	4	5	6	7	8	9	10	11	12	Al	Si	P	S	Cl	Ar
K	Ca	Sc	Ti	V	Cr	Mn	Fe	Co	Ni	Cu	Zn	Ga	Ge	As	Se	Br	Kr
Rb	Sr	Y	Zr	Nb	Mo	Tc	Ru	Rh	Pd	Ag	Cd	In	Sn	Sb	Te	I	Xe
Cs	Ba	La-Lu	Hf	Ta	W	Re	Os	Ir	Pt	Au	Hg	Tl	Pb	Bi	Po	At	Rn
Fr	Ra	Ac-Lr	Rf	Db	Sg	Bh	Hs	Mt	Ds	Rg	Cn	Uut	F1	Uup	Lv	Uus	Uuo

Zr, Hf and group V group elements (V, Nb, Ta and group VI elements Mo, W), and sulfur atoms (including S, Se, Te) composites. The general crystal structure is generally shown in Fig.1.6. Those transition metal chalcogenide bulk materials have similar structure with graphite (graphene precursor material) and hexagonal boron nitride. The interaction between layers are weak van der Waals which can be exfoliated effectively.

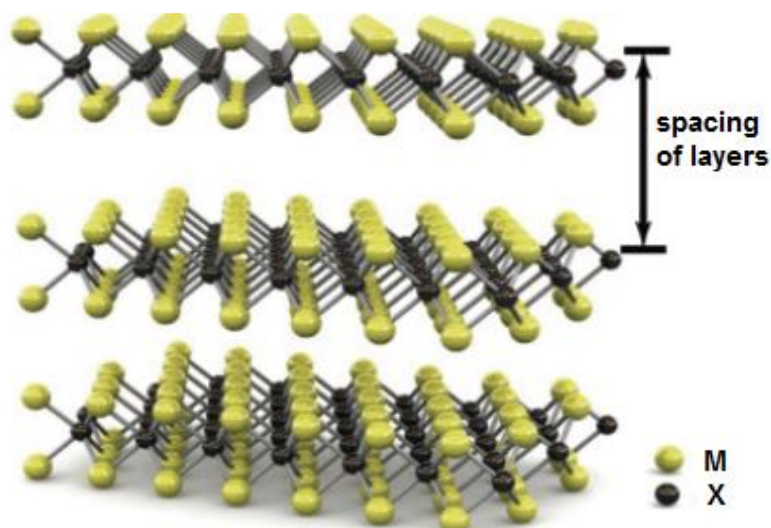


Fig. 1.6 The crystal structure of transition metal dichalcogenide.

Two-dimensional materials are characterized by their special structures, therefore the first issue is to find methods to accurately and efficiently characterize the two-dimensional layered structure. This can not only judge the preparation of two dimensional materials whether or not successful, but also better explore the relationship between structure and property of the graphene-like materials and promote their practical applications.

Generally, two-dimensional layered materials are characterized by various types of microscopy, including atomic force microscopy (AFM), scanning electron microscopy (SEM) and transmission electron microscopy (TEM) and so on. SEM and TEM measurement of the edge folds can also be used to identify the layers of two-dimensional materials roughly as shown in Fig. 1.7a-b. AFM is the most direct way to identify the layers of two-dimensional materials as shown in Fig. 1.7c as the height profile of the sample can be measured by AFM. Furthermore, Raman spectroscopy can also be used to characterize the two dimensional materials which is powerful, accurate, fast and will not destroy the crystal structure. Direct measuring the in-plane and out-of-plane vibration mode E^{12}_g and A^1_g Raman peaks different can be used to identify the average layer number of the fabricated sample. These results can be used to evaluate the exfoliation efficiency of fabrication method. Fig. 1.7d shows the Raman spectrum of the bulk, trilayer, bilayer and single-layer MoS_2 films.

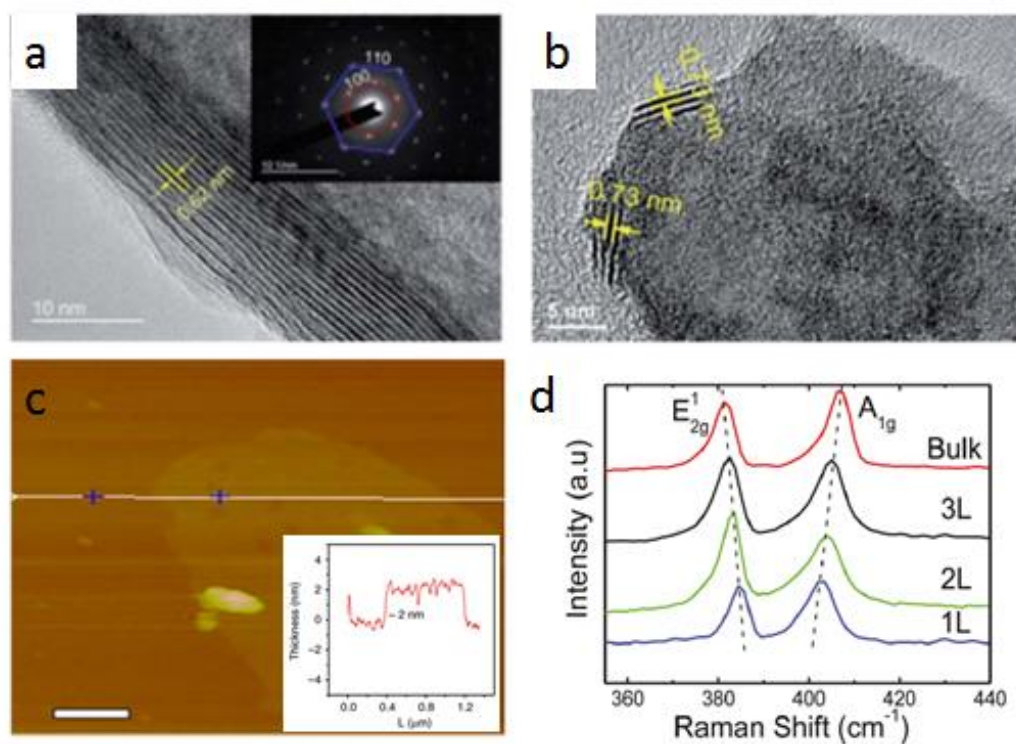


Fig. 1.7 Characterization methods of two-dimensional materials. (a) (b) TEM of MoS₂. Inset is the digital image of MoS₂ solution[30]; (c) AFM of exfoliated g-C₃N₄ nanosheets and corresponding thickness analysis taken around the white line [31]; (d) Raman spectra of MoS₂ nanosheet [32].

1.1.3 Application of two-dimensional materials

(a) Nonlinear optical application

A successful optical limiter should strongly attenuate intense, potentially for low-intensity ambient light. The development of viable photonic devices primarily depends on materials with remarkable specific optical properties, such as luminescence, non-linear optical responses and so forth [33]. The use of graphene based materials for making optical limiting products has been studied. GO dispersed in bisphenol-A polycarbonate exhibits excellent optical limiting performance as shown in Fig. 1.8 [34]. Also, graphene based materials have uniform absorption over

a broad waveband, high transmission at near infrared and strong absorption in the visible range and leads to relatively stronger two photon absorption at near infrared, which cover most of the mainstream high power laser system used within the industry and military e.g. Nd:YAG laser and Yb fiber laser operating near 1 micron [35, 36].

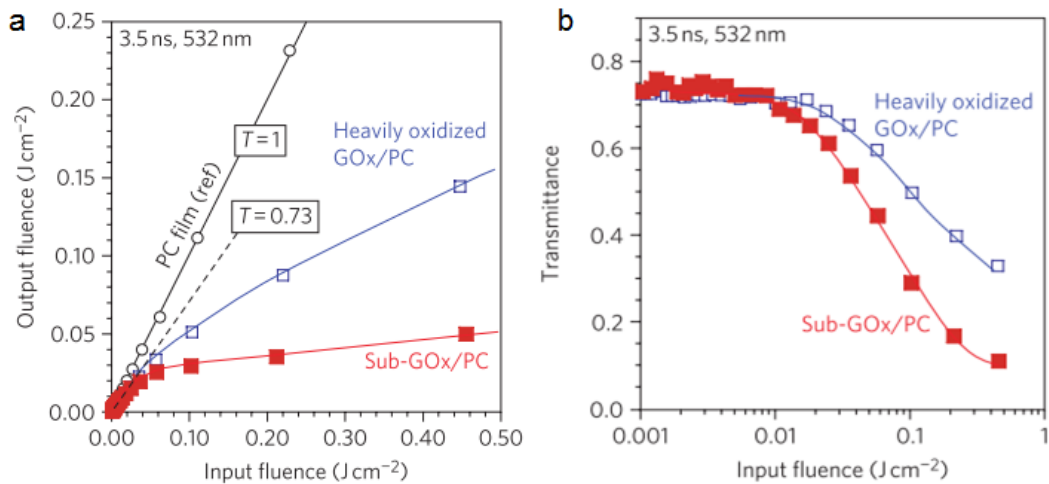


Fig. 1.1.8 Nonlinear transmittance characteristics of sub-GOx/PC film. (a) plot of output versus input fluence (b) plot of transmittance versus input fluence for 3.5 ns pulses are 532 nm [34].

However, due to the limit applications of the zero or small bandgap nature of graphene based materials, other innovation 2D materials e.g. TMDs materials, with larger natural bandgap ranged from visible to mid infrared has become very active research field [37 - 39]. While, its explored inorganic analogues with large intrinsic band gap and high carrier mobility, show great promise for optical applications for their unique properties, such as large surface area, high mechanical strength, high inplane charge mobility, and weak coupling between the layers [38]. The band gap energy of those TMDs, whose formula is MX_2 , (M - transition metal X -a chalcogen), e.g MoS_2 , WS_2 , TaS_2 , ZrS_2 , WSe_2 , Sb_2Se_3 and TiS_2 , can be engineered between 0.2

eV (6199 nm) to ~ 2 eV (~ 620 nm) by selecting different M and X [29]. With more than 40 different categories, TMDs material offers a range of features suitable for various wavelengths. Bulk WS_2 crystal or conventionally deposited WS_2 thin films possess no such properties, limiting the range of their use, for instance, in photonics [40]. While, few-layer MoS_2 or WS_2 exhibit excellent saturable absorb or optical limiting properties which can be seen in Fig. 1.9. [41]

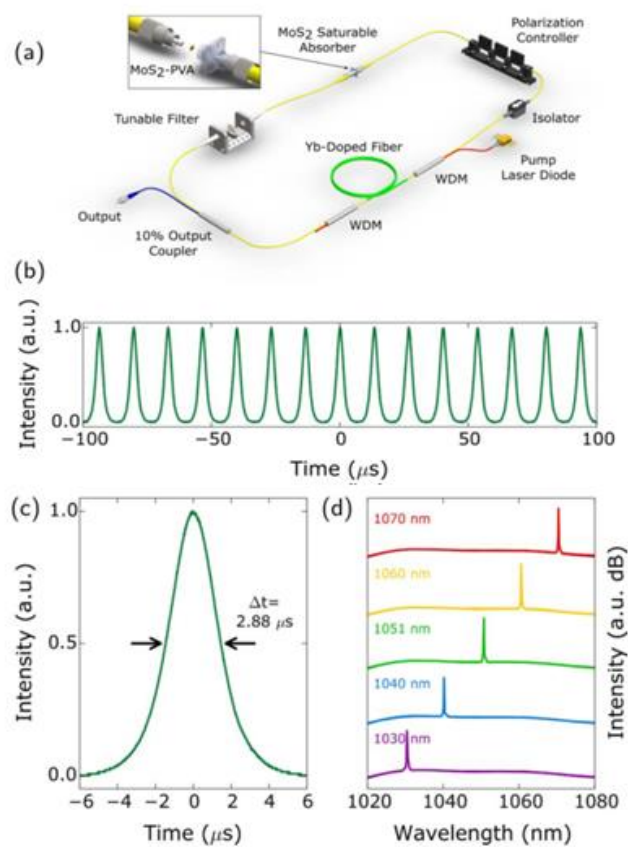


Fig. 1.1.9 Tunable MoS_2 Q-switched fiber laser. (a) cavity schematic, (b) output 74 kHz pulse train, (c) profile of single pulse, (d) various spectra at wavelengths within the continuous tuning range of 1030-1070 nm [41].

Therefore, it is a very meaningful research work to study nonlinear optical response with respect to those two dimensional materials. Besides the above

mentioned application, these TMDs materials have been applied for many other applications in the field of laser photonics, such as saturable absorber for Q-switching and mode locking laser generation [42, 43]; Optical limiter for human eyes and detectors protection [44, 45], optical switches for optical communication and computing, information data storage [46], laser pulse compression and two-photon fluorescence microscopy [47].

(b) Energy generation and storage

With the shortage of traditional energy sources, decreasing quality and environmental pollution problems, novel and sustainable green energy has become one of the important part of world's energy development. Chemistry has become the core of new energy industry revolution which can solve the randomness and volatility of new energy sources. Due to the unique property of two-dimensional materials, such as, special layered structure, variable atomic and electronic structure, strong interaction of phonons between electrons and lattice vibrations, the weak van der Waals forces between layers which is beneficial for the inserting and extracting of light metal ions (Li^+ , Na^+ , Mg^{2+} , etc), and the good charge storage capacity of the electrical double layer, those characteristics predict their high theoretical lithium storage capacity and as excellent chemical electrode materials [48, 49]. Furthermore, compared with bulk materials, two-dimensional materials have larger surface area, stronger adsorption capacity and higher reactivity which make them greater potential for energy storage application. A unique 2D MoS_2 /mesoporous carbon (MoS_2 /m-C) hybrid nanoarchitecture has been obtained which single-layer MoS_2 and m-C are sandwiched in alternating sequence. This superstructure, which is shown in in Fig.1.8 [50], forms excellent atomic interface contact between MoS_2 and

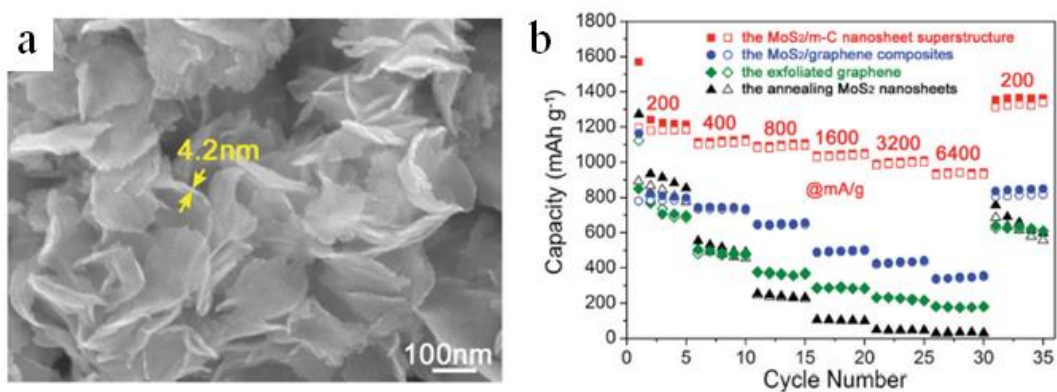


Fig. 1.10 (a) The MoS₂/m-C nanosheet superstructure; (b) the capacities retention of the MoS₂/m-C nanosheet superstructure, MoS₂/graphene composites, exfoliated graphene, and the annealed MoS₂ nanosheets at current densities from 200 to 6400 mA g⁻¹ [50].

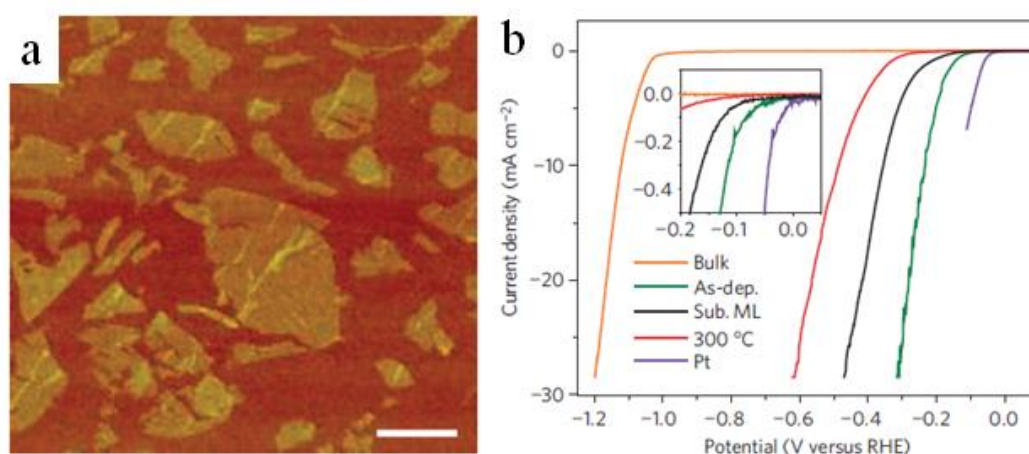


Fig. 1.11 (a) Typical AFM image of exfoliated nanosheets of WS₂; (b) Polarization curves of bulk and as-exfoliated WS₂ (as-deposited film of 1T phase, sub-monolayer as-exfoliated film, and 2H phase after annealing at 300 °C) along with those corresponding to Pt nanoparticles and bulk WS₂ powder for comparison [6].

carbon, leading to the maximization of synergistic interaction and their capacities retention. Voiry et al have used the chemically exfoliated monolayer 2H (trigonal prismatic) WS₂ as efficient catalysts for hydrogen evolution with very low over

potentials. Fig.1.9 show the typical AFM image of exfoliated WS₂ and its polarization curves compared with other phase WS₂ and Pt nanoparticles [6].

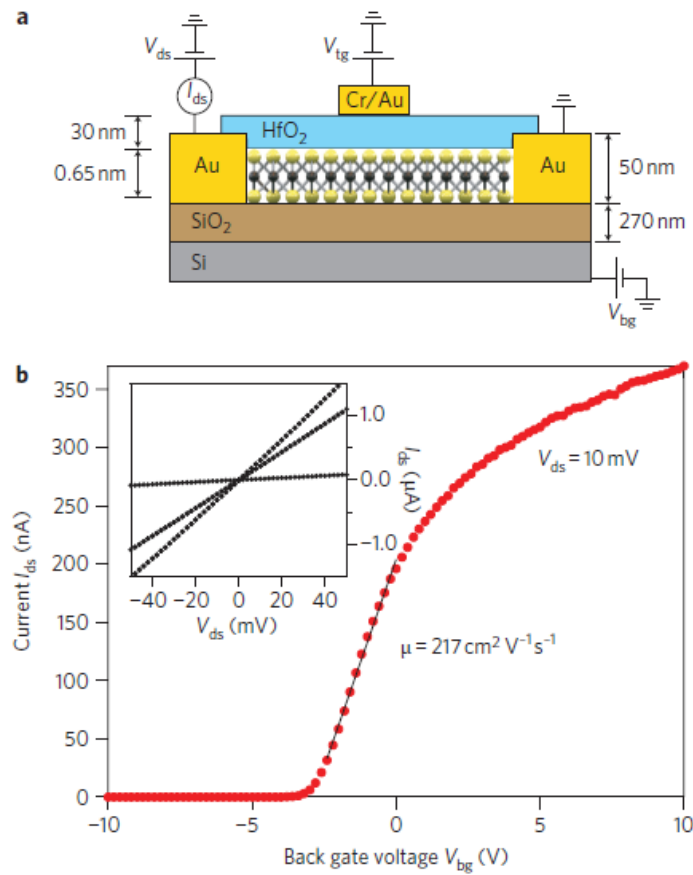


Fig. 1.12 Schematic structure and property of field effect transistor (FET) containing MoS₂ (a) schematic structure of FET; (b) room-temperature transfer characteristic for the FET with 10 mV applied bias voltage (V_{ds}) [14].

(c) Electronic devices

Field effect transistor (FET) is one of the important microelectronic technology, which mainly affect the electrical properties of semiconductor through changing the electric field. FETs are also named unipolar transistors for related single carrier type operation. Monolayer two dimensional materials are direct band gap semiconductors, therefore they can be used to prepare large switching current ratio, high carrier

mobility and low energy field effect transistor. Single-layer molybdenum disulfide has been prepared through the micro mechanical exfoliation method and then subsequently transfer on a silicon substrate, 50 nm thickness gold electrode was made through electron beam lithography, 30 nm thickness hafnium oxide was produced as gate dielectric layer by atomic layer method [14]. The schematic structure and transfer properties of FET are shown in Fig.1.10. Results show the threshold voltage is -4 V, the on/off current ratio is 108 and the electron mobility is $217 \text{ cm}^2 \cdot \text{V}^{-1} \cdot \text{s}^{-1}$.

(d) Organic light emitting diode.

An organic light-emitting diode (OLED) is a light-emitting diode (LED) in which the emissive electroluminescent layer is a film of organic compound that emits light in response to an electric current. The organic light emitting diode have many advantages including self-luminous, wide viewing angle, low power consumption, full color, etc, therefore it has broad applications in panel displays, solid state lighting and so on. Two-dimensional materials can be used as both host materials and hole injection layer of OLED. Wang et al demonstrated the few-layered graphene films which are used as anode in photovoltaic devices can improve the power conversion efficiency up to 1.71% [51].

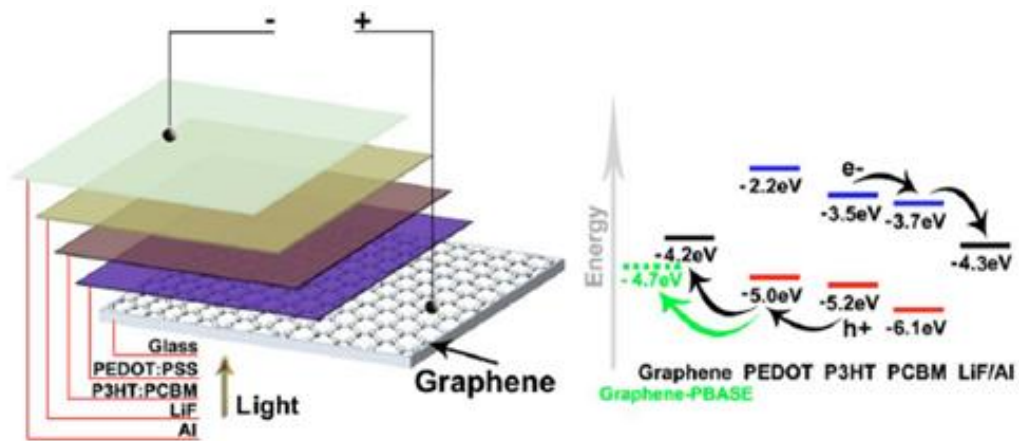


Fig. 1.13 Schematic and energy diagrams of the fabricated device with structure graphene/PEDOT:PSS/P3HT:PCBM/LiF/Al [51].

(e) Sensing devices

Due to their unique electronic properties, large specific surface area and layered structure which is in favor of adsorbed gas molecules, novel two dimensional materials have applications for gas sensing. Traditional metal oxide sensors not only are sensitive to oxidation and reducing gas but also need high working temperature (350°C or above). 1-4 layers molybdenum disulfide has been prepared successfully through micro mechanical exfoliation method and created field effect transistor device to detect the concentration of nitric oxide (NO) gas [52]. The detecting concentration range is 0.3×10^{-6} - 2×10^{-6} (volume fraction). This device is in good stability, high sensitivity as shown in Fig.1.12 and results demonstrate the two layers of molybdenum disulfide show the best detection performance.

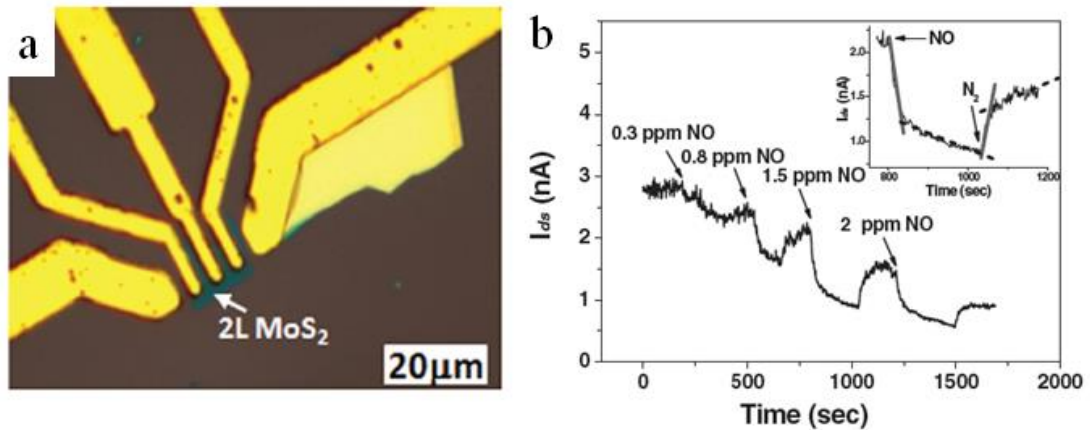


Fig. 1.14 (a) schematic structure of gas sensor; (b) real-time current response of the device exposed to NO with increasing concentration [52].

1.2 Nonlinear optical property

Nonlinear optics (NLO) is the discipline that describes the behavior of light in nonlinear media and the dielectric polarization P is nonlinear to the electric field E of the light. This nonlinearity is typically only observed under very high light intensities usually provided by laser source. In the past 40 years, the development of theory and working principles of nonlinear optics, discovery and research of new materials and its related applications remains active. It becomes one of the important branches of optics. Multi-photon absorption is one of the nonlinear optical phenomena, it has wide application in optical information storage, three-dimensional optical storage, bio-optics, material science and photochemistry. The study of multi-photon absorption material has been nearly half century, it has a rapid development in this area in the past 5-10 years.

When the high intensity laser interacts with materials, the relationship between polarization density and electric field which is nonlinear. For such interactions, the polarization density amplitude can be expressed as:

$$P(\gamma, t) = \varepsilon_0 \chi^{(1)} \cdot \overline{E} + \varepsilon_0 \chi^{(2)} \cdot \overline{EE} + \varepsilon_0 \chi^{(3)} : \overline{EEE} + \dots \quad (1-1)$$

$$P(\gamma, t) = P^{(1)} + P^{(2)} + P^{(3)} + \dots \quad (1-2)$$

Where ε_0 is the permittivity of free space, $\chi^{(n)}$ is the complex susceptibility tensor of order n, $\chi^{(1)}$ is the linear susceptibility tensor, $P^{(1)} = \varepsilon_0 \chi^{(1)} \cdot E$ represents the first order polarization or linear polarization. In the regime of weak fields, polarization density and electric field exhibits linear relationship, which is called linear polarization. $P^{(2)} = \varepsilon_0 \chi^{(2)} \cdot \overline{EE}$ and $P^{(3)} = \varepsilon_0 \chi^{(3)} : \overline{EEE}$ are the second- and third-order nonlinear polarization, where $\chi^{(2)}$ and $\chi^{(3)}$ are the second- and third-order nonlinear susceptibilities, and so on. When the light intensity is strong, the second order, third order and higher order will play important role on the overall polarization, therefore, materials will also exhibit higher-order nonlinear optical effects.

Nonlinear susceptibility can be expressed as follows:

$$\chi^{(3)} = \chi_R^{(3)} + i \cdot \chi_I^{(3)} \quad (1-3)$$

Where $\chi_R^{(3)}$ can be obtained:

$$\chi_R^{(3)} = 2 n_0^2 \cdot \varepsilon_0 \cdot c \cdot n_2 \quad (1-4)$$

Where $\chi_R^{(3)}$ is the real part, $\chi_I^{(3)}$ is the imaginary part, n_0 is the linear index of refraction, c is the speed of light in a vacuum, n_2 is the nonlinear index of refraction.

When the high intensity light interacts with materials, the refractive index of the materials will change which can be explained by different physical mechanisms. The overall effect depends on laser pulse duration as laser and materials interaction

period is critical. For example, (1) Under the interaction with intense light, the electron cloud surrounding the atoms and molecules become distorted, which induce refractive index change of the material. However, this process occurs rapidly, about $10^{-14} \sim 10^{-15}$ seconds. (2) The density of materials changes which is caused by the electrostriction effect under laser excitation and then lead to the change of refractive index, the response time of this process is about $10^{-8} \sim 10^{-9}$ seconds.

The relationship between the imaginary part of the nonlinear susceptibility and nonlinear absorption coefficient can be expressed as:

$$\chi_I^{(3)} = \frac{n_0^2 \cdot \epsilon_0 \cdot c^2}{\omega} \cdot \beta \quad (1-5)$$

Where ω is the angular frequency, β is the nonlinear absorption coefficient.

Nonlinear absorption refers to the change in laser transmittance with the change of intensity of incident laser. There are many mechanisms to explain nonlinear absorption. (1) the absorption of light decreases with increasing light intensity. Generally, with sufficient high incident laser intensity, atoms in the ground state become excited into an upper energy state, and there is not enough time for them to back to the ground state before the ground state becomes depleted as the ground state absorption cross section is larger than the excited state cross section, therefore the absorption subsequently saturates. Under this situation, the nonlinear absorption coefficient β is negative which represents the saturated absorption. (2) Reverse saturable absorption (RSA) can result in large absorption by the nonlinear absorber at high incident laser energies and weak absorption under low laser energies density. For this case, β is positive and absorption becomes strong at high optical intensity as the excited state absorption cross section is larger than the ground state cross section. (3) Two-photon absorption (TPA) is that the electron excited from the ground

state to the excited state by absorbing two-photon simultaneously under intense laser illumination. This process includes frequency degenerate two-photon absorption (absorbed photons have the same frequency) and frequency non-degenerate two-photon absorption (the absorbed photons have different frequency). (4) Free carrier absorption is the absorption coefficient increases with the increasing intensity of the incident laser which mainly occurs in the semiconductor materials. It happens when a material absorbs a photon, and a carrier (electron or hole) is excited from an already-excited state to another, unoccupied state in the same band (but possibly a different subband). The excited carrier is in an excited band, such as an electron in the conduction band or a hole in the valence band, and it is free to move.

Normally, optical limiting material exhibits at least one dominate nonlinear optical mechanism, including non-linear absorption (reverse saturable absorption, two photon absorption, excited-state absorption, or free-carrier absorption), non-linear refraction (excitation of free carriers, photorefraction, heating of the materials etc.), induced scattering (scattering centers formed by groups of non excited and excited molecules).

1.3 Objectives and organizations of the thesis

This thesis studies on the fabrication of novel two dimensional transition metal dichalcogenide materials, including the MoS₂ nanosheet, WS₂ nanosheet and WS₂ quantum dots, and embedded them into solid state matrix PMMA to measure their nonlinear optical absorption property. The thesis is composed of seven Chapters.

In Chapter 1, an overview related to two-dimensional materials, their preparation and optical properties, third-order optical property theory and related applications of those two-dimensional materials are presented. The objectives and

organizations of the thesis are also presented in this chapter.

In Chapter 2, the characterizations of two-dimensional materials dispersed into NMP suspension or embedded into solid state matrix PMMA are described. The two photon absorption theory and minimal enthalpy of the solution are also discussed in this chapter.

Chapter 3 presents the preparation and characterization of MoS₂ nanosheets and their nonlinear optical property embedded into solid state matrix PMMA. Few layered MoS₂ nanosheet was obtained through hydrothermal chemical reaction followed by ultrasonication. MoS₂ nanosheets have been characterized by X-ray diffraction (XRD), transmission electron microscopy (TEM), energy dispersive X-ray spectroscopy (EDS), Atomic force microscopy (AFM), Raman, Uv-Vis Absorption and Photoluminescence. Also, the interesting dependence of interlayer separation with respect to the layer number of MoS₂ has been successfully quantified and presented in this chapter. Furthermore, two different concentrations of MoS₂ nanosheets have been embedded into solid state matrix PMMA to investigate their nonlinear optical properties.

Chapter 4 presents the studies of optical limiting properties of MoS₂ nanosheets in two different environments - liquid NMP and solid state PMMA. Under the laser wavelength of 532 nm and 1064 nm illumination with different energy intensities, the changes in color of the MoS₂ in NMP suspension and size of MoS₂ nanosheets are presented. Furthermore, the changes of the MoS₂ nanosheets under 532 nm laser illumination have been studied through transmission electron microscopy (TEM), energy dispersive X-ray spectroscopy (EDS), Uv-Vis Absorption and Photoluminescence. Additionally, the optical limiting properties of the MoS₂ in

liquid NMP and in solid PMMA have been studied by using z-scan technique and their results are compared and discussed.

Chapter 5 presents WS₂ nanosheets with different size and thickness distribution fabricated by ultrasonication exfoliation method. With different centrifugation rate, WS₂ nanosheet with a series of size and thickness distribution range are obtained successfully which have been characterized by atomic force microscopy (AFM), Uv-Vis absorption, Raman spectrum. The mechanism of interesting shift of the characteristic peaks in absorption and Raman spectrum are also studied. Then, four WS₂ nanosheets samples with different size and thickness distribution are embedded into solid state PMMA to investigate their optical limiting properties. The relationship between the size and thickness of WS₂ nanosheets and their optical limiting performance have also been discussed in this chapter.

Chapter 6 presents ultra-small WS₂ quantum dots fabrication method. They are prepared through ultrasonication exfoliation method followed by high speed centrifugation in NMP. Two solutions are selected as solvent for sonication of the WS₂ powder. Surface energy analysis of the mixing enthalpy is consistent with the experimental results. The obtained WS₂ quantum dots are characterized by Transmission electron microscopy (TEM), Atomic force microscopy (AFM). Uv-Vis Absorption and photoluminescence. Furthermore, three different concentrations of WS₂ quantum dots embedded into solid state matrix PMMA have been used for Z-scan experiments under excitation of laser operating at both wavelengths of 532 and 1064 nm. The optical limiting parameters *e.g.* onset thresholds (F_{ON}), lower optical limiting thresholds (F_{OL}), and higher two-photon absorption coefficient (β) are measured. Additionally, the optical limiting performance of WS₂ nanosheet and

WS₂ quantum dots with similar thickness have been compared and discussed.

In Chapter 7, a conclusion of the two-dimensional materials preparation and their nonlinear optical properties embedded into solid state matrix PMMA and some suggested future work are provided in this Chapter.

CHAPTER 2

Two Dimensional Materials Characterization and Theoretical Analysis

During my PhD study, several types of two dimensional materials, *eg.* Molybdenum disulfide (MoS_2) nanosheet, Tungsten disulfide (WS_2) nanosheet and Tungsten disulfide (WS_2) quantum dots were fabricated and studied. In order to test their nonlinear optical properties, all are embedded into solid state matrix poly methyl methacrylate (PMMA) to stabilize their properties.

The morphologies and structure of these two dimensional materials are characterized by optical microscope, transmission electron microscopy, energy-dispersive X-ray spectroscopy, field emission scanning electron microscopy, and X-ray diffraction, respectively. Their optical properties are characterized by using transmission spectrum, absorption spectrum, photoluminescence spectrum, Raman spectrum, and Fourier transform infrared spectrum. Their nonlinear optical limiting performance are measured by open aperture Z-scan method using a 8 ns pulsed Nd:YAG Laser (Quanta-Ray GCR-168) for 532 and 1064 nm, respectively. Details regarding the characterization methods, background of these 2D materials are presented in this Chapter.

2.1 Characterization

2.1.1 X-ray diffraction

X-ray crystallography is a well-known characterization technique used for identifying the atomic and molecular structure of a crystal, in which the crystalline atoms cause a beam of incident X-rays to diffract into many specific directions. By measuring the angles and intensities of these diffracted beams, a crystallographer can produce a three-dimensional image of the density of electrons within the crystal through by performing the inverse Fourier transform on the diffracted electronic signals. From this electron density, the mean positions of the atoms in the crystal can be determined. Additionally, chemical bonds, their disorder and various other information of the crystal are obtained. The atomic planes of a crystal cause an incident beam of X-rays to interfere with one another as they leave the crystal. The phenomenon is called X-ray diffraction. It also has many useful applications in many aspects.

Features of XRD

- XRD is a nondestructive technique
- To identify crystalline phases and orientation
- To determine structural properties: Lattice parameters (10-4Å), strain, grain size, epitaxy, phase composition, preferred orientation (Laue) order-disorder transformation, thermal expansion
- To measure thickness of thin films and multi-layers
- To determine atomic arrangement
- Detection limits: ~3% in a two phase mixture; can be ~0.1% with synchrotron radiation

XRD diffraction measurements of the samples presented in this thesis are

carried out using a Rigaku automated multipurpose Smartlab X-ray diffractometer (XRD: Rigaku Corp., Tokyu, Japan). The digital image of the equipment is shown in Fig. 2.1.

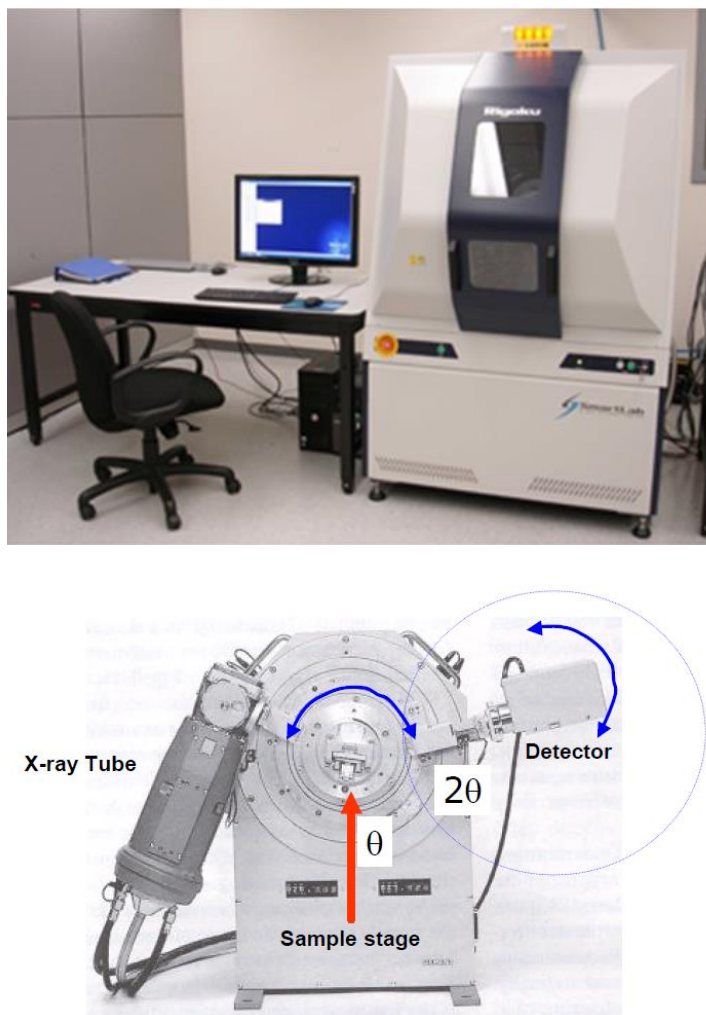


Fig. 2.1 Digital images of the Rigaku automated multipurpose Smartlab X-ray diffractometer.

2.1.2 Absorption and transmittance spectrum

Ultraviolet–visible spectroscopy or ultraviolet-visible spectrophotometry (UV-Vis or UV/Vis) refers to absorption spectroscopy or reflectance spectroscopy in the ultraviolet-visible spectral region. This means its operational waveband ranged

from near-UV and near-infrared [NIR]. The absorption or reflectance in the visible range directly affects the perceived color of the chemicals involved. In this region of the electromagnetic spectrum, molecules undergo electronic transitions. This technique is complementary to fluorescence spectroscopy, in that fluorescence deals with transitions from the excited state to the ground state, while absorption measures transitions from the ground state to the excited state.

The method is most often used in a quantitative way to determine concentrations of an absorbing species in solution, using the Beer-Lambert law:

$$A = \epsilon * L * c \quad (2-1)$$

Where A is the measured absorbance intensity of the incident light at a given wavelength, L the path length through the sample, and c the concentration of the absorbing species. For each species and wavelength, ϵ is a constant known as the molar absorptivity or extinction coefficient.



Fig. 2.2 Digital image of the Ultraviolet-visible spectrophotometer.

2.1.3 Fourier transform infrared spectroscopy

Fourier transform infrared spectroscopy (FTIR) is a technique which is used to obtain an infrared spectrum of absorption or emission of a solid, liquid or gas. An FTIR spectrometer simultaneously collects high spectral resolution data over a wide spectral range. This confers a significant advantage over a dispersive spectrometer which measures intensity over a narrow range of wavelengths at a time. This is a technique used to measure the samples absorption spectrum in the infrared range. Its absorption peaks are corresponding to the molecular vibrations of the functional groups. In our work, FTIR spectra of WS₂ nanosheets collected by different centrifugation speed were recorded using a VERTEX 70 spectroscopy which is presented in Fig. 2.3.

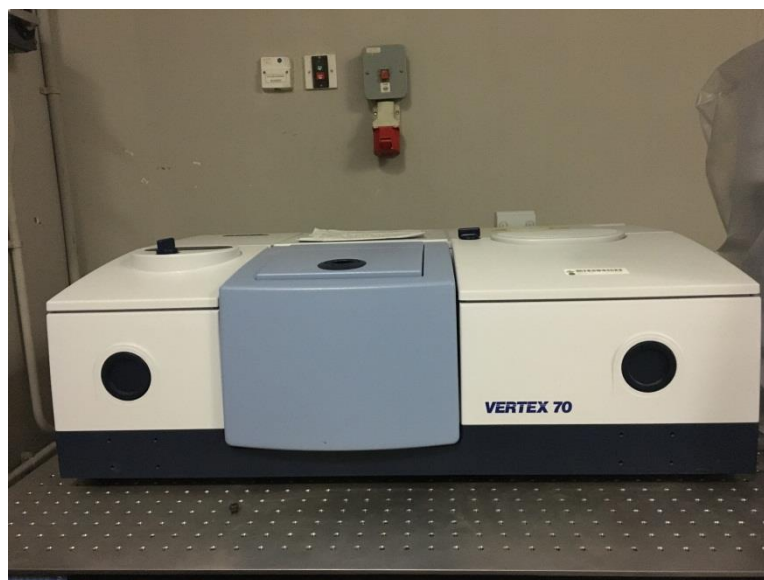


Fig. 2.3 Digital image of the Fourier transform infrared spectrophotometer.

2.1.4 Photoluminescence spectra

Photoluminescence (abbreviated as PL) is light emission from any form of matter after the absorption of photons (electromagnetic radiation). It is one of many forms of luminescence (light emission) and is initiated by photoexcitation. Following

excitation various relaxation processes typically occur in which other photons are re-radiated. Time periods between absorption and emission may vary: ranging from short femtosecond-regime for emission involving free-carrier plasma in inorganic semiconductors up to milliseconds for phosphorescent processes in molecular systems; and under special circumstances delay of emission may even span to minutes or hours.

All excitation and emission spectra of two dimensional materials nanosheets and quantum dots were obtained using an Edinburgh Instruments FLS920 Steady-State shown in Fig. 2.4. All measurements are performed at room temperature.



Fig. 2.4 Digital image of the photoluminescence spectrophotometer.

2.1.5 Raman spectrum

Raman spectroscopy is a spectroscopic technique used to observe vibrational,

rotational and other low frequency modes of the two dimensional materials. Raman spectroscopy is commonly used in chemistry to provide a fingerprint by which molecules can be identified. The laser light can interact with the molecular vibrations and cause the energy of laser photons being shifted up or down, and the information about the materials can be obtained through measuring the energy shift. Raman spectrum can also be used to determine the phonon energy of two dimensional materials. In this PhD study, all the Raman spectra were measured using a HORIBA Jobin Yvon HR800 Raman spectrometer with a 488 nm laser excitation source which is shown in Fig. 2.5.



Fig. 2.5 Digital image of the Raman spectrophotometer.

2.1.6 Atom force microscopy

Atomic Force Microscopy (AFM) provides nanoscale 3D image of the material surface, it is an important method to analyze the surface of materials. The working

principle is shown in Fig. 2.6. The AFM consists of a cantilever with a sharp tip at its end which is used to scan the specimen surface. When the tip is brought into proximity of a sample surface, forces between the tip and the sample lead to a deflection of the cantilever.

It has three modes of measurement, contact mode, tapping mode and non-contact mode. Among them, tapping mode is most common. For this mode of operation, the probe slightly taps on the sample surface during scanning, contacting the surface at the bottom of its swing. This mode has many advantages, including overcome problems associated with friction, adhesion and so on. The AFM images of graphene oxide presented in this thesis was carried out using a Bruker Nanoscope 8 atomic force microscope.

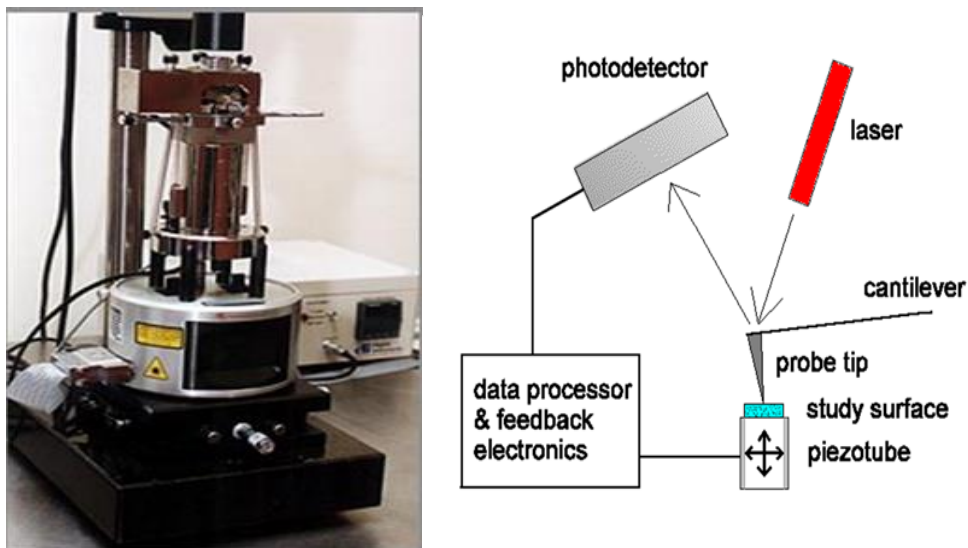


Fig. 2.6 Digital image of scanning probe microscope nanoscope IV.

2.1.7 Transmission Electron Microscopy

Transmission Electron Microscopy (TEM) is an effective way to characterize the morphology and structure of materials. The principle is that a beam of electrons

from the electron gun interact with the materials when they pass through the specimen, and the image is formed from the interacted electrons transmitted through the specimen. TEM/HRTEM images and electron diffraction patterns presented in this thesis were obtained by a JEOL Model JEM-2100F transmission electron microscope which is shown in Fig.2.7.

The uniqueness of TEM is the ability to obtain full morphological (grain size, grain boundary and interface, secondary phase and distribution, defects and their nature, etc.), crystallographic, atomic structural and microanalytical such as chemical composition, bonding (distance and angle), electronic structure, coordination number data from the sample.

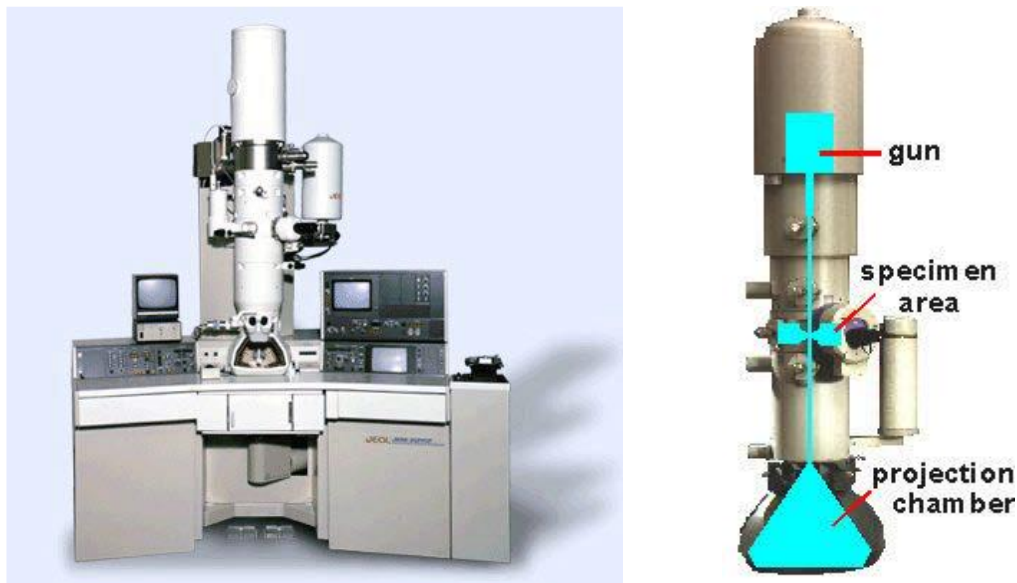


Fig. 2.7 Digital image of Transmission electron microscopy.

2.1.8 Scanning Electron Microscopy

Scanning electron microscopy (SEM) technique uses a focused beam of high-energy electrons to generate a variety of signals at the surface of solid specimens. The accelerated electrons in an SEM carry significant amounts of kinetic

energy, and this energy is dissipated as a variety of signals produced by electron-sample interactions when the incident electrons are decelerated in the solid sample. These signals include secondary electrons (that produce SEM images), backscattered electrons (BSE), diffracted backscattered electrons (EBSD that are used to determine crystal structures and orientations of minerals), photons (characteristic X-rays that are used for elemental analysis and continuum X-rays), visible light (cathodo-luminescence-CL), and heat. Secondary electrons and backscattered electrons are commonly used for imaging samples. SEM analysis is considered to be “non-destructive”; that is, X-rays generated by electron interactions do not lead to volume loss of the sample, so it is possible to analyze the same materials repeatedly.

With regarding to the field emission SEM (FESEM), it has several advantages compared to SEM as following:

- ◆ FESEM produces clearer, less electro statically distorted images with spatial resolution down to 1-0.5 nm. That’s 3 to 6 times better than conventional SEM.

- ◆ Smaller-area contamination spots can be examined at electron accelerating voltages compatible with Energy Dispersive X-ray Spectroscopy.

- ◆ Reduced penetration of low kinetic energy electrons probes closer to the immediate material surface.

- ◆ High quality, low voltage images are obtained with negligible electrical charging of samples. (Accelerating voltages range from 0.5 to 30 kV.)

◆Need for placing conducting coatings on insulating materials is virtually eliminated.

◆For ultra-high magnification imaging, can use, eg, In-lens FESEM.

The structure and composition of GO-APTES doped gel glasses presented in this thesis were investigated using a JEOL Model JSM-6490 scanning electron microscope (SEM) equipped with an energy dispersive X-ray spectroscopy detector. Gold was previously coated on the sample surface to create the clear image.



Fig. 2.8 Digital image of Scanning electron microscopy.

2.1.9 Nonlinear optical properties

The nonlinear optical properties of MoS₂/PMMA, WS₂/PMMA, WS₂QD/PMMA composites are measured through Nd: YAG solid state lasers. The digital image of Nd: YAG laser system is shown in Fig. 2.9a. In this Ph.D study, those composites were investigated using a 8 ns laser pulses from a Nd:YAG laser at a repetition of 10 Hz. The energy densities in front of and behind the sample were measured by an energy detector. In chapter 3 and 5, the pulse energies are ~2000 μ J corresponding to the laser intensity of 8.9 GW/cm² and 28 GW/cm² at the laser focal

point for 532 and 1064 nm, respectively. In chapter 4, four different energy densities were used to irradiate the suspension, 0.05 J/cm², 0.10 J/cm², 0.16 J/cm², 0.28 J/cm² for 532 nm wavelength. Three different energy densities were used to irradiate the suspension, 0.77 J/cm², 3.35 J/cm², 3.72 J/cm² for 1064 nm wavelength. The pulse energies in front of and behind the sample were measured by an energy detector. All the measurements were operated at room temperature. The experimental setup for Z-scan measurement is also shown in Fig. 2.9a. Samples move along the Z-direction.

2.2 Theoretical calculations

2.2.1 Two photon absorption theory

Due to the novelty of two-dimensional materials, there are not much papers discuss the exact details mechanism of the NLO properties of these two dimensional materials. Two major mechanisms were proposed to explain the optical limiting properties of 2D materials including nonlinear scattering and nonlinear absorption. For the nonlinear scattering, the high input laser intensity is scattered into different direction, therefore, a reduction of the transmitted light intensity is observed. The effective scattering center comes from the generation of solvent bubbles, ionization of nanoparticles and the refractive index discontinuity due to the thermal effect of the solvents surrounding the nanosheets. It is believed that it is possible to happen within 2D materials incorporate within the solution. We believe the nonlinear scattering within our solid state matrix should be very weak. The nonlinear absorption should be the dominant mechanism for the optical limiting properties observed in our solid state samples. The optical limiting properties can be explained two-photon or multiple-photon absorption. The bandgap of monolayer of MoS₂ or WS₂ is nearly 2.0

eV. The bandgap of our sample is about 1.7 eV. Therefore, as illustrated in the Fig. 3b, the energy of one 1064 nm photon is not enough to excite the electron from the valence band to conductive band and leads to high optical transmission under low input intensity. However, when the input intensity is getting high the electron from the ground state can be promoted to a virtual intermediate state, follow the absorption of a second 1064 nm photon that takes the electron to the conduction band. Since the intermediate state for such transitions is virtual, energy need not be conserved in the intermediate state but only in the final state. Under the high laser irradiation, these two or multiples photon absorption will become dominant. This two photon absorption of our two dimensional nanosheets can be strong due to their unique bandgap structure and broad absorption band as shown in Fig. 3. The prepared nanosheets have high surface area to volume ratio and more dangling bonds on the surface leading to the more exposed free active edges that can benefit for the TPA process [27]. Also, the impurity in the nanosheets can become the sub-bandgap that broaden its absorption spectrum which is favourable to the TPA process [28].

Two-photon absorption is the simultaneous absorption of two photons of identical or different frequencies in order to excite a molecule from one state (usually the ground state) to a higher energy electronic state which is illustrated in Fig.2.10. The energy difference between the involved lower and upper states of the molecule is equal to the sum of the energies of the two photons. Graphite and transition metal sulfide (TMDs, the formula MX_2 , wherein M represents a transition metal, X represents a sulfur group elements) are all two-dimensional layered bulk materials. When changing from block to single layer, they exhibit changes of properties e.g. the bandgap structure. However, the band structure of graphene and TMDs materials are

very different. Graphene has zero energy bandgap as shown in Fig.2.11. Compared with conventional carbon materials, such as carbon nanotube, carbon black [29, 33,

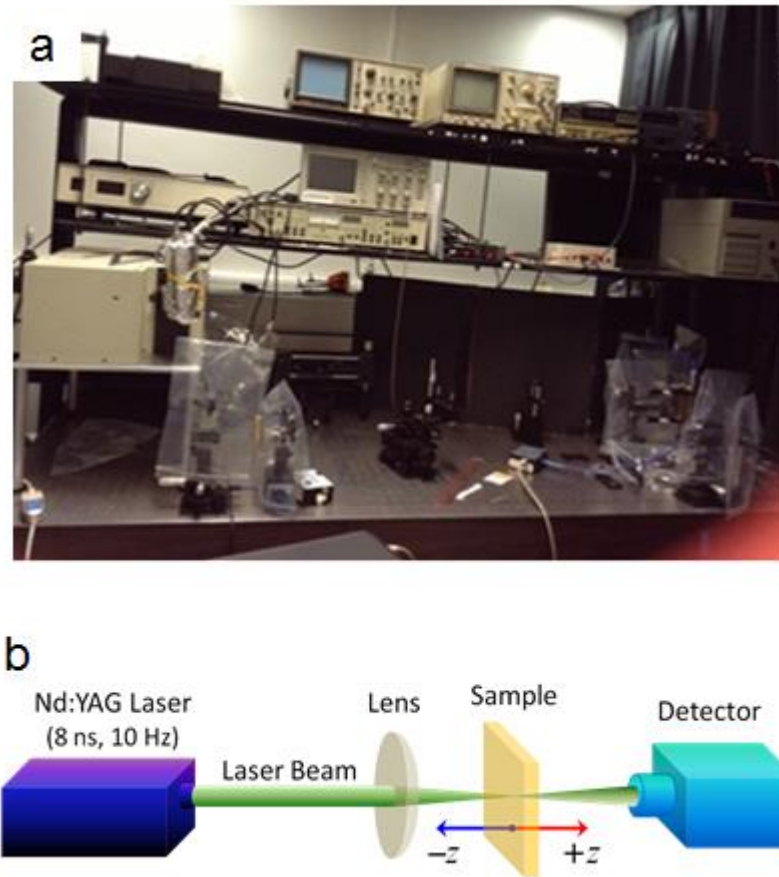


Fig. 2.9 Digital image of Nd:YAG laser system (a) and the experimental setup for Z-scan measurement (b).

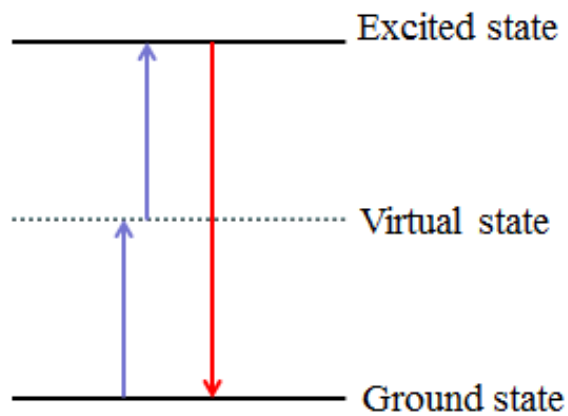


Fig. 2.10 Energy scheme of a two photon excitation up conversion process.

53, 54] graphene exhibits a lower threshold of nonlinearity, and strong optical limiting effects. Graphene has uniform and weak absorption rates in the visible and near infrared spectrum, which lead to the high linear transmittance. As for the graphene oxide, its band gap becomes larger showing in Fig.2.12, however, its absorption is stronger in the ultraviolet and weak in visible spectrum, resulting in low near-infrared two-photon absorption efficiency, therefore, its application in near-infrared region is limited. Some of the two-dimensional transition metal dichalcogenide materials are semiconductors, their band gaps range from 0.2 eV (6199 nm) to ~ 2 eV (~ 620 nm), so that TMDs materials can be used for fabricating broadband optical devices. As shown in the Fig. 2.13, MoS₂ has weak absorption at the wavelength which is larger than its bandgap such as 808 nm, 980 nm and 1064 nm and other commonly used high-power near infrared laser, so it has a high linear transmittance at near infrared. However, it has a high two-photon absorption effect, ensuring the high optical limiting linear transmittance and high nonlinear absorption effects. The potentially sensitive optical limiting wavelength range of those TMDs materials are 700 nm-1300 nm, it has low single photon absorption and a relatively high two-photon absorption. According to the literature and experimental data

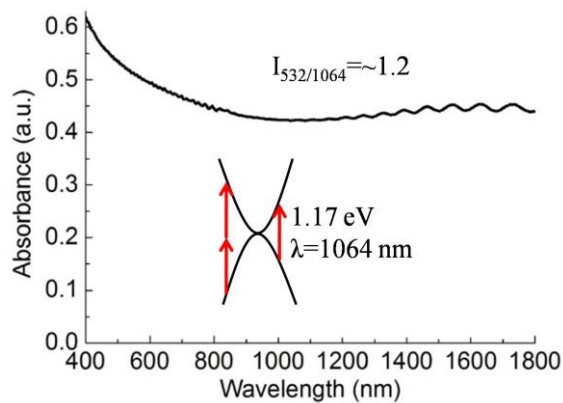


Fig. 2.11 Absorption spectra of graphene and its band gap structure [55].

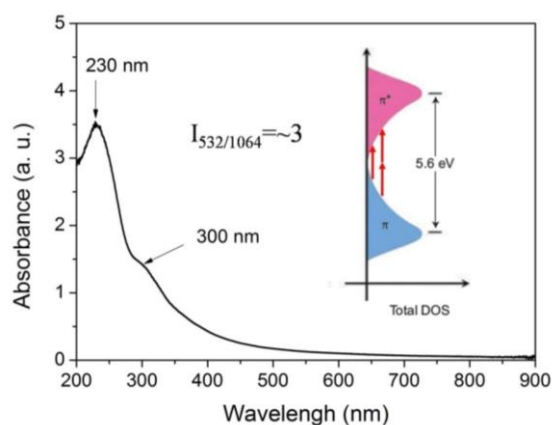


Fig. 2.12 Absorption spectra of graphene oxide and its band gap structure, the absorption at 1064 nm refer to [56].

obtained in this thesis, graphene, graphene oxide, MoS₂ and WS₂ absorbance at 532 nm and 1064 nm intensity ratio at about 1.2, 3, 14 and 5, respectively, which can be seen in Fig. 2.11-2.14. Compared with graphene and graphene oxide, TMDs materials MoS₂ WS₂ based on the 1064 nm laser at low power density can have a high linear transmittance, but has a strong two-photon absorption at high power density shown by experimental data.

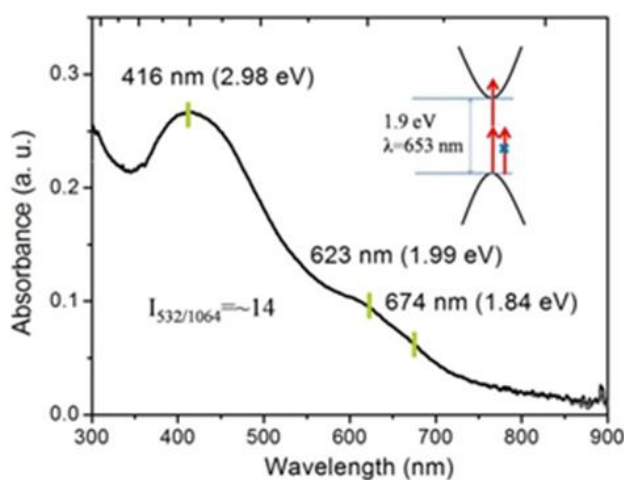


Fig. 2.13 Absorption spectra of MoS₂ nanosheet and its band gap structure, the absorption at 1064 nm refer to [57].

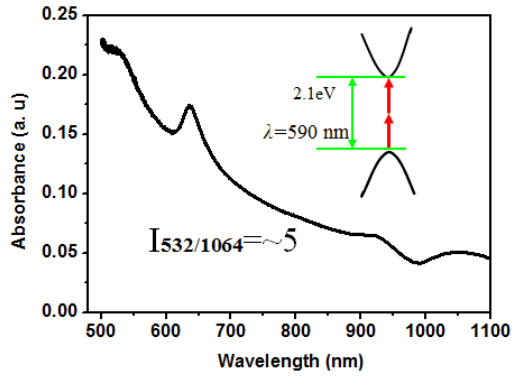


Fig. 2.14 Absorption spectra of WS₂ nanosheets and its band gap structure.

2.2.2 The minimal enthalpy of mixing solution

Some common solvents have been used for the effective exfoliation of layered materials by sonication method. With the surface energy of the solvent being well matched with that of the layered material, the energy required for exfoliation is minimized [38]. In this thesis, some solutions, *eg*, 1-Methyl-2-pyrrolidone (NMP) and water ethanol mixture, are selected as solvent for sonication of the TMDs materials bulk.

The solubility of non-polar solute in non-polar solvent will depend on their mixing enthalpy. Minimizing the mixing enthalpy would give the best solvent for the solute [58, 59]. In other words, minimizing the difference in surface energy of non-polar solvent and solute would give the best solvent for solute.

With Gibb's Free Energy, G , and Enthalpy, H , the surface tension γ could be expressed as below [60].

$$\gamma = \left(\frac{\partial G}{\partial A} \right)_{T,P,N} = \left(\frac{\partial H}{\partial A} \right)_{T,P,N} - T \left(\frac{\partial S}{\partial A} \right)_{T,P,N} \quad (2-2)$$

$$-\left(\frac{\partial \gamma}{\partial T} \right)_A = S_A \quad (2-3)$$

where $\left(\frac{\partial S}{\partial A}\right)_{T,P,N} = S_A$ is the surface entropy and $\left(\frac{\partial H}{\partial A}\right)_{T,P,N} = E_{\text{Surface}}$ is the

surface energy. The S_A could be determined experimentally with equation 2 by measuring the change of surface tension with respect to temperature.

$$\gamma = E_{\text{Surface}} - TS_A \quad (2-4)$$

Equation 2-2 is then rewritten as equation 2-4 and it implies that the surface energy E_{Surface} could be estimated from sum of surface tension and entropy energy. The surface tension of solution does not change much with respect to temperature [61, 62]. Hence, the dimensionless surface tension σ^* could be given as a temperature independent equation below.

$$\sigma^* = \frac{\sigma_{\text{water}} - \sigma_{\text{Mixture}}}{\sigma_{\text{water}} - \sigma_{\text{Alcohol}}} = \frac{1 + a(1 - x_{\text{Alcohol}})}{1 - b(1 - x_{\text{Alcohol}})} x_{\text{Alcohol}} \quad (2-5)$$

where σ_{water} is the pure water surface tension, σ_{Alcohol} is the pure alcohol surface tension, σ_{Mixture} is the surface tension of solutions mixture, x_{Alcohol} is the mole fraction of alcohol, constant a, b are fitting parameters.

CHAPTER 3

MoS₂ Nanosheet Preparation And MoS₂/PMMA Composite For Nonlinear Optical Application

3.1 Introduction

Due to the relatively weak van der Waals (VDW) force between interlayers, few-layer MoS₂ nanosheets are prepared using simple ultrasonic exfoliation method and incorporated in PMMA. The good nonlinear optical (NLO) property of the MoS₂/PMMA composite for the nanosecond pulsed laser at both 532 and 1064 nm has been first reported. The size, thickness and atomic structure of MoS₂ nanosheets have been characterized by transmission electron microscopy (TEM) and atomic force microscopy (AFM). The interesting dependence of interlayer separation with respect to the layer number of MoS₂ has been successfully quantified. The average interlayer separation of the MoS₂ nanosheets increases and deviates much from the theoretical value of 0.31 nm with reducing the layer number. Such few-layer MoS₂ nanosheets have been homogeneously incorporated into solid-state PMMA, which shows low optical limiting thresholds, 0.4 and 1.3 J/cm², low limiting differential transmittance (T_C), 2% and 3% for the nanosecond laser operating at 532 nm and 1064 nm, respectively. The results suggest that MoS₂ nanosheets incorporated PMMA is a promising candidate of solid NLO material for optical limiting

application.

Recently, thin two-dimensional (2D) layer materials such as graphene, [34, 63, 64] hexagonal boron nitride (h-BN) [65, 66], and layer transition metal dichalcogenides (LTMDs) [29, 38, 67 - 69] have attracted substantial attention due to their favorable electrical and optical properties. MoS₂ is one type of LTMDs materials with a sandwiched consisted of an atomic plane of molybdenum between two atomic planes of sulfur. The distance between the neighbouring S-Mo-S layers is 0.62 nm [70], much larger than that of the carbon layers (0.34 nm) in graphite [71], leading to weaker van der Waals (VDW) force between inter-layers. This makes thin layer MoS₂ sheet easier to be separated from bulk MoS₂. Various physical and chemical methods such as mechanical cleavage [70, 72 - 74], electrochemical Li-intercalation exfoliation [57, 75], and ultrasonic exfoliation [19, 76] have been developed for this purpose. Among these methods, ultrasonic exfoliation has been employed in this research due to its relatively simple and scalable feature.

It has been demonstrated that the energy band structure of MoS₂ changes from indirect to direct bandgap owing to the electron motion confinement and the absence of interlayer perturbation in monolayer MoS₂ when it is thinned from bulk to monolayer, resulting in the emergence of the characteristic absorption peaks which can not be observed in the bulk MoS₂ and also a great improvement of photoluminescence [57, 74, 77]. Such interesting optical transition has attracted much attention, and the electrical and photoluminescence properties of thin MoS₂ have been studied extensively [74, 78 - 80]. However, there has been not much research work done on its nonlinear optical (NLO) properties up to now, except for the ultrafast saturable absorption property of few-layer MoS₂ reported by K. P. Wang

et al [39] and reverse saturable absorption of graphene/MoS₂ composite at 532 nm reported by Q. Y. Ouyang *et al* [81]. Nowadays, high energy Q-switched nanosecond lasers operating at 1064 nm and frequency doubled into 532 nm are readily available and very popular for various commercial, industrial and military applications. Therefore, it becomes critically emergent and significant to explore novel and excellent NLO materials capable of protecting human eyes, detectors, sensors and cameras from high power laser damage for these laser systems. Few-layer MoS₂ shows strong absorption at 266 nm and 532 nm, indicating the high chance of two-photon absorption (TPA) at 532 nm (half the energy of 266 nm) and 1064 nm (half the energy of 532 nm). Thus, MoS₂ can be potentially better optical limiter for its high transmission at low intensity and high absorption for its TPA at high pumping intensity for most of commercially available high power laser operating around 1 μm and its frequency doubled wavelength around 0.5 μm, e.g., Yb fiber laser and Nd:YAG crystal lasers [82 - 86].

Currently, NLO properties of 2D carbon materials such as graphene, graphene oxide (GO) and reduced graphene oxide (RGO) are being studied intensively [87 - 89]. GO is usually obtained from graphite by using Hummer's method. In detail, the graphite is pretreated with a lot of strong oxidant, such as KMnO₄, concentrated H₂SO₄, H₂O₂ and so on, to decrease the connection between the carbon layers, and followed by ultrasonic treatment, to finally obtain the resultant thin GO sheets [90, 91]. RGO is prepared by reducing the GO with reductants such as NaBH₄ and N₂H₄ [88], however, the fabrication processes are complicated, dangerous and unfriendly to the environment. Graphene sheets can be obtained from graphite just by ultrasonic exfoliation method [92]. Considering the much larger interlayer distance of MoS₂

than graphite, the thin MoS₂ sheets can be obtained more easily through the simple ultrasonic exfoliation method. Therefore, it is very meaningful to explore NLO properties of these thin MoS₂ sheets and its potential photonic applications. Optical limiters can be in liquid or solid form, but the liquid based has very limited practical use due to its high rate of evaporation and contamination, leakage caused by container damage, high losses originating from the refractive index mismatch between the liquid and solid interfaces, relatively easy aggregation as well as the lack of flexibility and stability. Thin film based optical limiters have very short absorption length and easy to be damaged. Therefore, it is better to incorporate the NLO materials into bulk solid state optical matrix so as to stabilize and isolate it from outside environment, which offers more advantages e.g., withstanding higher optical power, avoiding aggregation and well suitable for producing commercial photonics products.

In this chapter, we incorporate few-layer MoS₂ in solid PMMA matrix to isolate it from outside environment and avoid the oxidization. The fabricated MoS₂/PMMA composite shows good NLO properties. To our best knowledge, there has been no report on this so far. The few-layer MoS₂ nanosheets are obtained through ultrasonic exfoliation of the powder synthesized by hydrothermal method in advance. Transmission electron microscopy (TEM) and atomic force microscopy (AFM) results indicate that the prepared MoS₂ sheets are very thin (<5 layers), and an interesting phenomenon is found that the interlayer separation depends a lot on the layer number. The few-layer MoS₂ nanosheets are well homogeneously incorporated in PMMA matrix without any complicated functionalization like graphene [93]. PMMA is a good optical host material with advantages such as high optical

transparency, excellent mechanical property, low cost, moldable and so on, and more significantly, it shows good and stable NLO property, demonstrating its great potential acting as a novel NLO material for optical limiting application.

3.2 Experimental section

Hydrothermal preparation of MoS₂ powder has been previously reported using (NH₄)₂MoS₄ as raw material [94]. In detail, Na₂MoO₄·H₂O (0.3 g) and CS(NH₂)₂ (0.4 g) were dissolved in DI water (30 mL) under vigorous stirring, followed by transferring the transparent solution to a 50-mL-capacity Teflon autoclave and keeping it at 240 °C for 24 hours. After hydrothermal process, the formed black suspension was centrifuged and washed with DI water several times and dried at 60 °C in vacuum. Finally, black MoS₂ crystalline powder was obtained.

Few-layer MoS₂ nanosheets were first obtained by ultrasonic exfoliation method. MoS₂ (16 mg) powder was dispersed in N-methyl-2 pyrrolidone (NMP, C₅H₉NO, 80 mL) under vigorous stirring, followed by ultrasonic treatment for 18 h, and then the suspension was centrifuged at 3000 rpm for 20 min to remove the thick MoS₂ nanosheets. The left MoS₂ suspension was kept for incorporation into PMMA. MMA (20 mL) and MoS₂ suspension were first mixed and heated at 75 °C for 10 min, and then BPO (0.023 g) was added and heated at 75 °C for another 10 min. Followed by heat treatment at 105 °C for 20 min. Finally, it was kept at 75 °C for 30 h and solid transparent MoS₂/PMMA was obtained. The incorporated MoS₂ concentrations in our experiment MoS₂/PMMA-1 and MoS₂/PMMA-2 are about 0.008 mg/cm³ and 0.016 mg/cm³, respectively.

3.3 Structure and morphology of MoS₂ nanosheet

We have developed a hydrothermal method to prepare MoS₂ bulk and using ultra-sonication process to exfoliate bulk into few layered nanosheets. Then MoS₂ nanosheet is embedded into solid state matrix PMMA to investigate its nonlinear optical property. Its structure and morphology has been characterized by XRD, TEM, EDS and AFM. Due to the relatively weak van der Waals (VDW) force between interlayers, few-layer MoS₂ nanosheets are prepared using simple ultrasonic exfoliation method and incorporated in PMMA. The good nonlinear optical (NLO) property of the MoS₂/PMMA composite for the nanosecond pulsed laser at both 532 and 1064 nm has been first reported. The size, thickness and atomic structure of MoS₂ nanosheets have been characterized by transmission electron microscopy (TEM) and atomic force microscopy (AFM). The interesting dependence of interlayer separation with respect to the layer number of MoS₂ has been successfully quantified. The average interlayer separation of the MoS₂ nanosheets increases and deviates much from the theoretical value of 0.31 nm with reducing the layer number. Such few-layer MoS₂ nanosheets have been homogeneously incorporated into solid-state PMMA, which shows low optical limiting thresholds, 0.4 and 1.3 J/cm², low limiting differential transmittance (T_C), 2% and 3% for the nanosecond laser operating at 532 nm and 1064 nm, respectively. The results suggest that MoS₂ nanosheets incorporated PMMA is a promising candidate of solid NLO material for optical limiting application.

3.3.1 XRD, TEM and EDS of MoS₂ nanosheet

Fig. 3.1a shows the X-ray diffraction pattern of the MoS₂ prepared by hydrothermal method, which is black powder as shown in the inset. The diffraction peaks located at $2\theta = 14^\circ, 33^\circ, 40^\circ, 50^\circ, 59^\circ$ correspond to the planes of (002), (100),

(103), (105) and (110), respectively, agreeing well with the hexagonal MoS₂ (JCPDS card No. 37-1492). Fig.3.1b displays the TEM image of the MoS₂ obtained through hydrothermal method, with the flake size of around 200 nm. From the HRTEM image (Fig.3.1c), it can be found that the obtained MoS₂ nanosheet is ~16 layers thick, and the interlayer separation is determined to be 0.62 nm, identical to the theoretical layer distance along the c-axis direction [70]. The selected area electron diffraction (SAED) pattern of the MoS₂ nanosheet is presented in Fig.3.1c inset that reveals the hexagonal lattice structure and well stacked single crystal layer feature, with the mark of the diffraction points ascribed to the (100) and (110) planes. Fig.3.1d shows the SEM image of MoS₂ powder bought from Aladdin-Reagent Company, showing its flake size of several micrometers, much larger than the MoS₂ sheets obtained through hydrothermal method. The large size starting material is unfavourable to obtaining thin MoS₂ nanosheets through ultrasonic exfoliation, which has been confirmed by the K. P. Wang *et al* [39]. In their work, MoS₂ sheets with large size (hundreds of nanometers) and thickness (dozens of nanometers) were obtained from large commercial MoS₂ powder as starting material. It is well known that the thinner MoS₂ is, the stronger optical response will be obtained [27, 78]. And, moreover, the MoS₂ sheets need to be small enough for a perfect dispersion in liquid and solid matrix aiming to minimize the optical scattering losses. Therefore, using small raw MoS₂ powder prepared through hydrothermal method has the edge over using large commercially available MoS₂.

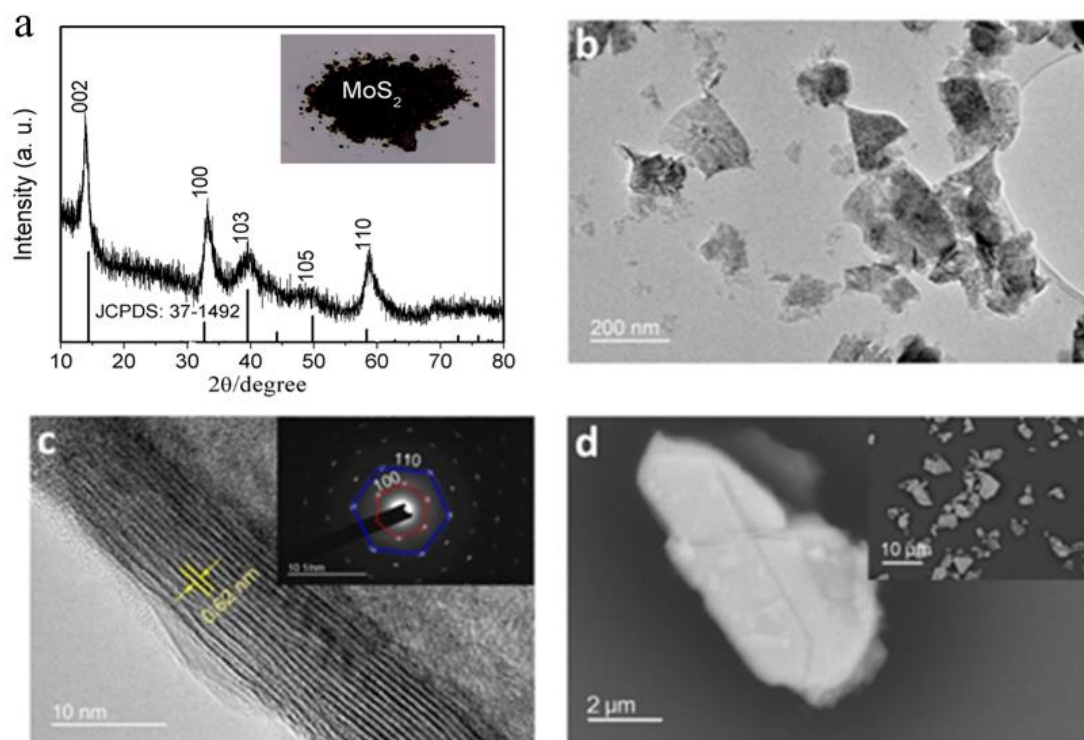


Fig. 3.1 (a) XRD pattern, (b) TEM and (c) HRTEM images of as-prepared MoS₂. Inset of (a) is the digital photo of MoS₂ powder. Inset of (c) is the SAED pattern of the MoS₂ sheet. (d) SEM image of the commercial MoS₂ bought from Aladdin-Reagent Company. Inset is the SEM image with lower magnification.

As is well known, the connection between the S-Mo-S layers is weak VDW force, making it easy to be separated. In this study, few-layer MoS₂ is obtained by employing ultrasonic exfoliation method. Fig. 3.2a shows the TEM image of the MoS₂ nanosheets after 18 h ultrasonic treatment, demonstrating obtained MoS₂ below 100 nm. As analyzed from the SAED pattern given in Fig. 3.2a inset, the multi-group hexagonal diffraction points with a certain angle misplace indicate that the MoS₂ sheets consist of several few-layer single crystal MoS₂ stacked in different orientations. The elemental composition of the sheets is confirmed by energy dispersive spectrometer (EDS) result shown in Fig. 3.2b, and the Cu peak recorded is due to the copper mesh support for measurement.

It has been recognized as a common method to determine the layer number of 2D layer material from the HRTEM image of the folded edge. [95, 96] As directly evidenced from the folded edge in Fig. 3.2c, the obtained MoS₂ nanosheets through 18 h ultrasonic exfoliation contains three layers. Fig. 3. 2d shows the HRTEM image

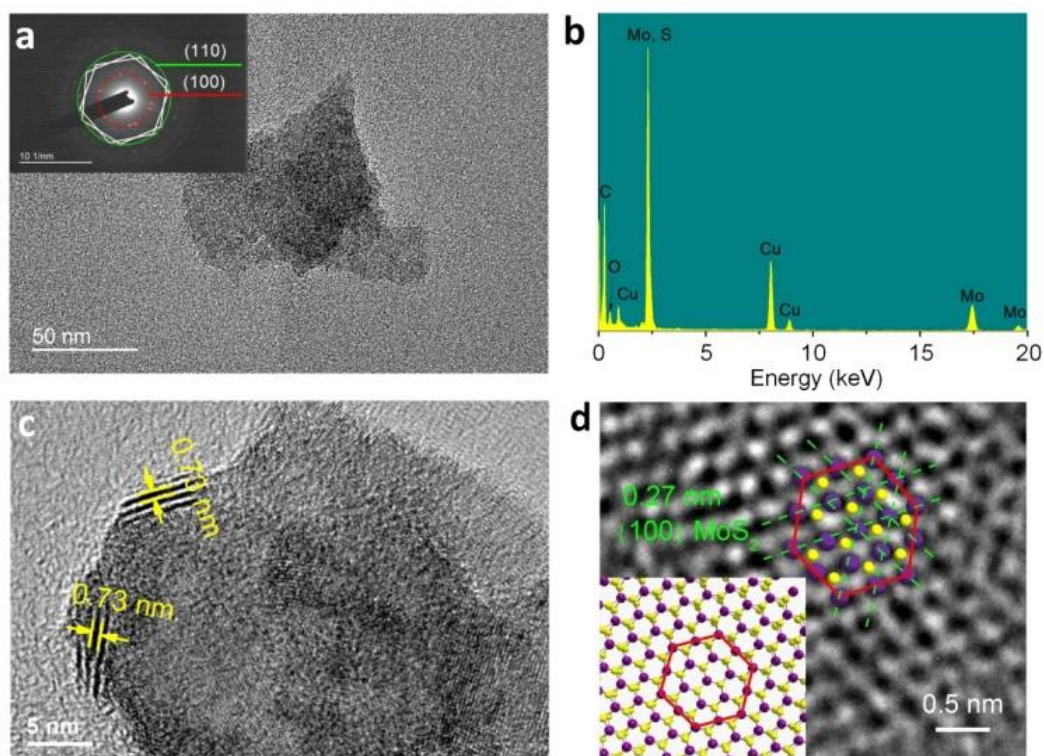


Fig. 3.2.(a) Low-magnification TEM image of MoS₂ nanosheets obtained after ultrasonic exfoliation, inset shows the SAED pattern. (b) EDS spectrum of MoS₂ nanosheets. (c) HRTEM image showing layer information of the MoS₂ sheets. (d) HRTEM image indicating atomic structure of MoS₂, inset illustrates the schematic structure with yellow and purple balls corresponding to S and Mo atoms, respectively.

of MoS₂ at the atomic scale, the large black points are Mo atoms and the small black points are S atoms; they are marked by purple balls for Mo atoms and yellow balls for S atoms, respectively. The 0.27 nm interplane distance matches well with the

(110) planes, indicating a top view through c-axis direction. As shown in Fig. 3.2d inset, the corresponding atomic structural model viewing through c-axis direction can foster deep understanding of the MoS₂ structure indicated by the high resolution TEM image.

3.3.2 AFM of MoS₂ nanosheet

Fig. 3.3a shows the 2D AFM topographical image of the MoS₂ nanosheets with thickness below several nanometers obtained after 18h ultrasonic exfoliation, confirming again the successful preparation of thin MoS₂ nanosheets through ultrasonic treatment. With clearly observable difference of thickness, the layer number is definitely labelled in the stepped height-type AFM image (Fig3.3b). In order to precisely analyze the thickness of the areas with different colours, the height profiles of the sections marked in Fig. 3.3b are plotted in Fig. 3.3c, with the precise thickness given in it. In fact, the measured thickness of MoS₂ is a summation of three contributions: the distance from MoS₂ to the substrate (D), the height of S-Mo-S layers (L) and the interlayer separations (S). Taking the bi-layer MoS₂ for an example, the measured thickness equals to $D+2L+S$, where L is 3.08 Å [70], and D is determined to be 4.03 Å according to the measured thickness of monolayer MoS₂. And then, the interlayer separations of MoS₂ with different layers are obtained and plotted in Figure 3d. It is interesting to find that the interlayer separation is much closer to the theoretical value 0.31 nm [70] as the layer number increase, and much

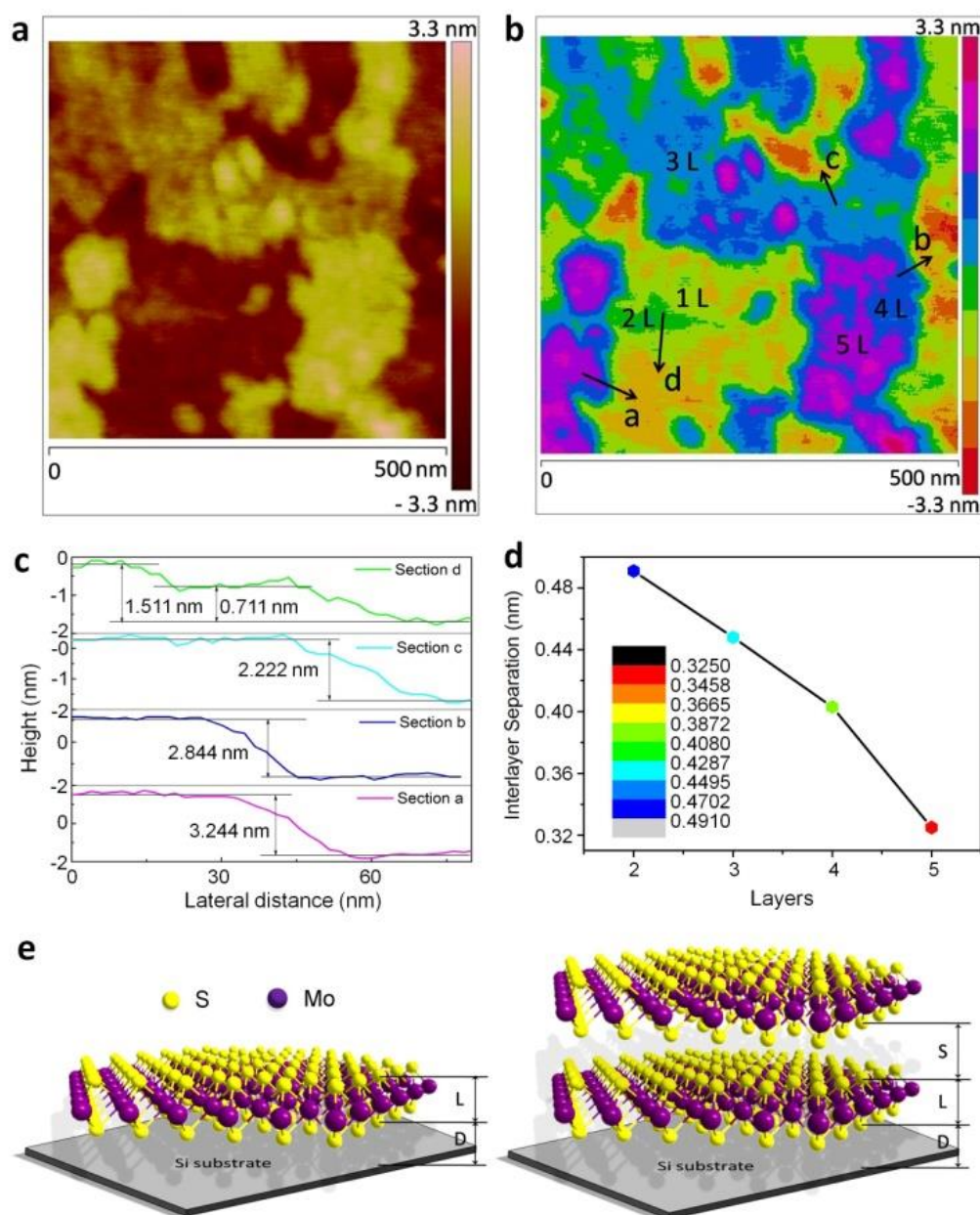


Fig. 3.3 (a) 2D topographical and (b) 2D stepped height-type AFM images of few-layer MoS₂ nanosheets. (c) Height profiles of the sections marked in (b). (d) Interlayer separation dependence on the layer number. (e) Schematic diagram of monolayer and double layer MoS₂ on Si substrate. (L: the thickness of S-Mo-S layer; D: the distance from MoS₂ to the substrate; S: the separation between the S-Mo-S layers.)

larger when it contains fewer layers. This is similar as the few-layer graphene reported by Y. X. Ni *et al* [97]. As the connection between the S-Mo-S layers comes from VDW force, the larger interlayer separation of thinner MoS₂ can be ascribed to the weaker attractive VDW force between the layers because of the fewer atoms, as well as the increased interlayer repulsive force due to the active edge effect of the smaller nanosheets[98, 99]. Fig. 3.3e shows the schematic structure of mono- and bi-layer MoS₂ sheet. For the monolayer MoS₂, the measured thickness is exactly the summation of the S-Mo-S bond distance (L) and the distance between MoS₂ and the substrate (D), as L is 3.08 Å and the D is variable. This explains why the thickness of single layer MoS₂ deviates largely in different works (i.e., changing from 0.5 to 0.9 nm) [24, 27, 70, 100].

3.3.3 Raman and PL of MoS₂ nanosheet

The Raman spectrum of the MoS₂ sheets obtained after 18 h ultrasonic exfoliation is given in Fig. 3.4a. The two characteristic vibration modes E_{2g}^1 (in-plane) and A_{1g} (out-of-plane) located at 384 and 410 cm⁻¹, respectively, are observed. The locations of these two peaks are in agreement with the few-layer MoS₂ reported [78]. The full-width-half-maximum (FWHM) of E_{2g}^1 and A_{1g} bands are calculated to be 10.2 and 7.4 cm⁻¹, respectively, much broader than other reported results [24, 27, 101]. It has been recognized widely that the locations of E_{2g}^1 and A_{1g} peaks of MoS₂ show a little shift with varying layers: E_{2g}^1 shifts to higher frequency while A_{1g} shifts to lower frequency for thinner MoS₂ [79, 101, 102]. Therefore, the broader FWHM of Raman spectrum also indicates the co-existence of MoS₂ nanosheets with different layers.

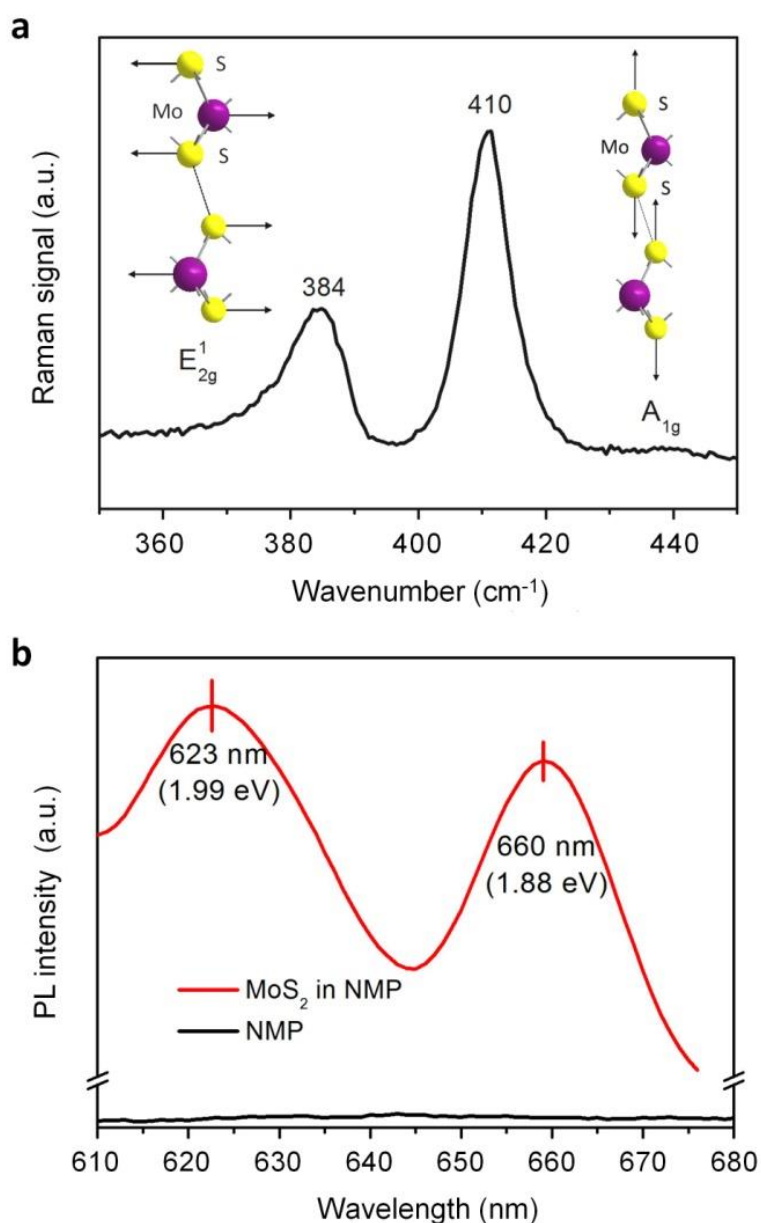


Fig. 3.4 (a) Raman spectrum and (b) Photoluminescence spectrum of MoS₂ nanosheets obtained after ultrasonic exfoliation. Insets of (a) show the schematic of the vibration modes at 384 cm⁻¹ (left) and 410 cm⁻¹ (right).

Fig. 3.4b shows the photoluminescence spectrum of MoS₂ in NMP under 532 nm excitation. The two characteristic emission peaks located at 623 and 660 nm are ascribed to the B and A direct excitonic transitions from the lowest conduction band to the highest spin-split valence band at the K-point of the Brillouin zone [27, 74],

respectively, indicating that the layer number of MoS₂ has been successfully reduced and it has become a direct gap semiconductor.

3.3.4 Absorption of MoS₂ nanosheet and MoS₂ /PMMA

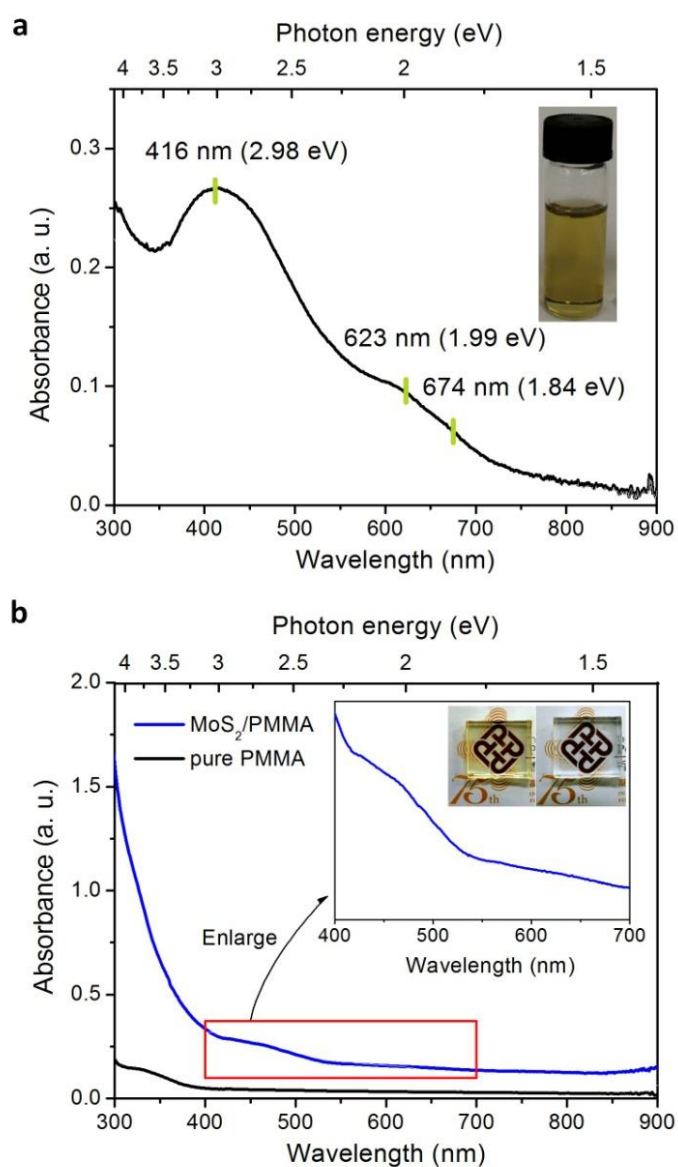


Fig. 3.5 (a) Absorption spectrum of the few layer MoS₂ suspension in NMP. Inset shows the digital photo of such sample. (b) Absorption spectra of pure PMMA and MoS₂/PMMA composite bulks. Insets show the enlarged absorption within 400-700 nm region, and digital photos of MoS₂/PMMA (left) and PMMA (right).

The absorption spectrum of the few-layer MoS₂ nanosheets suspension in NMP is shown in Fig. 3.5a. It can be observed that the two characteristic absorption peaks at 623 nm (1.99 eV) and 674 nm (1.84 eV) arise from direct transition from valence band to conduction band at the K-point of the Brillouin zone, known as the B and A transitions, respectively [39, 57, 68, 74], are recorded. Such two peaks with little energy difference is due to the spin-orbital splitting of the valence band [39, 74]. In addition, the broad absorption band centered at 416 nm (2.98 eV) arising from the complicated C and D transitions is also observed [39, 57, 76]. As shown in Fig.3.5a inset, the suspension shows the characteristic yellow-green color of few-layer MoS₂, similar to other reports [57, 76]. The above results have confirmed that few-layer MoS₂ nanosheets are obtained through ultrasonic exfoliation in this contribution, agreeing well with the above TEM and AFM analysis. The MoS₂ nanosheets have been incorporated in PMMA, the well-known organic optical glass, in order to realize various optical applications such as saturable absorber, optical limiter and so on. Fig. 3.5b gives the absorption spectra of pure PMMA and MoS₂/PMMA composite bulks, the characteristic absorption peaks between 400-700 nm corresponding to MoS₂ are recorded. And the homogeneous yellow-green colour (see Fig. 3.5b inset) indicates that MoS₂ has been not only successfully incorporated into PMMA matrix but also in a homogeneous dispersion.

3.4 Nonlinear optical property of MoS₂ /PMMA composite

Fig. 3.6a and Fig. 3.6b show the plots of output fluence F_{out} versus input fluence F_{in} for PMMA and MoS₂/PMMA composite bulks measured at 532 and 1064 nm, respectively. The ratio F_{out}/F_{in} in the limit of zero fluence gives the linear

transmittance (T_L), and the values are shown in Table 3-1. The measured results reveal that the transmittance of MoS₂/PMMA remains the same initially and then decreases with the increase of the input fluence at both 532 and 1064 nm, showing the typical feature of optical limiting materials. In contrast, only linear optical property observed in pure PMMA reveals that PMMA has no contribution to the NLO response of MoS₂/PMMA composite. The NLO onset threshold (F_{ON}) and optical limiting threshold (F_{OL} , defined as the input fluence point at which the normalized transmittance drops to 50%) are vital parameters to evaluate the NLO performance of a given material. Herein F_{ON} and F_{OL} values are determined and listed in Table 3-1. For the sample MoS₂/PMMA-2, F_{ON} are 0.01 J/cm² and 0.04 J/cm², and F_{OL} are 0.40 J/cm² and 1.30 J/cm² for MoS₂/PMMA at 532 nm and 1064 nm, respectively. Although these thresholds are higher than the single-layer graphene dispersion [34], they are much lower than or comparable to other NLO materials including few-layer graphene [53, 88, 103], graphene oxide [88, 90, 104, 105], reduced graphene oxide [105], carbon nanotube [88, 106 - 108] and various metal nanostructures [109 - 111]. At high input fluence, the slope dF_{out}/dF_{in} gives the limiting differential transmittance (T_C), indicating the output clamping characteristics of samples. T_C for the sample MoS₂/PMMA-2 are 2% and 3% at 532 nm and 1064 nm, respectively, even lower than the single-layer graphene dispersion,

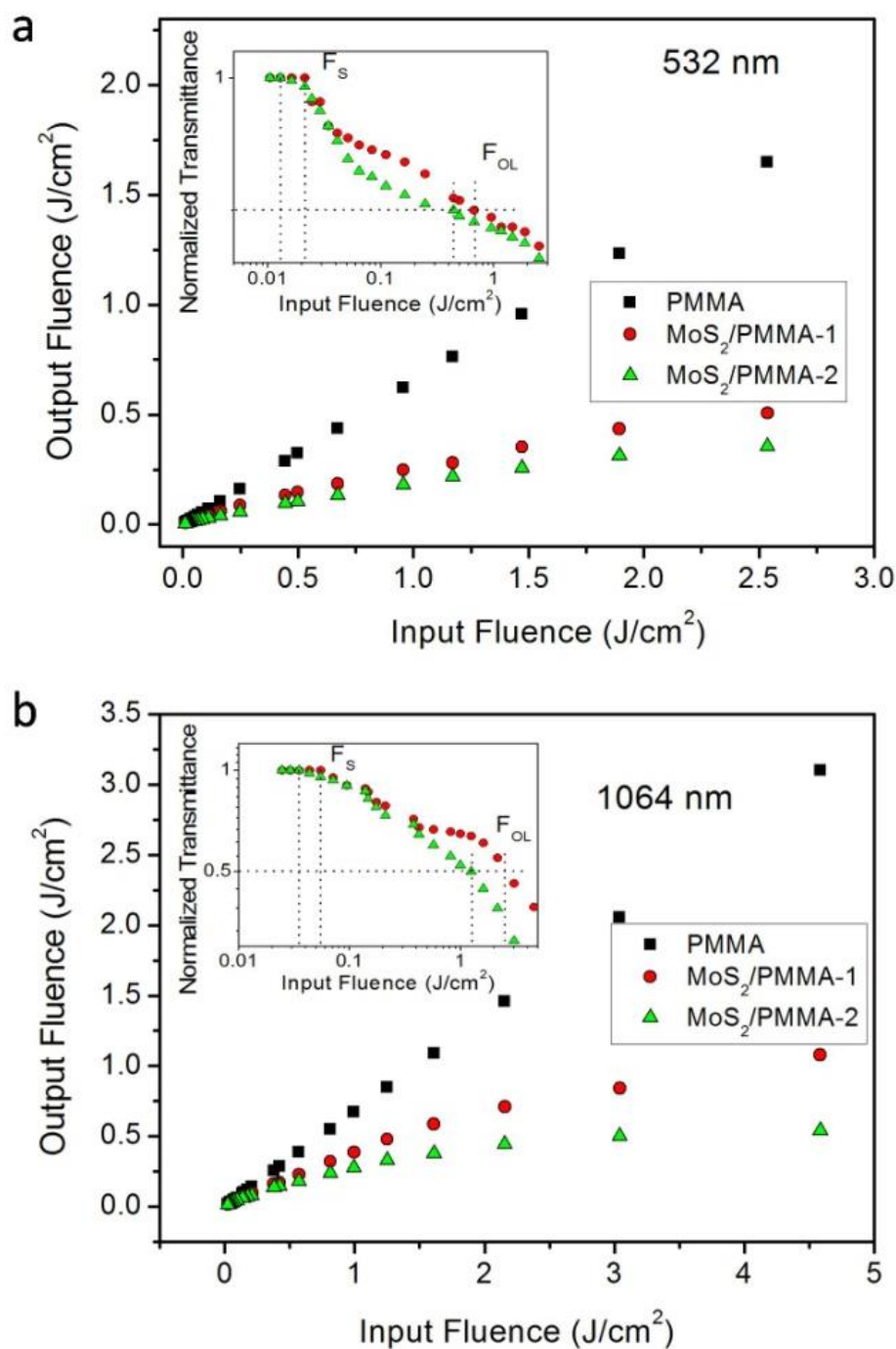


Fig. 3.6 The output fluence dependence on the input fluence at 532 nm (a) and 1064 nm (b), respectively. Insets are the corresponding normalized transmittance dependence on the input fluence. The concentration of MoS₂ in MoS₂/PMMA-1 and MoS₂/PMMA-2 are 0.008 and 0.016 mg/cm³, respectively.

further indicating its better optical limiting performance [34]. All these results suggest that MoS₂/PMMA composite has great potential as a type of excellent NLO material for optical limiting applications.

Two-photon absorption (TPA) and nonlinear scattering (NLS) have been acknowledged as the dominant mechanisms for NLO properties of optical limiting materials. Since NLS is usually resulted from the bubbles formed in the solution based NLO materials, it is reasonable to assume that TPA process makes dominant contribution to the NLO performance of solid-state MoS₂/PMMA composite bulk. And the TPA coefficient (β) subsequently can be obtained by the following equation: [112].

$$I_0 = \frac{I_i e^{-\alpha L}}{1 + (1 - e^{-\alpha L}) \beta I_i / 2\sqrt{2}\alpha} \quad (3-1)$$

where I_i and I_o are the input and output laser power respectively, α is the linear absorption coefficient, and L is the path length. The β values are fitted and given in Table 3-1. Such β values are larger than or compatible to the carbon materials[90, 113 - 115], indicating efficient TPA process in such MoS₂/PMMA composite bulk at both 532 and 1064 nm and hence leading to good NLO performance for optical limiting application. A table with actual linear transmittance, onset thresholds and optical limiting thresholds has been added in chapter 6 to compare the optical limiting performance between our samples and the above mentioned materials.

Table 3-1 Optical parameters of linear transmittance (T_L), Two-photon absorption (TPA) coefficient, NOL starting threshold (F_{ON}) and Optical limiting threshold (F_{OL}) threshold of MoS₂/ PMMA composites (sample 1 and 2).

Samples	532 nm				1064 nm			
	T_L	β_{TPA}	F_{ON}	F_{OL}	T_L	β_{TPA}	F_{ON}	F_{OL}
MoS ₂ /PMMA-1	55	62	0.02	0.7	60	27	0.06	2.3
MoS ₂ /PMMA-2	44	70	0.01	0.4	53	55	0.04	1.3

Note: The units of T_L , TPA, F_{ON} and F_{OL} are %, cm GW^{-1} , J cm^{-2} and J cm^{-2} , respectively. The concentration of MoS₂ in MoS₂/PMMA-1 and MoS₂/PMMA-2 are 0.008 and 0.016 mg/cm^3 .

3.4 Summary

In conclusion, good NLO property of the novel 2D material MoS₂ at both 532 and 1064 nm is studied and reported in this contribution. By employing ultrasonic exfoliation method, few-layer MoS₂ sheets are successively prepared. The interlayer separation in such few-layer MoS₂ has an interesting dependence on the layer number, primarily due to the weaker van de Waals force and increased interlayer repulsive force resulted from the active edge effect of the smaller nanosheets. Z-scan results of MoS₂/PMMA composite bulk further demonstrate the low NLO onset threshold F_{ON} , low optical limiting threshold F_{OL} , low optical limiting differential transmittance T_C , and high two-phonon absorption coefficient β at both 532 and 1064 nm, confirming the good NLO property. Hence, the few-layer MoS₂ nanosheets incorporated PMMA bulk can be a kind of novel NLO material with great potential

for optical limiting applications.

CHAPTER 4

Effect Of Laser Illumination On few-layer MoS₂

Nanosheet In NMP And PMMA

4.1 Introduction

Recently, great attention has been paid to two dimensional (2D) nanomaterials for its ultrathin atomic layer structure and interesting optical, electronic and mechanical properties [37, 38, 116 - 119]. Those 2D nano materials include graphene and layered transition metal dichalcogenides, TMDs - whose formula is MX₂, where M is a transition metal of groups 4–10 and X is a chalcogen, e.g MoS₂, WS₂, TaS₂, ZrS₂ and WSe₂ [29]. Nanosheets of TMDs have been explored for a wide range of applications associated with their ultra-thin thickness and 2D morphology, such as transistor, photoswitches, supercapacitors, additives for mechanical reinforcement, gas sensors, and electrochemical catalysis[120 - 128].

Graphene based materials have shown great applications in the field of laser photonics, e.g. optical limiting, saturable absorption, optical switches[104, 129 - 131]. Like graphene, layered structure MoS₂ also exhibits exceptional optical response when changed from bulk to few-layer structure. Owing to the specific 2D confinement of electron motion and the absence of interlayer perturbation, the MoS₂ monolayer possesses a direct band gap and shows dramatic improvement in

photoluminescence quantum efficiency by a factor of 10^4 in comparison with the bulk counterpart [57, 74]. This material will also bring new opportunities for the future development in the field of laser photonics, including optical limiting applications and saturable absorber for short pulsed laser [41, 132, 133], because of its strong nonlinear optical properties. Furthermore, the properties change in these materials under high optical density illumination is a very important research topic because of its unknown stability in suspension under high laser density. In this paper, we have studied the changes in size, optical absorption spectrum and photoluminescence with respect to two different laser wavelengths (532 and 1064 nm) at various optical energy densities. The nonlinear absorption properties of MoS₂ changes in N-methyl pyrrolidinone (NMP) and Polymethylmethacrylate (PMMA) before and after laser illumination for a period of time have been measured and compared.

4.2 Experimental section

Na₂MoO₄·H₂O (0.3 g) and CS(NH₂)₂ (0.4 g) were dissolved in DI water (30 mL) under vigorous stirring, followed by transferring the transparent solution to a 50-mL-capacity Teflon autoclave and keeping it at 240 °C for 24 hours. After the hydrothermal process, the formed black suspension was centrifuged and washed with DI water several times and dried at 60 °C in vacuum. Finally, black MoS₂ crystalline powder was obtained. Then few-layer MoS₂ nanosheets were first obtained by ultrasonic exfoliation method. MoS₂ (16 mg) powder was dispersed in NMP (80 mL) under vigorous stirring, followed by ultrasonic treatment for 18 h, and then the suspension was centrifuged at 3000 rpm for 20 minutes to remove the thick MoS₂ sheets. Then the MoS₂ nanosheets suspension was kept in NMP solution. The

concentration of the suspension is about 0.1 mg/mL. The MoS₂ suspension in NMP was in cuvette, then 532 nm and 1064 nm laser with repetition rate of 10 Hz was used to illuminate the suspension for 30 minutes and 60 minutes, respectively. During this experiment, the cuvette shook for 1 minute after laser illumination for every 10 minutes to keep the uniformity of the suspension.

4.3 Effect of laser illumination of morphology change of MoS₂

nanosheet in NMP

Two dimensional (2D) materials and laser interaction is a very important research topic due to the unique properties of 2D materials, making them a promising candidate for high power applications such as optical limiter and saturable absorber for mode locking laser generation. In this chapter, we have analysed the morphology and optical property changes of few layers MoS₂ nanosheet in NMP solution under the illumination of Q-switched laser with operational wavelength of 532 and 1064 nm with respect to various laser energy densities. The experimental results show significant changes caused by the oxidization of molybdenum disulfide (MoS₂) into molybdenum oxide (MoO₃). Due to its stronger absorption in visible range, 532 nm have stronger oxidization effect compared with 1064 nm as illumination wavelength. The nonlinear optical absorption properties of the MoS₂ in liquid NMP and in solid PMMA have been studied by using z-scan technique and their results are compared. It has been shown experimentally that the nonlinear optical absorption properties of MoS₂ in NMP disappeared but without changes in MoS₂/PMMA composites after laser illumination. It confirms that the MoS₂ is relatively much more stable within PMMA for preserving nonlinear absorption properties under high laser density

illumination.

4.3.1 Color changing of prepared MoS₂ suspension in NMP under laser

illumination

Fig. 4.1 shows the changing colour of the suspension after 532 laser illumination with different energy densities over 30 minutes. The MoS₂ suspension in NMP prepared by ultrasonic exfoliation is dark brown as shown in the Fig. 4.1a, after 532 nm 10 Hz nanosecond laser with increasing energy densities of 0.05 J/cm², 0.10 J/cm², 0.16 J/cm², 0.28 J/cm². The color of the suspensions changes from dark brown (Fig. 4.1b), bright yellow (Fig. 4.1c), yellow green (Fig. 4.1d) to colorless (Fig. 4.1e), successively.

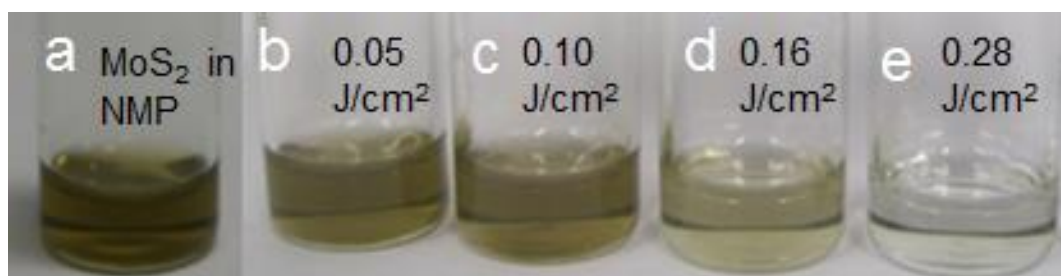


Fig. 4.1 Digital photos of prepared MoS₂ suspension in NMP after 532 nm laser illumination with different laser energy densities. The illumination time is 30 minutes.

Fig. 4.2 shows the changing colour of the suspension after 1064 nm laser illumination with different energy densities. The MoS₂ suspension in NMP prepared by ultrasonic exfoliation is dark brown as shown in the Fig. 4.2a, The color of the solution only become lighter by 1064 nm nanosecond laser for 60 minutes with energy densities of 0.77 J/cm², 3.35 J/cm², 3.72 J/cm², respectively, as shown in Fig. 4.2b, Fig. 4.2c and Fig. 4.2d. It indicates more color change of the MoS₂ suspension

in NMP under 532 nm illumination in comparison with that of 1064 nm.

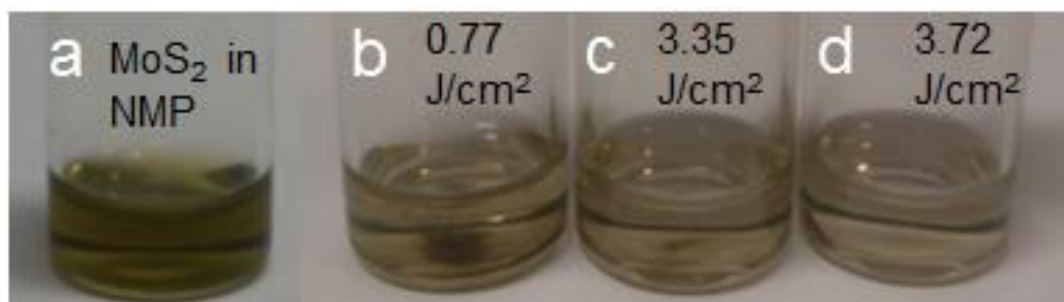


Fig. 4.2 Digital photos of prepared MoS₂ suspension in NMP after 1064 nm laser illumination with different laser energy densities. The illumination time is 60 minutes.

4.3.2 Morphology and size change of MoS₂ suspension in NMP before and after 532 nm laser illumination

The TEM images of MoS₂ suspension in NMP before and after 532 nm laser illumination under different energy densities are shown in Fig. 4.3a-4.3e. It can be seen from Fig. 4.3, the size of MoS₂ nanosheet decreases with the increasing 532 nm laser energy density. However, after laser illumination under laser density of 0.28 J/cm², the smaller nanosheets tends to aggregate together as shown in Fig. 4.3e, making it difficult for size measurement.

The size distributions of MoS₂ nanosheet after different energy densities of laser illumination are presented in Fig. 4.4. From Fig. 4.4a, the most frequency size of the MoS₂ nanosheet prepared by ultrasonic exfoliation is about 132 nm. After 30 minutes 532 nm laser illumination with laser densities of 0.05 J/cm², 0.10 J/cm² and 0.16 J/cm², the most frequent size of the nanosheet reduced to 103 nm, 94 nm and 58 nm

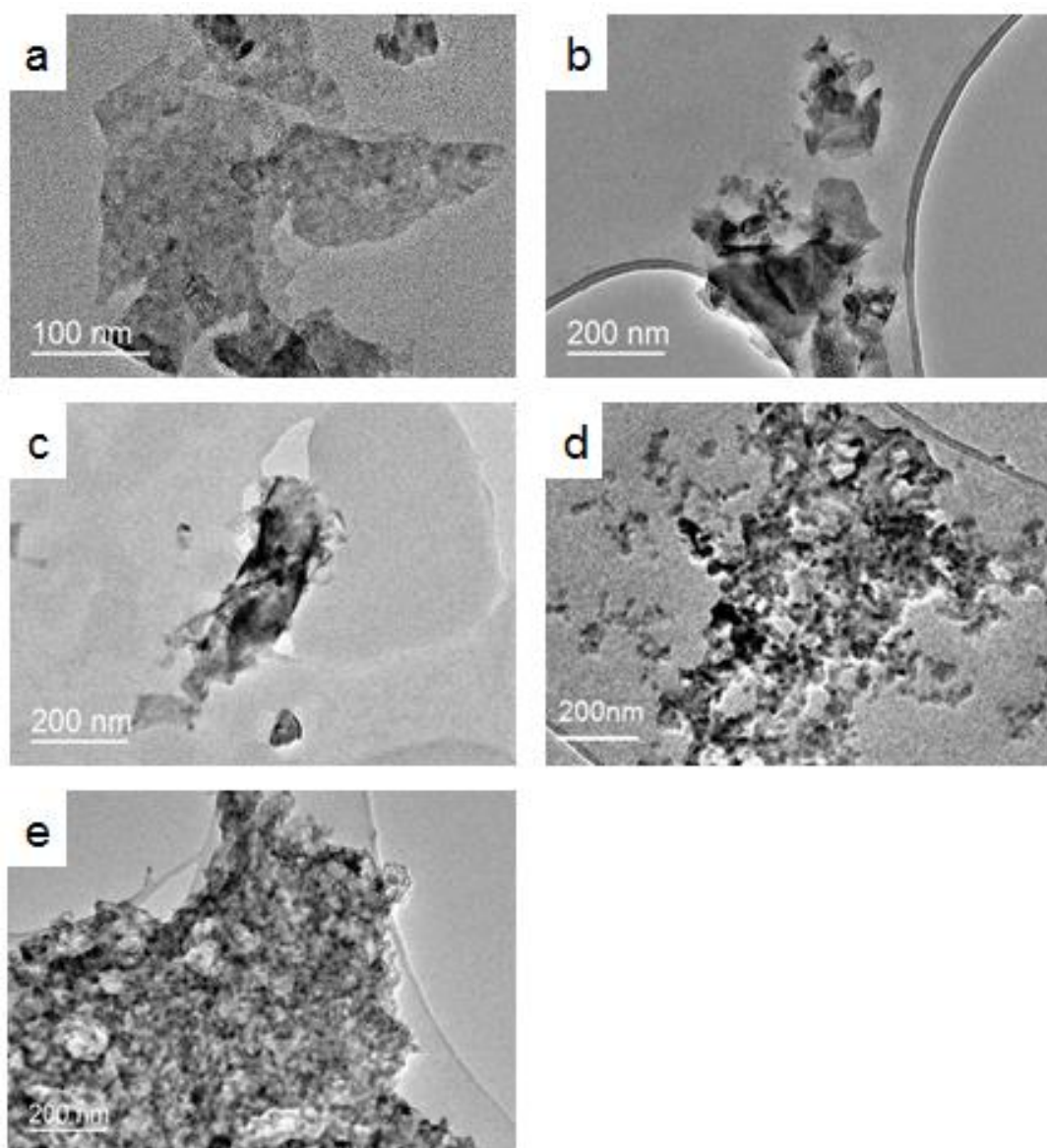


Fig. 4.3 TEM images of MoS₂ suspension in NMP before and after 532 nm laser illumination under different energy densities, (a) before laser illumination; (b) 0.05 J/cm²; (c) 0.10 J/cm²; (d) 0.16 J/cm²; (e) 0.28 J/cm².

respectively, as shown in the Fig. 4.4b - Fig. 4.4d. Fig. 4.4e illustrates the most frequent size of nanosheet becomes smaller after laser illumination. The higher the illumination laser energy density is, the smaller the nanosheet size will be under the same period of laser exposure time.

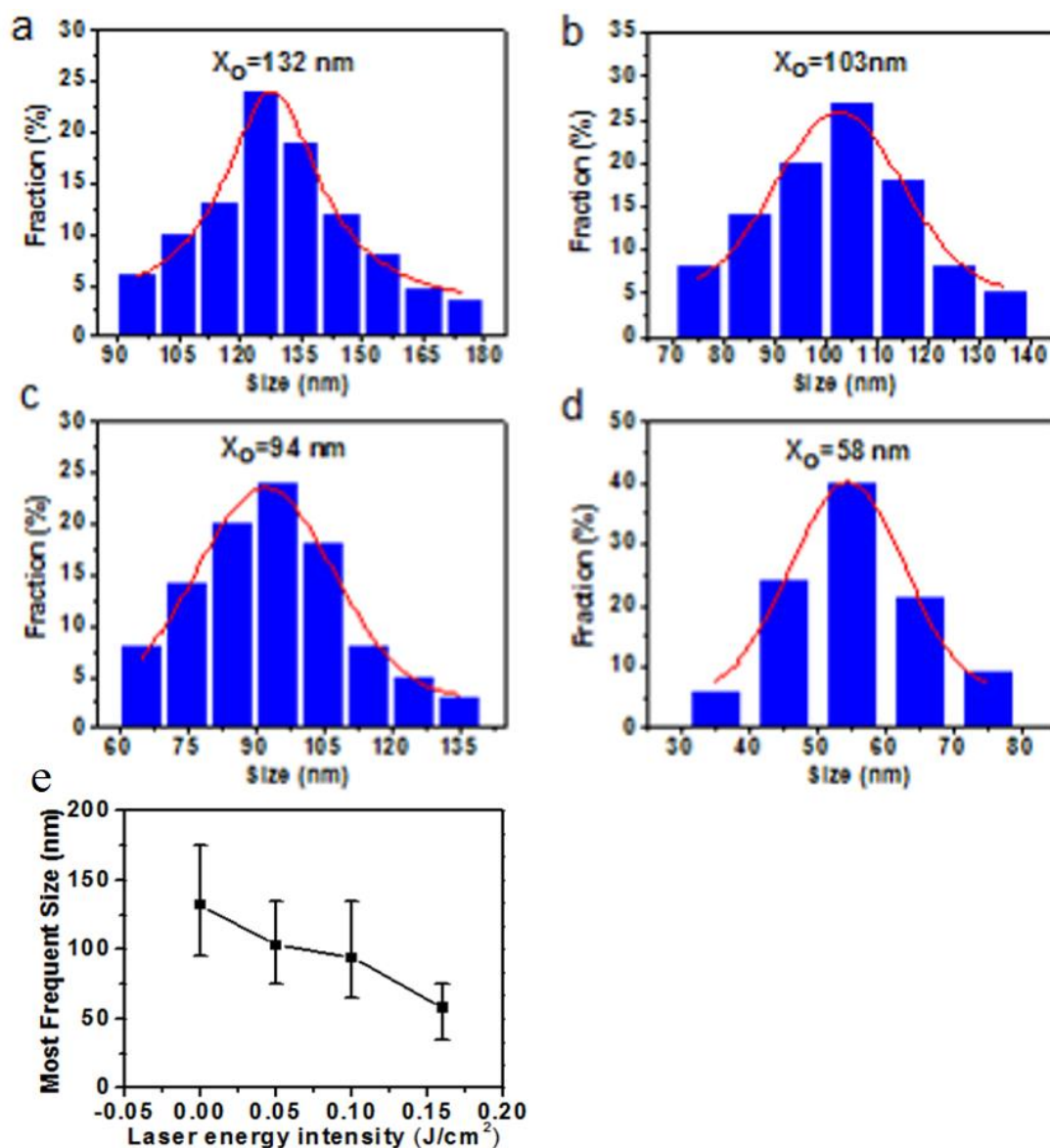


Fig. 4.4 Size distributions of MoS₂ nanosheet in NMP before and after 532 nm laser illumination under different energy densities (a) before laser illumination; (b) 0.05 J/cm²; (c) 0.10 J/cm²; (d) 0.16 J/cm²; (e) the most frequent size distribution with different energy intensities of illumination laser.

Fig. 4.5 shows the EDS of MoS₂ nanosheet before 532 nm laser illumination and after laser illumination with energy density of 0.28 J/cm². The selected area electron diffraction (SAED) pattern after 532 nm laser illumination in Fig. 4.5c contains signals for both MoO₃ and MoS₂. The (011) and (110) indexed diffraction

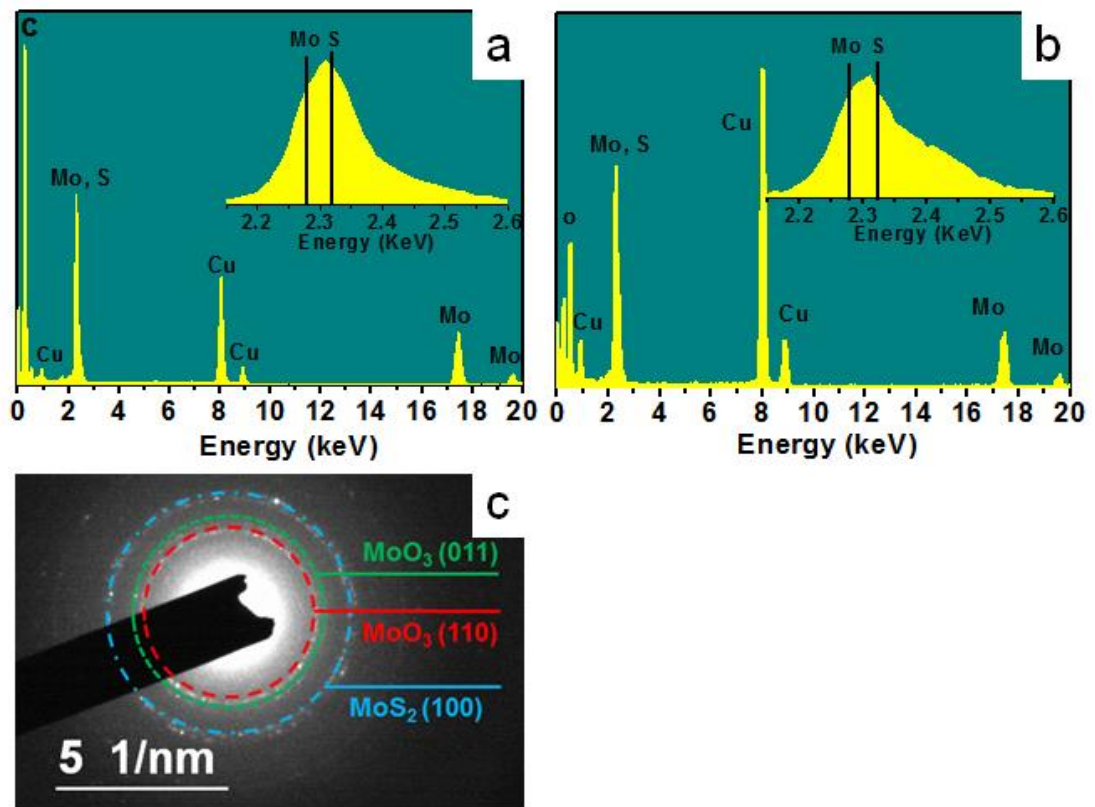


Fig. 4.5 EDS spectrum of the sample before laser illumination (a); EDS spectrum (b) and SAED pattern (c) of MoS₂ nanosheet after laser density of 0.28 J/cm². Insets(a-b) show the enlarged EDS within the 2.15-2.60 keV region.

spots for MoO₃ and (100)-indexed diffraction spots for MoS₂ can be seen clearly in one SAED pattern. As analyzed from the EDS patterns between before (Fig. 4.5a) and after laser illumination (Fig. 4.5b), the appearance of O element and the decreasing of S element after laser illumination which can be found from the insets of Fig. 4.5a and 4.5b confirming the oxidization process of the 2D materials. Under strong laser excitation, we expected the crystallinity of the obtained MoO₃ is not good. Due to the low concentration and low crystallinity, we did not see any observable changes in Raman spectroscopy and X-ray diffraction.

4.3.3 Size change of MoS₂ nanosheet after 1064 nm laser illumination

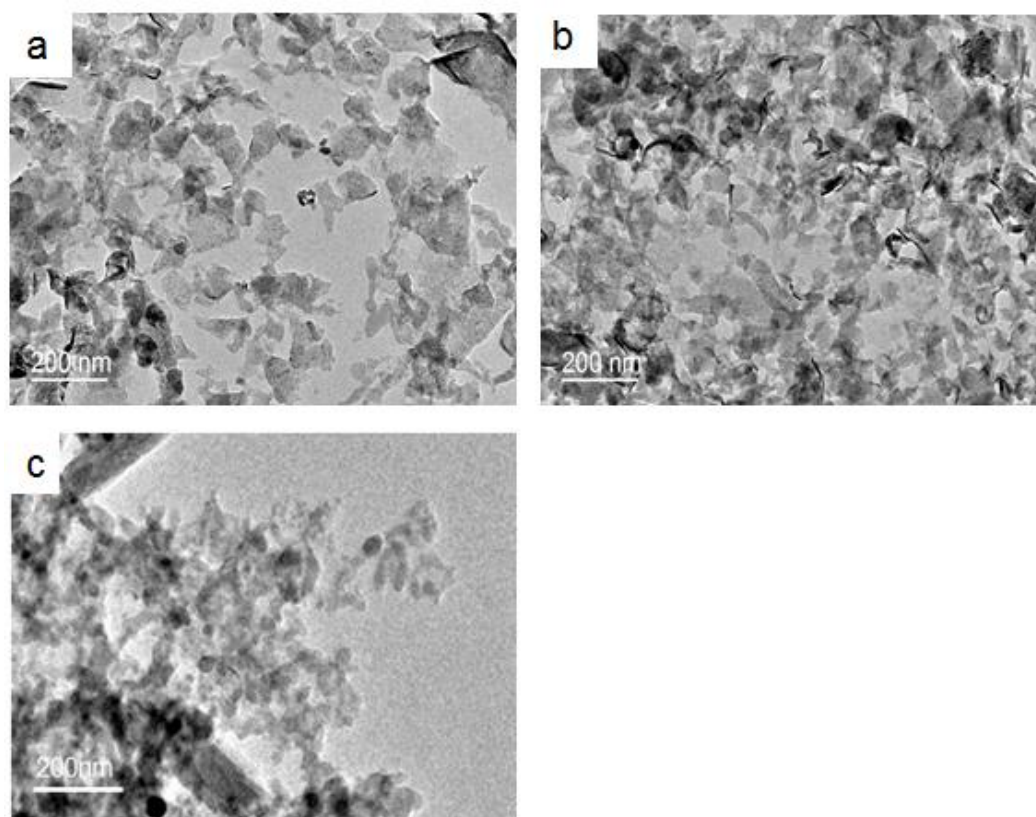


Fig. 4.6 TEM images of MoS₂ suspension in NMP after 1064 nm laser illumination for 60 minutes under different laser energy intensities (a) 0.77 J/cm²; (b) 3.35 J/cm²; (c) 3.72 J/cm².

The TEM images of MoS₂ suspension in NMP before and after 1064 nm laser illumination under different energy densities are shown in Fig. 4.6a-4.6c. After 1064 nm laser illumination with laser densities of 0.77 J/cm², 3.35 J/cm², and 3.72 J/cm² for the exposure time of 60 minutes, the most frequent size of the nanosheets changes from 132 nm to 105 nm, 100 nm and 92 nm as shown in the Fig. 4.7a-4.7c. Fig. 4.7d illustrates the most frequent size of nanosheet after laser illumination with different energy densities. The size of the nanosheet do not change much when compared to laser operating at 532 nm as the illumination source.

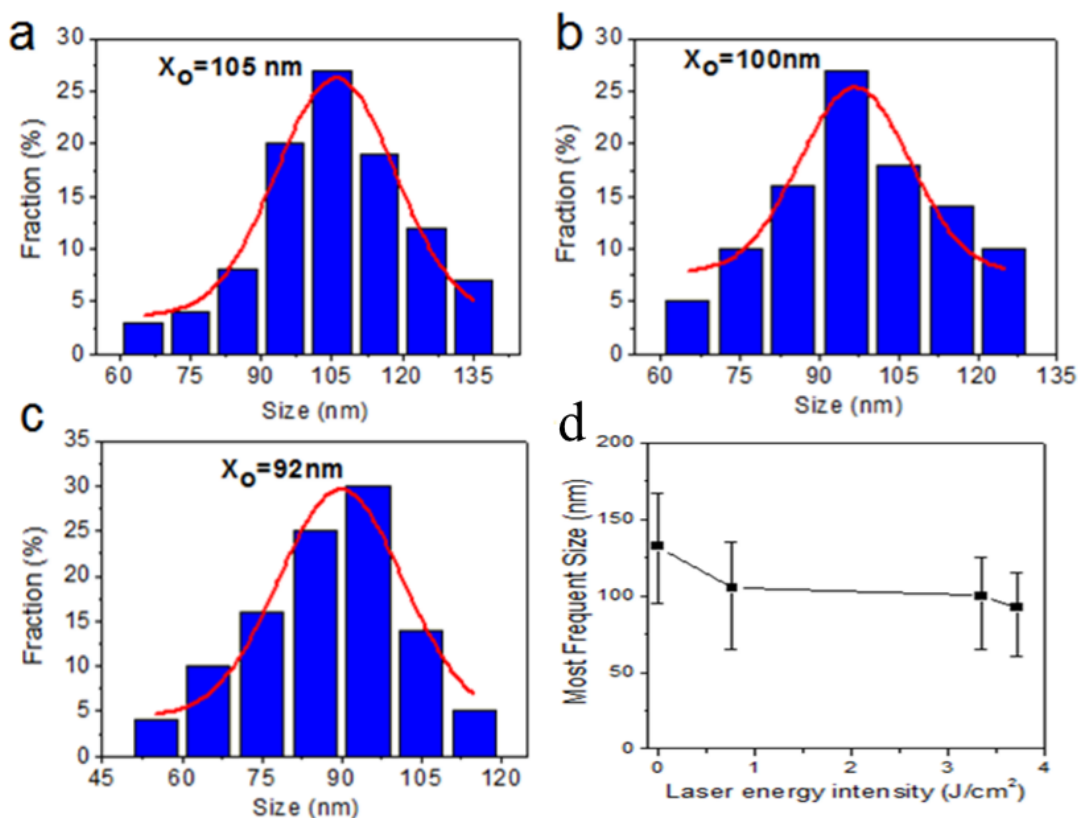


Fig. 4.7 Size distribution of corresponding samples MoS₂ suspension in NMP after 1064 nm laser illumination for 60 minutes under different laser energy intensities (a) 0.77 J/cm²; (b) 3.35 J/cm²; (c) 3.72 J/cm²; (d) the most frequent size distribution.

4.3.4 UV/Vis absorption spectrums before and after laser illumination

Fig. 4.8a-4.8b shows the normalized UV/Vis absorption spectra of MoS₂ suspension in NMP after 532 nm and 1064 nm laser illumination with respect to various laser densities. Due to the low concentration, the MoS₂ suspension in NMP prepared by ultrasonic exfoliation shows a broad absorption band centered at 416 nm with two very weak characteristic absorption peaks at 623 nm and 674 nm because of direct transition at the K-point of the Brillouin zone for the B and A transitions respectively [68, 76]. After 532 nm laser illumination, even with the lowest laser of 0.05 J/cm², all the three characteristic peaks at 416, 623 and 674 nm disappear and a new broad absorption band centered at 320 nm is observed, as shown clearly from

the Fig. 4a. With the highest illumination laser density of 0.28 J/cm^2 , there is another new broad absorption band centered at 650 nm was observed due to the formation of MoO_3 [134, 135]. While, under 1064 nm laser illumination, the characteristic absorbance peaks of 623 and 674 nm disappear gradually, as shown in Fig.4b. This result is also in good agreement with the color changes observed in Fig.1c. The broad absorption band centered at 416 nm also disappears and a broad absorption peak centered at 320 nm rises under the illumination of 1064 nm. Compared with 532 nm laser illumination, there is no clear absorption band at 650 nm even though the input laser density is 13 times higher than that of 532 nm for longer exposure time up to 60 minutes. The different effects caused by 532 nm and 1064 nm laser illumination is due to the absorption difference between both wavelengths (The absorption ratio of two wavelengths $I_{532/1064} \approx 9$ [57]). It means the absorption of MoS_2 at 532 nm is 9 fold of that of 1064 nm so that more 532 nm laser energy can be used to break the MoS_2 sheets into smaller pieces and oxidized into MoO_3 , leading to the smaller size of nanosheets and absorption reduction. Also, the considerable quantum-confinement effect might also cause the enhanced absorption to speed up the oxidization process further. The smaller size, the stronger the absorption will be, which has been reported in MoS_2 as well [136]. From the absorbance spectrum, it could be concluded that MoS_2 suspension in NMP could be oxidized into MoO_3 under the high density 532 nm laser illumination, with stronger oxidization effect compared with 1064 nm laser as illumination source.

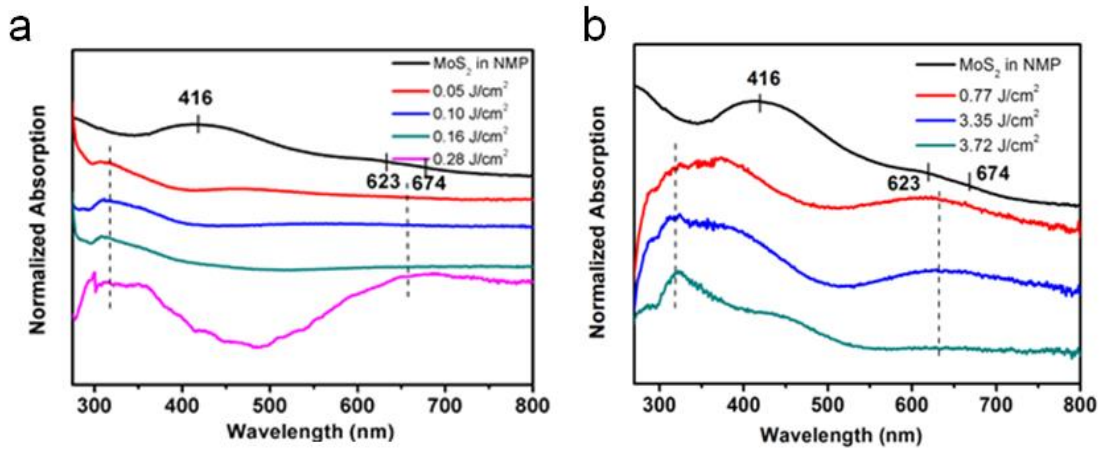


Fig. 4.8 Normalized UV/Vis absorption spectrum of MoS₂ suspension in NMP after laser illumination of 532 nm (a) and 1064 nm (b), respectively.

4.3.5 Photoluminescence spectrums before and after laser illumination

Fig. 4.9a and 4.9b show the normalized photoluminescence spectra of MoS₂ suspension in NMP before and after 532 nm and 1064 nm laser illumination, respectively. Fig. 4.9a can clearly identify two characteristic emission peaks of MoS₂ located at 623 and 660 nm before laser illumination [27, 74]. However, the two characteristic peaks gradually disappear with the increasing laser density of 532 nm due to the conversion from MoS₂ to MoO₃. However, two obvious characteristic peaks of MoS₂ only reduce slightly under the 1064 nm laser illumination due to lower absorption at this wavelength.

In this study, the excitation wavelength of photoluminescence is 532 nm. From the Fig.4.8a, the absorption at 532 nm is decreasing with the increasing intensity of illumination laser which lead to the decreasing intensity of photoluminescence in Fig.4.9b. During the illumination process, MoS₂ nanosheet is oxidized into MoO₃, therefore it is expected that the absorption characteristic peaks of MoS₂ should disappear and change into the shape of absorption spectrum of MoO₃ gradually.

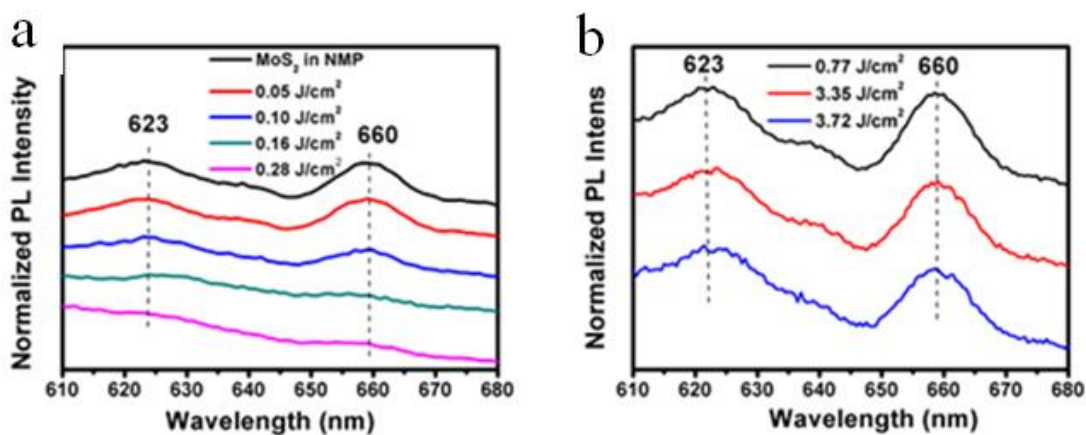


Fig. 4.9 Normalized photoluminescence spectrum of MoS₂ suspension in NMP after laser illumination of 532 nm (a) and 1064 nm (b), respectively.

4.4 The difference of nonlinear optical property between MoS₂ nanosheet in NMP and PMMA

To investigate the optical properties of MoS₂ before and after laser illumination in different host matrix, a z-scan experiment is employed with the same details described in ref [30]. Fig.4.10 shows the transmittance of MoS₂ suspension in NMP and PMMA matrix with respect to various input fluence created by moving the samples across the laser focus for both wavelengths of 532 and 1064 nm, respectively. Then the optical properties, e.g. initial transmittance at the same spot have been measured and compared. The initial transmittance of MoS₂ in different matrixes is presented in Table 4-1. Before laser illumination, MoS₂ suspension in NMP exhibits certain nonlinear optical absorption property under both 532 and 1064 nm wavelengths. After the illumination of 532 nm with energy density of 0.28 J/cm² for 30 minutes and 1064 nm with energy density of 3.72 J/cm² for 60 minutes, the initial transmittance of MoS₂ suspension in NMP becomes higher from 69 % to 95 % and 72 % to 85 %, for 532 nm and 1064 nm respectively, and their transmittance

becomes constant, with complete disappearance of non-linear optical absorption as shown in Fig. 5a to 5d. The disappearing nonlinear optical property of MoS₂ in NMP suspension can be explained by two possible reasons. Firstly, the optical limiting property of the suspension could be due to the nonlinear scattering which is usually size-dependent [45, 137]. Before laser illumination, larger size MoS₂ nanosheet in suspension exhibits stronger optical limiting response. However, the size of nanosheet and nonlinear scattering was reduced after laser illumination and the optical limiting property reduced. Secondly, MoS₂ is oxidized into MoO₃ gradually and loss its optical limiting properties after laser illumination.

However, compared with MoS₂ in NMP, MoS₂/PMMA composite exhibit much stronger optical limiting property even before laser illumination due to the thermophoresis phenomenon in NMP solution, leading to faster MoS₂ movement and local concentration reduction within the volume under the laser illumination. Of course the reduction of nonlinear optical absorption is also attributed to the oxidation of MoS₂. However, the MoS₂/PMMA composite shows almost no change in initial transmittance and non-linear absorption properties before and after laser illumination as shown in Fig. 4.10e and 4.10f. Compared with liquid suspension, solid state matrix can hold the MoS₂ into the fixed position and protect MoS₂ against oxidation so that the optical limiting property of MoS₂ nanosheets can be preserved, thus making it a very interesting research topic to investigate its nonlinear optical properties of these 2D materials embedded in solid state matrix [44, 104, 138].

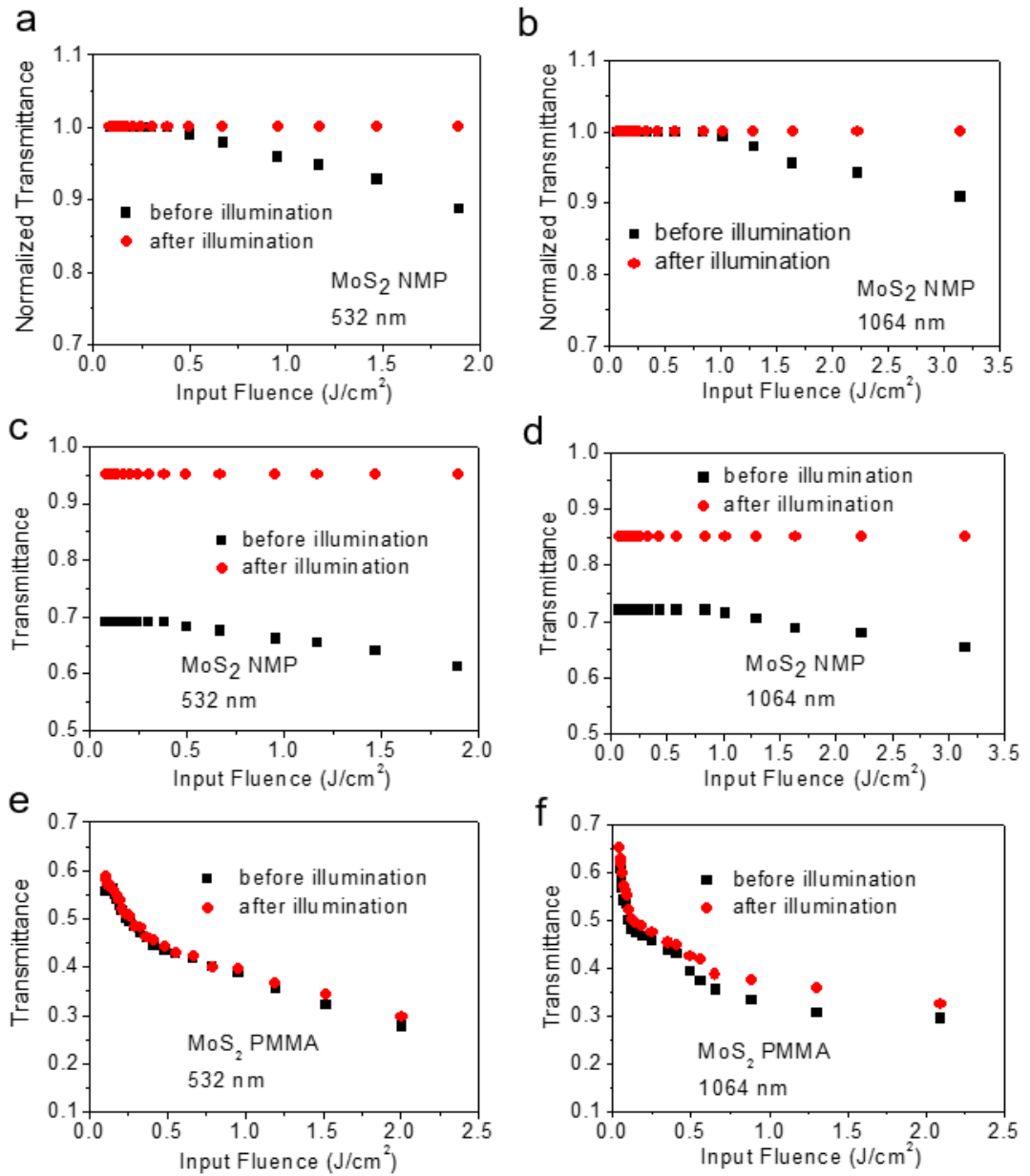


Fig. 4.10 (a) (b) normalized transmittance; (c) (d) transmittance of MoS₂ suspension in NMP and (e) (f) transmittance of MoS₂ /PMMA before and after the 532 nm and 1064 nm laser illumination, respectively.

Table 4-1 Transmittance of MoS₂ suspension in NMP and embedded into PMMA matrix before and after 532 nm, 1064 nm laser illumination, respectively.

The transmittance of MoS₂ in NMP and embedded in PMMA

Samples	532 nm		1064 nm	
	Before	After	Before	After
MoS ₂ NMP	0.69	0.95	0.72	0.85
MoS ₂ PMMA	0.55	0.59	0.63	0.66

4.5 Summary

In conclusion, MoS₂ suspension in NMP could be reduced in size and chemically oxidized into MoO₃, leading to the changes in optical properties including absorption, photoluminescence and nonlinear optical absorption properties after laser illumination. However, the illumination wavelength of 532 nm has relatively stronger effect on MoS₂ suspension compared to 1064 nm because of its higher optical absorption at 532 nm. Thus, 532 nm laser can oxidize MoS₂ to MoO₃ easily with even lower laser density compared with 1064 nm. Compared with the samples of MoS₂ in NMP, we have found that the initial transmittance and nonlinear optical absorption property of MoS₂ nanosheet in PMMA do not change much after laser illumination. Therefore it can be concluded that the stability of MoS₂ can be greatly enhanced when it is incorporated into PMMA solid state matrix.

CHAPTER 5

WS₂ Nanosheet Preparation And WS₂/PMMA Composite For Nonlinear Optical Application

5.1 Introduction

Graphene, the earliest discovered two-dimensional (2D) material, has become well known for its excellent electrical, optical, magnetic, mechanical properties, and so on [139 - 141]. However, it remains a challenge to tune its electronic and optical properties because opening or engineering the zero-bandgap structure of graphene usually involve complicated processes to break the lattice symmetry [33, 142]. As a kind of newly emerging 2D layered materials, transition metal dichalcogenides (TMDs) are different from zero-bandgap graphene, offering a wide range of intrinsic open bandgap structure and properties by changing different combination of transition metal groups and chalcogen. The dependence of bandgap structure of TMDs on the thickness results in its thickness-tunable bandgap properties, as well as tunable optical, electrical and electrochemical property, arousing considerable interest among researchers around the world because of their wide applications including solar cells, photodetectors, transistors, water splitting, and so on [6, 14, 37, 39, 143 -145].

WS₂ is a typical TMD material with large layer distance, making it easier to be

separated from the bulk to few-layer through various physical and chemical methods. In this research, ultrasonic exfoliation method was used because of its simplicity and scalability. When WS₂ is thinned from bulk to single layer, its bandgap changes from 1.3 eV indirect to 2.1 eV direct bandgap structure [146]. And the resulting enhancement of UV-Vis absorption has significant implications for solar cell, photodetector, photocatalysis, and other optical applications [6, 145]. Moreover, these bandgap changes will improve the transition probability from the valence band to the conduction band of the material, leading to the enhancement of the nonlinear optical absorption (NOA) such as two photon absorption (TPA) [30].

Being able to control the nonlinear optical properties of nanoscale materials is one of the most fundamental manipulations of light for the development of micro-photonics [147]. Therefore, a cost effective method to tune the nonlinear optical properties of the nanoscale TMDs have attracted enormous research interest due to its wide potential applications including optical limiting, bioimaging, optical communication, optical computer, data storage, drug delivery, and photodynamic therapy [148 - 150].

In this study, WS₂ flakes were exfoliated by an ultrasonic technique followed by a gradient centrifugation separation as shown in Fig. 5.1. In brief, 0.05 g WS₂ powder was dispersed in 50 ml N-methyl-pyrrolidone (NMP) and treated with ultrasonic for 15 h at a power of 400 W. A simple gradient centrifugation was then employed to select the size and thickness of WS₂ in a certain range. Subsequently, the WS₂ sheets were incorporated in Polymethylmethacrylate (PMMA) to form a solid composite for the NOA studies. The detail of this fabrication method is discussed in the experimental section.

5.2 Experimental procedures

WS₂ nanosheets are first prepared through ball milling and ultrasonic exfoliation method followed by a gradient centrifugation process. In order to obtain smaller WS₂ powder, the raw material tungsten sulfide (WS₂) powder (~6 μm, 99.99%) which were purchased from Aladdin in Shanghai were grinding through a ball milling solvent thermal induced method. A detailed gradient centrifugation process is shown in Fig. 5.1. In detail, 0.05 g WS₂ powder after ball milling was dispersed in 50 ml NMP and treated with ultrasonic for 15 h at a power of 400 W. The obtained exfoliated WS₂ sheets dispersion was then centrifuged at a successive rate, ω , equal to 7000, 5000, 1000 and 500 rpm for 30 min, respectively. The concentrations of all these four dispersions were adjusted to the same 0.087 mg/ml. Then, solid state WS₂/PMMA composites were fabricated, 20 ml MMA and 2 ml WS₂ sheets or quantum dots dispersions were first mixed and heated at 75°C for 10 mins, and then 0.023 g BPO was added and heated again at 75 °C for another 10 mins, followed by another heat treatment at 105 °C for 20 min. Finally, they were kept at 75 °C for 30 hours and four different solid transparent WS₂/PMMA samples with a series of different size and thickness were obtained.

5.3 Structures and morphology of WS₂ nanosheet in NMP

WS₂ nanosheet with different size and thickness are prepared by gradient centrifugation method and characterized by various methods shown below.

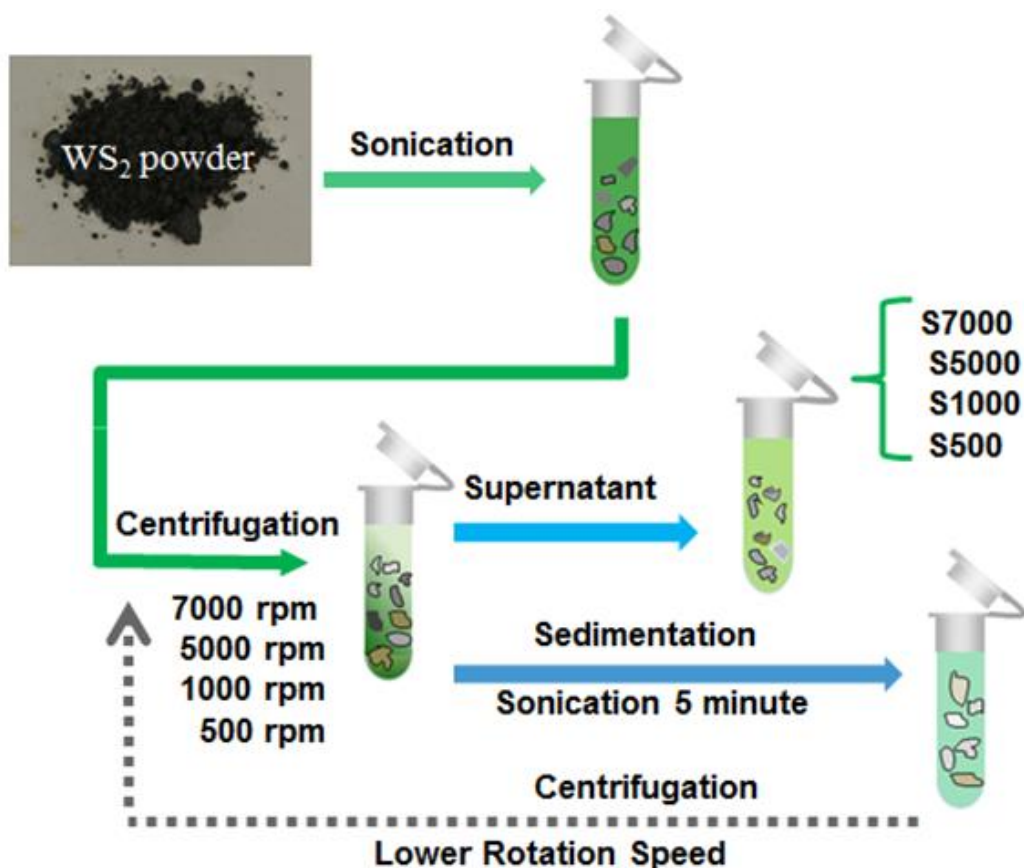


Fig. 5.1 Experimental procedures for fabricating WS₂ nanosheets with different size and thickness distribution.

5.3.1 Height profile of WS₂ nanosheet

Fig. 5.2a-2d show the atomic force microscopy (AFM) images of the WS₂ sheets obtained after 15 hours of ultrasonic exfoliation and subsequent centrifugation at 500, 1000, 5000, 7000 rpm, which were named after S500, S1000, S5000 and S7000 samples, respectively. With the increasing centrifugation rate, smaller and thinner WS₂ sheets can be obtained, which has also been confirmed by K. G. Zhou *et.al.* [151], and smaller WS₂ sheets would be beneficial for the TPA process [152]. Fig.5.3a-3d is the corresponding three-dimensional AFM images of WS₂ sheet. All

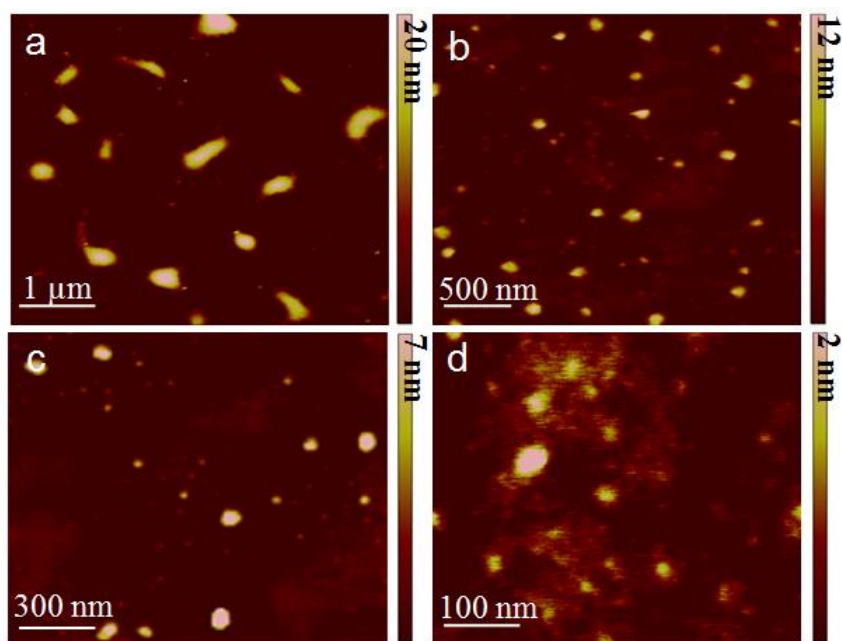


Fig. 5.2 (a-d) AFM images of WS₂ sheets exfoliated in NMP and subsequently separated under different centrifugation rates of 500, 1000, 5000, and 7000 rpm, respectively. For each WS₂ sample, about 50 sites were sampled for size and thickness analysis.

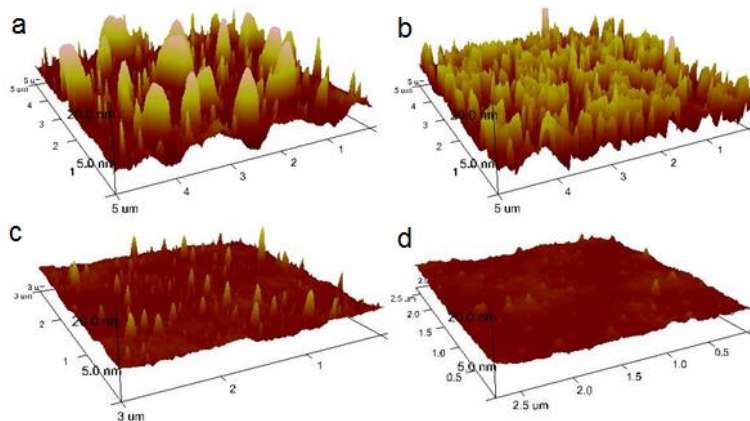


Fig. 5.3 (a-d) AFM images of WS₂ sheets exfoliated in NMP and subsequently separated under different centrifugation rates of 500, 1000, 5000, and 7000 rpm, respectively. For each WS₂ sample, about 50 sites were sampled for size and thickness analysis.

the height coordinate is 200 nm, it can be seen the thickness of four different samples

decrease gradually with the higher centrifugation rotation speed.

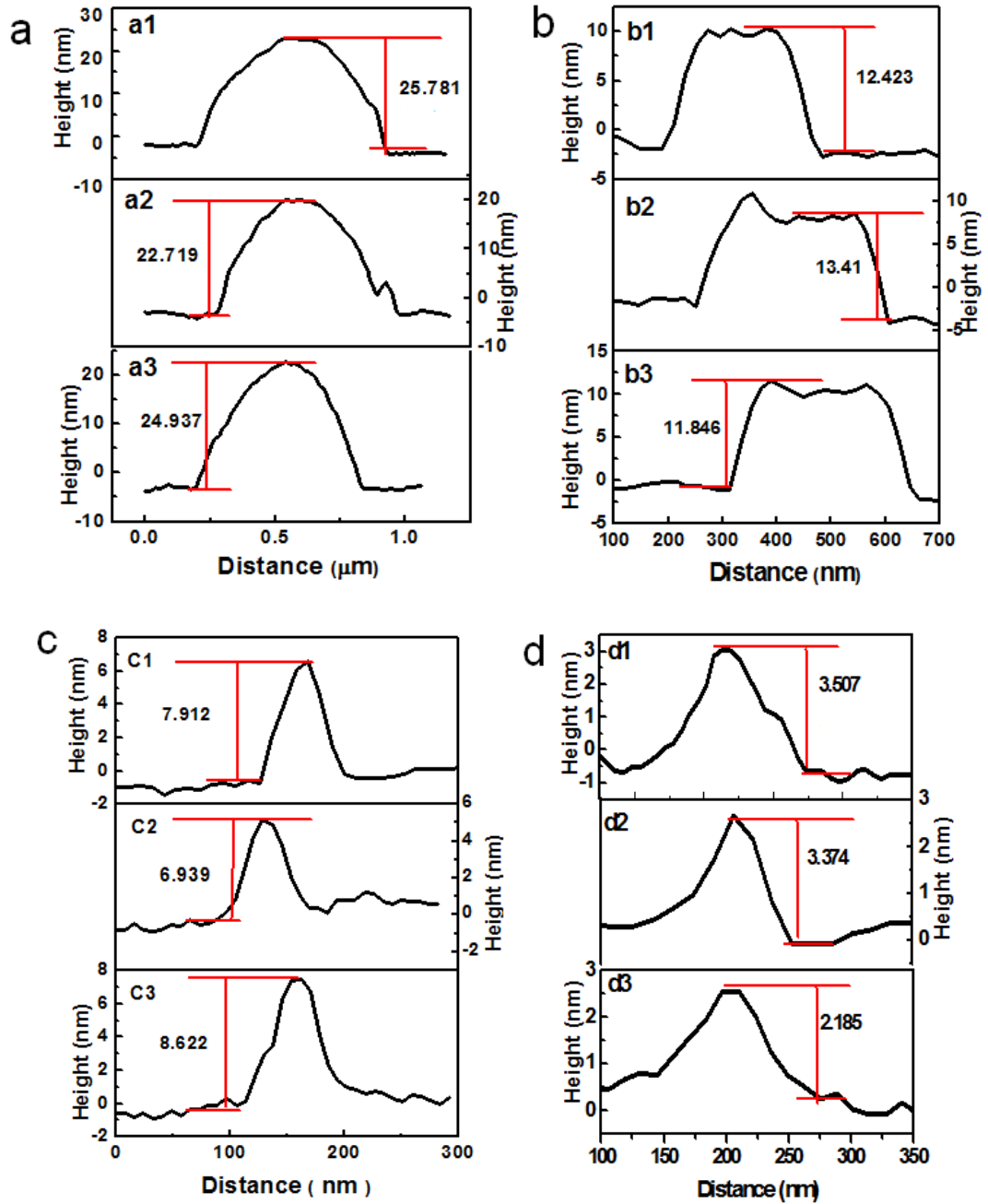


Fig. 5.4 Randomly selected section height profiles of WS₂ sheets exfoliated in NMP and subsequently separated under different centrifugation rates of a-500, b-1000, c-5000, and d-7000 rpm, respectively. The interlayer space of WS₂ is 0.62 nm.

Fig.5.4 (a-d) is the corresponding height profile of three randomly selected WS₂ sheet from samples collected by various centrifugation rates. The average thickness

of the three randomly selected nanosheet with different centrifugation rotation speed is 24.48 nm, 12.56 nm, 7.83 nm and 3.02 nm, corresponding to the layer number of 39 L, 21 L, 13 L and 4 L, respectively.

5.3.2 Thickness distribution of WS₂ nanosheet

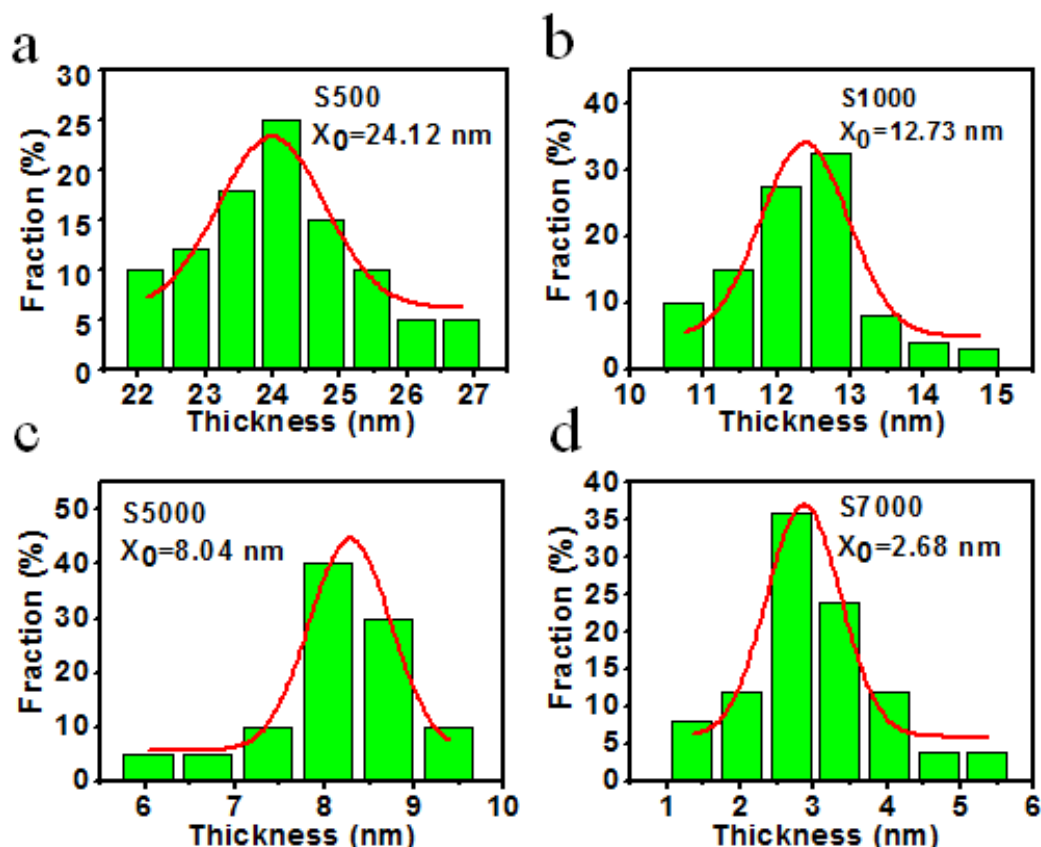


Fig. 5.5 Thickness distribution of WS₂ sheets exfoliated in NMP and subsequently separated under different centrifugation rates of a-500, b-1000, c-5000, and d-7000 rpm, respectively. The interlayer space of WS₂ is 0.62 nm.

From the thickness distributions shown in Fig. 5.5, it is confirmed that WS₂ sheets with different thickness (layer number) ranges from 40 layers to 4 layers. It can be seen that the different layer WS₂ sheets can be separated effectively from bulk

form through the simple ultrasonic exfoliation and centrifugation method.

5.3.3 Size distribution of WS₂ nanosheet

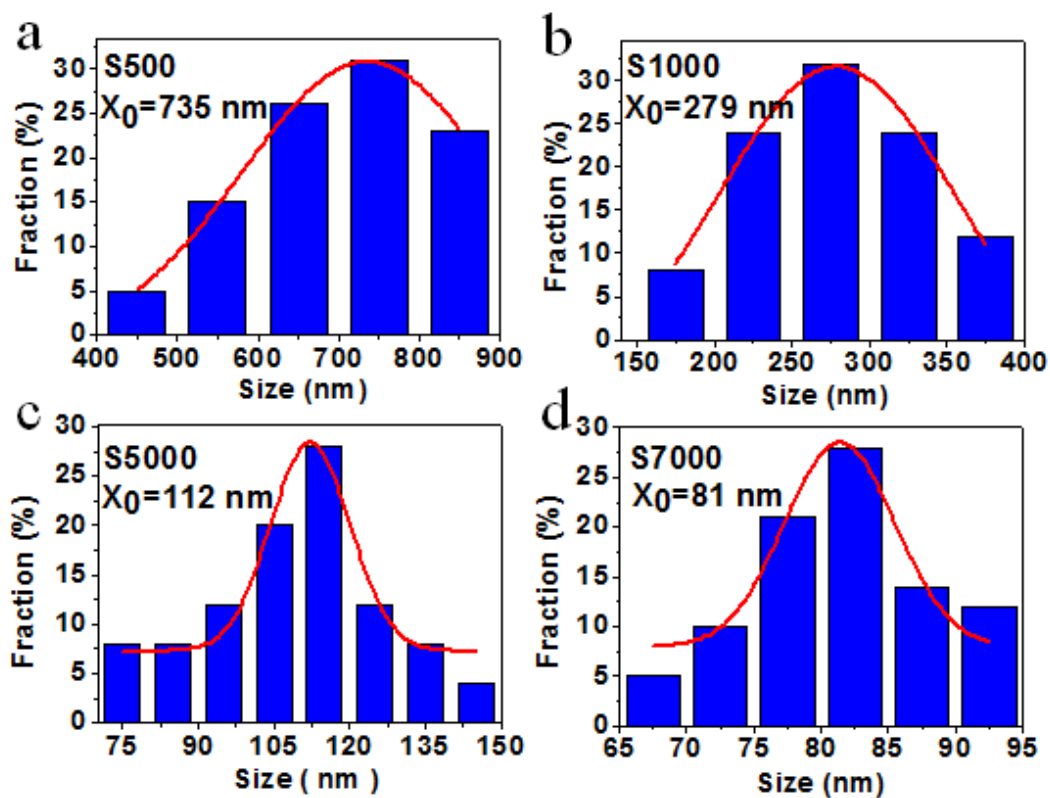


Fig. 5.6 Size distribution of WS₂ sheets exfoliated in NMP and subsequently separated under different centrifugation rates of a-500, b-1000, c-5000, and d-7000 rpm, respectively.

The size distributions of 4 different samples are shown in Fig. 5.6, it is confirmed that WS₂ sheets with different size ranges from 740 nm to 81 nm. The

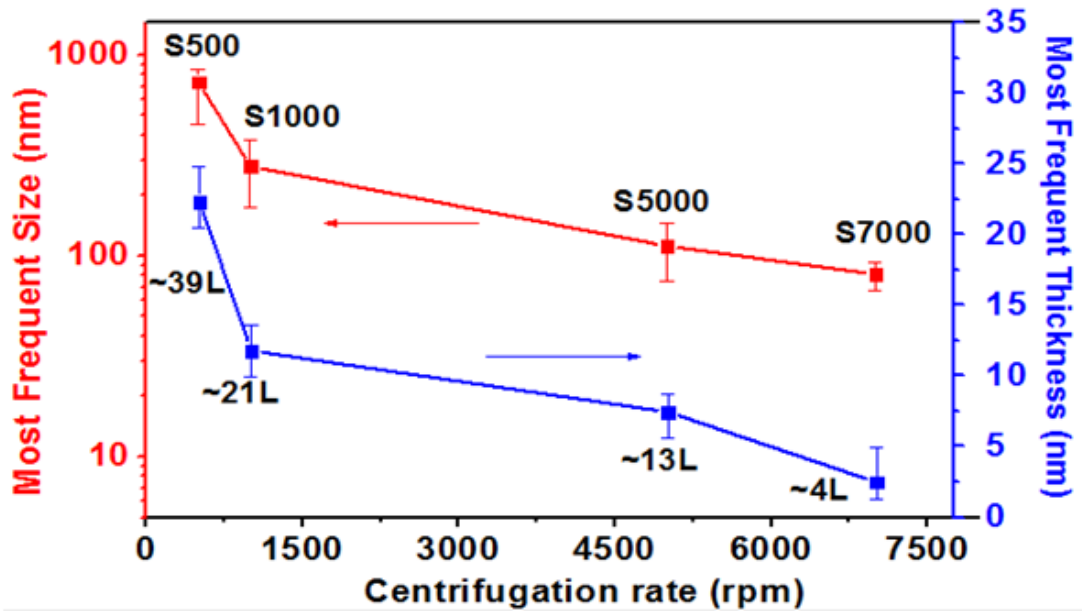


Fig. 5.7 Most frequent size and thickness of the four samples, L - Estimated layer number.

quantified changes agree well with the AFM images shown in Fig. 5.2 and Fig. 5.3.

The most frequent size and thickness of the four samples are presented in Fig. 5.7. The most frequent size decreases from about 1 to 0.1 μm and the most frequent thickness decreases from about 24.1 nm to 2.6 nm for the samples from S500 to S7000.

5.3.4 Raman spectra of WS₂ nanosheet

The Raman spectra of WS₂ sheets suspensions in NMP collected at different centrifugation rates were measured and given in Fig. 5.8. Two characteristic Raman peaks, E_{2g}¹ and A_{1g} of WS₂ are observed in Fig. 5.8a. E_{2g}¹ is hardened with the decreasing layer number, which is due to increasing long range Coulombic interaction of the in-plane vibrations of Mo atoms, resulting in the blue shift of E_{2g}¹

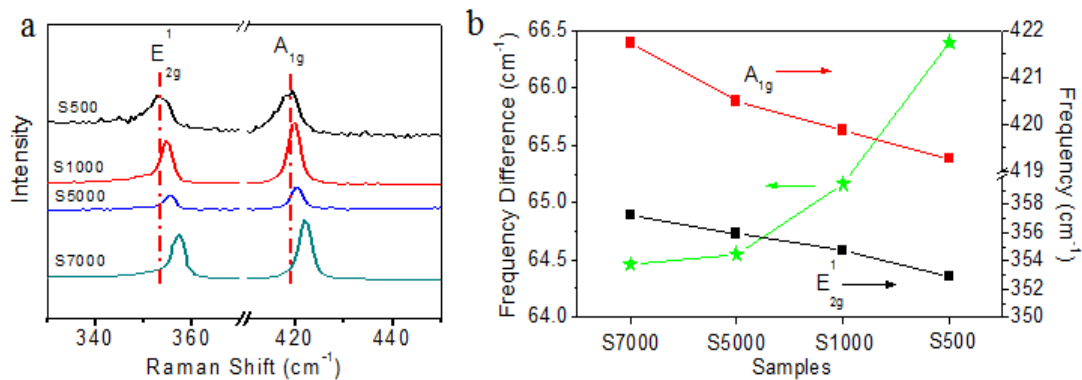


Fig. 5.8 (a) Raman spectra (b) The peak frequency of E_{2g}¹, A_{1g} and their frequency difference.

peak, as shown in Fig. 5.8a and 5.8b [153]. A_{1g} mode is related to the out-of-plane vibration of S atoms which is also hardened and shows a blue shift with the decreasing layer number as presented in Fig. 5.8a and 5.8b. The blue shift of the A_{1g} peak with decreasing layer number is different from the previous reported one [154] [155]. This phenomenon may be explained by the size effect. With the decreasing size of WS₂ sheets, the momentum conservation will be relaxed and the Raman active modes will not be limited to be at the center of the Brillouin zone, causing the blue shift of A_{1g} peak which has been reported in the TiO₂ nanoparticles and Si nanosolid [156, 157].

5.3.5 Absorption spectra of WS₂ nanosheet

The normalized UV-Vis-NIR absorption spectra of WS₂ sheets suspensions in NMP collected at different centrifugation rates were measured and given in Fig. 5.9. Fig. 5.9a presents the absorption intensity in the UV-Vis range showing a significant increase for the smaller and thinner WS₂ sheets collected at higher

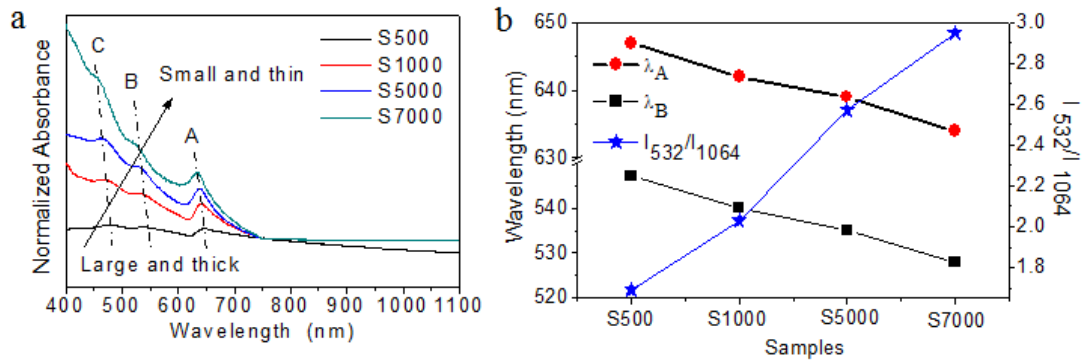


Fig. 5.9 (a) Absorption spectra; (b) Peak positions of the characteristic peaks A and B, and ratios of absorption intensity at 532 nm to 1064 nm (I_{532}/I_{1064}) of WS₂ suspension in NMP selected at 500 rpm, 1000 rpm, 5000 rpm and 7000 rpm centrifugation rate, respectively.

centrifugation rate, consequently making it closer to direct bandgap semiconductor with stronger bandgap absorption. The two characteristic excitonic absorption peaks A and B of WS₂ are observed along with a higher energy density of states peak C. The excitonic absorption peaks A and B are due to the direct transition from the valance band to the conduction band involving a spin-orbit split valence band at the K point of the Brillouin zone [155]. With increasing centrifugation rate, all the three peaks show blue shifts, being consistent with the results reported by Coleman et al [158]. As presented in Fig. 5.9b, the peak wavelength of A and B bands gives a similar decline tendency (λ_A and λ_B) with the increase of collecting centrifugation rate for obtaining smaller and thinner WS₂. Such behavior was observed in other TMDs, such as MoS₂ and WSe₂ [57, 159]. The ratios of absorption intensity at 532 nm to 1064 nm is also plotted in Fig. 5.9b, showing a considerable I_{532}/I_{1064} change with a two fold increase from S500 to S7000. This result indicates the relative absorption at 532 nm is stronger than that at 1064 nm for smaller and thinner WS₂ sheets.

5.4 Nonlinear optical absorption performance of WS₂/PMMA composites



Fig. 5.10 Digital photographs of prepared WS₂/PMMA composites, they are S500, S1000, S5000 and S7000 from the left to right, respectively.

WS₂ nanosheet with same concentration of different size and thickness are embedded into the PMMA. The digital images of WS₂/PMMA composites are presented in Fig. 5.10. Composites turn from colorless to bright yellow with smaller and thinner WS₂ flakes embedded.

A standard open aperture Z-scan apparatus was used to measure the NOA properties of WS₂ incorporated in PMMA. All experiments were performed by using a 8-ns Nd:YAG pulsed Q-switched laser operating at a repetition of 10 Hz. The beam was focused using a 5 cm focal length lens. Schematic diagram of the experimental setup is shown in Fig. 2.9.

The output fluence (F_{out}) was measured with respect to various input fluence (F_{in}) created by moving the sample along the z-direction around the focus. Fig. 5.11 presents the NOA performance of the WS₂/PMMA composite samples. At both 532 and 1064 nm, the output fluence shows a linear dependence on input fluence for the

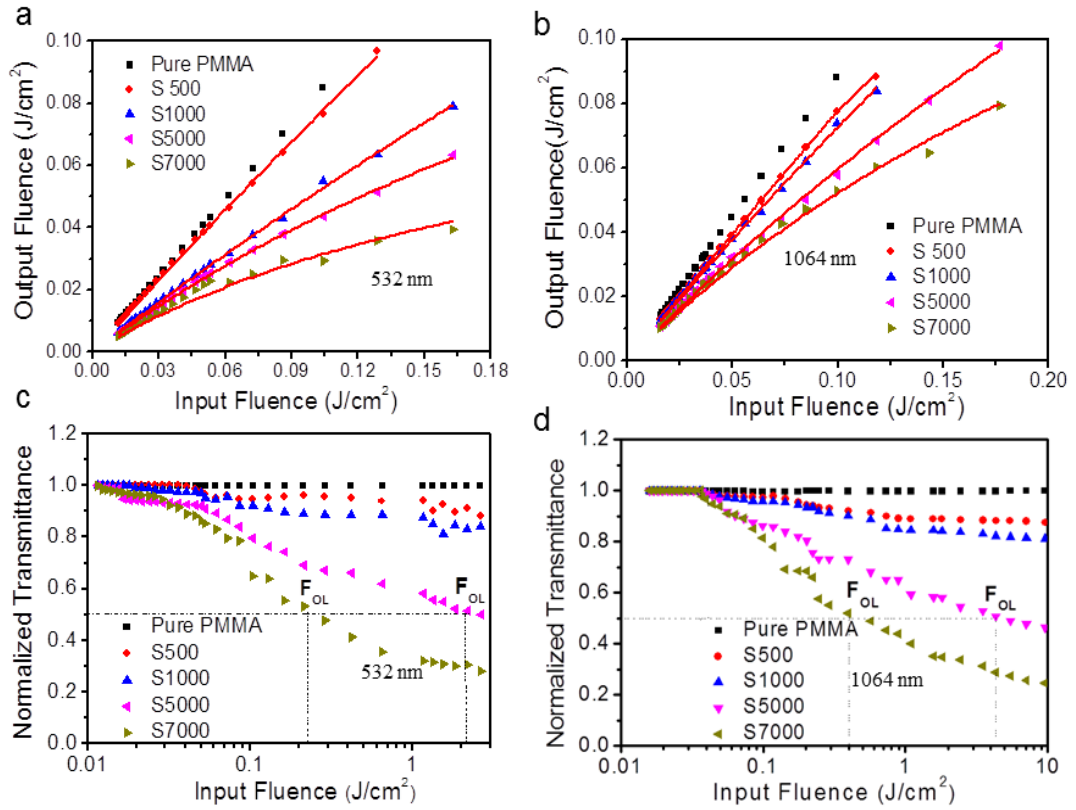


Fig. 5.11 Nonlinear optical absorption performance of WS₂/PMMA composites. (a) and (b) are the output influence dependence on input fluence, the red lines are the fitting curve according to the TPA model. (c) and (d) are the corresponding normalized transmittance dependence on the input fluence at 532 nm and 1064 nm.

pure PMMA contrast to its nonlinear dependence after WS₂ sheets are embedded, indicating the matrix PMMA has no contribution to the NOA property of WS₂/PMMA. Fig. 5.11a and 5.11b present plots of F_{out} versus F_{in} for the WS₂/PMMA composites at 532 and 1064 nm, respectively. The ratio F_{out}/F_{in} in the limit of zero fluence gives the linear transmittance (T_L), All WS₂/PMMA composites exhibit a gradually reduced transmission with increasing incident energy for both wavelengths 532 and 1064 nm, indicating clearly a broad NOA response. Here, only the nonlinear optical reverse saturable absorption (RSA) property of WS₂ is observed

but not saturable absorption (SA) reported by others [152]. It is believed that the pumping laser intensity of these experiments is too high to observe the SA phenomenon of WS₂ occurred under lower pumping intensity [45, 160]. Fig. 5.11c and 5.11d show the variation of normalized transmittance as a function of the input fluence for different WS₂/PMMA samples under excitation wavelengths of 532 and 1064 nm, respectively. The NOA onset threshold (F_{ON}) is defined as the input fluence at which the normalized transmittance begins to deviate from linearity, and the optical limiting threshold (F_{OL}) is defined as the input fluence at which the normalized transmittance dropped to 50%. The values of F_{ON} and F_{OL} obtained from Fig. 5.11 are presented in Table 5-1. As two-photon absorption (TPA) is considered as the major mechanism for the optical limiting effect of WS₂ [133, 161], the TPA coefficient (β) are also obtained by fitting the NOA data according to the TPA model and shown in Table 5-1 [30]. The T_L , F_{ON} , F_{OL} show a remarkable decrease with decreasing the size and thickness, indicating that smaller size and fewer layers of WS₂ sheets hold more sensitive NOA property with greater two-photon absorption (TPA) coefficient β . However, when comparing the sample S5000 to S7000, the most frequent size only dropped slightly 28% but the most frequent thickness reduced in 67% that lead to significant drops in F_{ON} and F_{OL} by 31% and 91%, respectively. These results indicate that the thickness plays a key role in tuning the NOA property. Sample S7000 exhibits excellent nonlinear optical property at both wavelengths of 532 and 1064 nm. For instance, the values of F_{ON} and F_{OL} at 532 nm are measured to be $0.011 \text{ J}\cdot\text{cm}^{-2}$ and $0.245 \text{ J}\cdot\text{cm}^{-2}$, respectively.

Table 5-1 Optical parameters of linear transmittance (T_L), two-photon absorption (TPA) coefficient (β), NOA onset thresholds (F_{ON}) and optical limiting thresholds (F_{OL}) for various $WS_2/PMMA$ composites.

Samples	532 nm				1064 nm			
	T	β	F_{ON}	F_{OL}	T	β	F_{ON}	$F_{OL}(J$
	$L(\%)$	(cm/GW)	(J/cm ²)	(J/cm ²)	$L(\%)$	(cm/GW)	(J/cm ²)	/cm ²)
S500	79	3.91	0.035	—	80	2.29	0.05	—
S1000	54	6.52	0.026	—	78	6.26	0.044	—
S5000	52	21.51	0.016	2.6	67	11.35	0.039	4.32
S7000	44	44.46	0.011	0.245	65	21.87	0.036	0.48

5.5 Discussion

The improved NOA property for the smaller and thinner WS₂ sheets can be attributed to the following two possible reasons. On the one hand, with the thickness of WS₂ sheet being reduced from around tens of layers (S500) to few layers (S7000), its bandgap structure gradually changes from indirect to direct due to an interlayer interaction, thus greatly enhancing the transition probability from the valence band to conduction band and resulting in the enhanced absorption. Also, with considerable quantum-confinement effect, smaller size will lead to stronger absorption. This has been observed in MoS₂ as well [136]. Therefore, the absorption coefficient of WS₂ is enhanced greatly as shown in Table 5-3. And the enhanced absorption of the thin layer WS₂ can benefit TPA at both wavelengths of 532 and 1064 nm. With the highest absorption coefficient of sample S7000, the transition probability of photon from the valence band to conduction band would also be the highest, resulting in the best NOA performance. Moreover, the ratio I_{532}/I_{1064} of S7000 is about twice that of S500, indicating the potential enhancement of the NOA property. On the other hand, with the smallest size of WS₂ sheets, sample S7000 has the largest surface area to volume ratio and more exposed free active edges, which also benefit to the TPA process [158].

Table 5-2 The absorption coefficient α ($\text{L g}^{-1} \text{cm}^{-1}$) of different samples at 532 and 1064 nm, respectively.

Samples	S500	S1000	S5000	S7000
α ($\text{L g}^{-1} \text{cm}^{-1}$) @ 532 nm	13.98	21.84	27.92	32.21
α ($\text{L g}^{-1} \text{cm}^{-1}$) @1064 nm	8.26	10.78	10.85	10.95

5.6 Summary

In summary, the WS_2 sheets in different size and thickness ranges have been successfully fabricated using simple and effective liquid phase exfoliation technique. The NOA property of WS_2 sheet incorporated in PMMA show a close dependence on both size and thickness, and it has been confirmed that the smaller and thinner WS_2 contributes to a remarkably enhanced NOA performance (lower F_{ON} and F_{OL}). The widely tunable NOA properties have been achieved through a control of size and thickness.

CHAPTER 6

WS₂ Quantum Dots: Preparation, Characterization And Its Optical Limiting Effect In PMMA

6.1 Introduction

Two-dimensional (2D) layered materials, such as graphene and transition metal dichalcogenides (TMDs), are very attractive materials for the next generation of micro- or nano-structure electronic or optoelectronic devices development due to their favorable electronic and optical properties and very compact layered structure. In addition, those 2D materials open up enormous applications in the field of optics and optoelectronics, such as conductors [169], transistors [170], photoluminescence [74], and photodetectors [171, 172] etc. Studying the non-linear optical properties of these 2D materials is a very important research topic as these novel materials can be used to manipulate light intensity nonlinearly and leading to many important optoelectronic applications including optical switching [173] and saturable absorbers for short pulsed lasers generation [85, 174, 177], and optical limiters[30, 104, 178]. Usually optical limiting properties of these 2D materials can be observed under high optical excitation intensity [30, 104, 178].

Layered structured WS₂ has a thickness depending on bandgap varying from 1.3 eV (indirect) to 2.1 eV (direct) as it changed from bulk to single layer structure [178]. Recently we have demonstrated that non-linear optical limiting properties of WS₂ can be further enhanced by engineering its size and layer structures. The previous study shows the WS₂ quantum dot (WS₂ QD) also exhibits strong optical

limiting properties[178]. However, its nonlinear optical property has not been investigated systematically. When becoming 0 dimension - quantum dots, those two dimensional materials exhibit high tunability of properties due to quantum confinement and size effect and demonstrate various applications including electroluminescent optical switches, solar cells, and biological imaging etc [179 - 181]. Therefore, increasing interest has been paid to study the optical properties of the quantum dots and its related fabrication methods [182, 183].

The theoretical and experimental analysis show that the surface energies of the selected solvents, N-methyl-2-pyrrolidone (NMP), match very well with that of WS₂, resulting in a minimal energy needed for overcoming the van der Waals forces between two WS₂ sheets, resulting in possible effective production of WS₂ quantum dots through liquid phase exfoliation method in NMP [38]. This paper will discuss the synthesis procedures of the WS₂ quantum dots via a facile liquid exfoliation method and the results for characterization. Previous reports show that the nonlinear optical properties of the 2D TMDs materials are more stable and stronger within solid state matrix [184]. Therefore, the nonlinear optical absorption properties of this fabricated WS₂ quantum dots incorporated into polymethylmethacrylate (PMMA) matrix with respect to different concentrations was also characterized by Z-scan technique. The WS₂ QD/PMMA with concentration of 0.027 mg cm⁻³ shows the onset threshold F_{ON} and optical limiting threshold F_{OL} comparable with the lowest thresholds obtained by using graphene [34], much lower compared with other nonlinear optical materials e.g. organics, fullerenes and carbon nanotube.

6.2 Experimental section

Preparation of WS₂ quantum dots: WS₂ powder was bought from Aladdin. In detail, 0.05 g WS₂ were dissolved in 50 ml NMP solution under ultrasonication for 15 h at the 29°C, and then the formed black suspension was centrifuged at 10000 rpm and kept in bottles.

Preparation of WS₂ QD /PMMA: 3 ml MMA and 0.3 ml / 0.6 ml / 1 ml WS₂ QD suspension was first mixed and heated at 75 °C for 10 min, and then 0.023 g BPO was added and heated at 75 °C for another 10 min, followed by heat treatment at 105 °C for 20 min. Finally, it was kept at 75 °C for 30 h and solid transparent WS₂ QD /PMMA was obtained.

6.3 Preparation and the structure of WS₂ quantum dots

According to the calculation of minimal entropy of mixture solution, by making use of reported data [61], for 35% ethanol-water solution prepared at 30°C, fitting parameters a and b were found to be -0.03985 and 0.9584. Therefore, the surface tension for ethanol-water solution at 30°C was found to be about 26.18 mJm⁻². Previous experimental data found that the NMP surface tension would be 40.38 mJm⁻² at 30°C [62]. The surface entropy of ethanol-water solution was reported as 0.078 mJm⁻²K⁻¹ around 0.3 mole fraction of ethanol [185]. Thus surface energy of ethanol-water solution was estimated to be 49.8 mJm⁻². As the surface entropy of different pure liquids was reported to be about 0.1mJm⁻²K⁻¹ [185 - 188], the surface energy of NMP was estimated to be 70 mJm⁻² which is consistent with the report [19].

6.3.1 The structure and morphology of the WS₂ QD

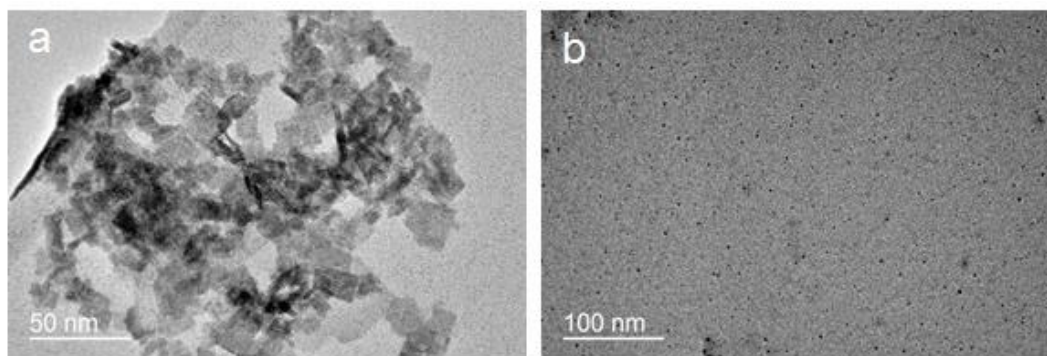


Fig. 6.1 TEM images of WS₂ nanosheet in ethanol and water mixture (a) and NMP suspension (b) sonicated by 15 h, respectively.

Fig.6.1a shows the Transmission Electron Microscope (TEM) morphology of WS₂ nanosheet in ethanol and water mixture after 15 h ultrasonic exfoliation. It clearly shows the WS₂ powder becomes relatively large nanosheet with average size around 20 nm with irregular shape and size. However, when WS₂ powder is ultrasonicated within NMP solution for 15 h, WS₂ nanosheets becomes quantum dots with much smaller average size around 2.4 nm and uniformly distributed within NMP as illustrated in Fig. 6.1b. It demonstrated that WS₂ powder can be effectively ultrasonicated into small quantum dots and uniformly dispersed within NMP solution due to the matching surface energy. WS₂ quantum dots are prepared by liquid exfoliation with centrifugation speed rate at 10000 rpm.

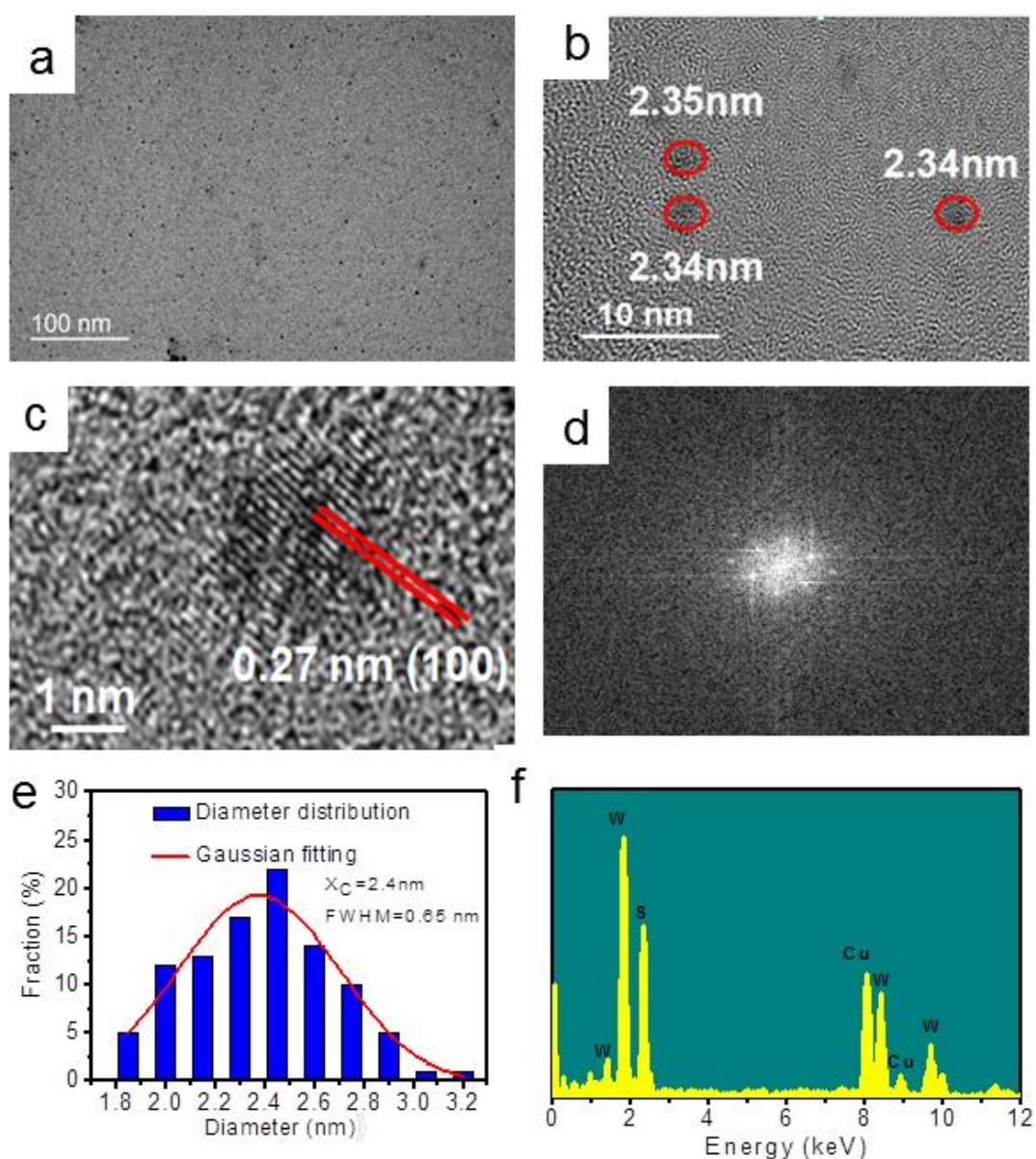


Fig. 6.2 TEM images of the WS₂ quantum dots (a); (b, c) HRTEM images; and corresponding selected area FFT image (d); diameter distribution of WS₂ quantum dots (e); EDS spectrum of WS₂ quantum dots (f).

In this study, the WS₂ QDs are successively obtained by ultrasonic WS₂ flakes in NMP for 15 hours but with a much higher centrifugation rate up to 10000 rpm. Fig. 6.2a shows the transmission electron microscopy (TEM) images of the WS₂ QDs. This agrees well with the HRTEM image of several typical WS₂ QDs (Fig. 6.2b). As

presented in Fig. 6.2c, a single WS₂ QD of diameter 3.12 nm with an in-plane lattice spacing of 0.27 nm matches well with the (100) planes, in which the lattice fringes of the WS₂ QDs is also clearly observed. The corresponding selected area Fast Fourier Transform (FFT) image is shown in Fig. 6.2d, revealing the hexagonal crystalline structure. It is clearly observed that the preparation of WS₂ QDs is successful within the range of 1.8 to 3.2 nm with average diameter at 2.4 nm and FWHM of 0.65 nm as shown in Fig. 6.2e, suggesting the prepared WS₂ quantum dots are ultra-small and possess excellent uniformity. The elemental composition of the WS₂ quantum dots is confirmed by the EDS results presented in Fig. 6.2 (f). The Cu peak is due to the copper mesh support for the measurement.

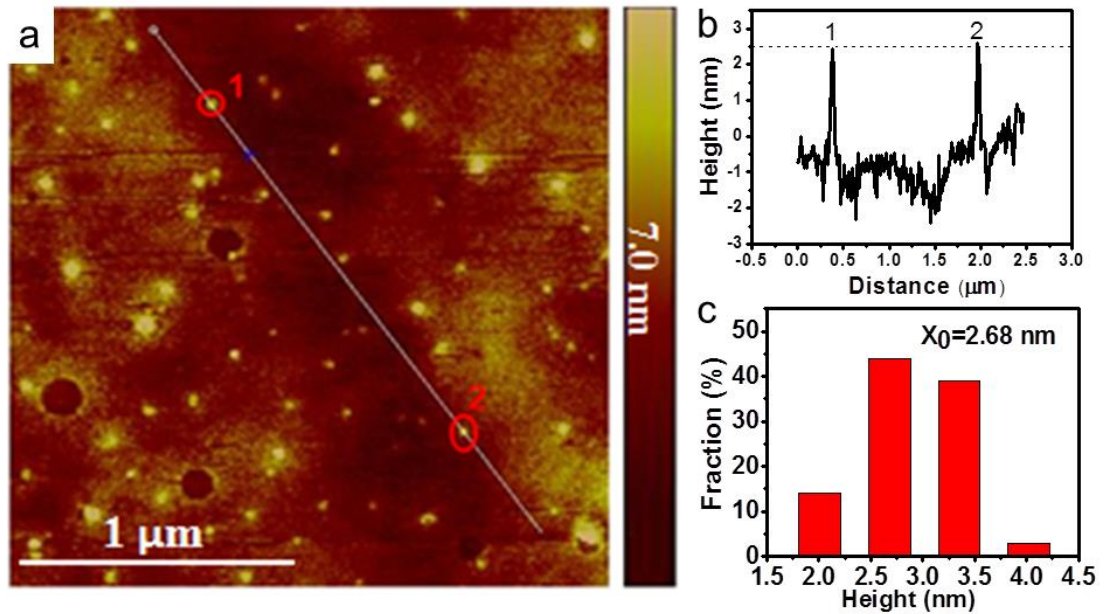


Fig. 6.3 (a) AFM topography image of WS₂ QDs. (b) height profile of the section marked in (a). (c) Height distribution of the WS₂ QDs.

Fig. 6.3a gives the topography image of WS₂ QDs with the height profiles of the

two randomly selected WS₂ QDs labeled as 1 and 2 shown in Fig. 6.3b. The average height of these WS₂ QDs is about 2.7 nm, corresponding to a few (~4) atomic layers of WS₂ QDs. The height distribution of the WS₂ QDs obtained from the AFM image is shown in Fig. 6.3c, indicating most of the WS₂ QDs are of 4 or 5 layers. From the data statistics, WS₂ QDs have the similar diameter and height due to the random orientation, then it can be regarded as sphere.

6.3.2 Absorption and Photoluminescence spectrum of WS₂ QD

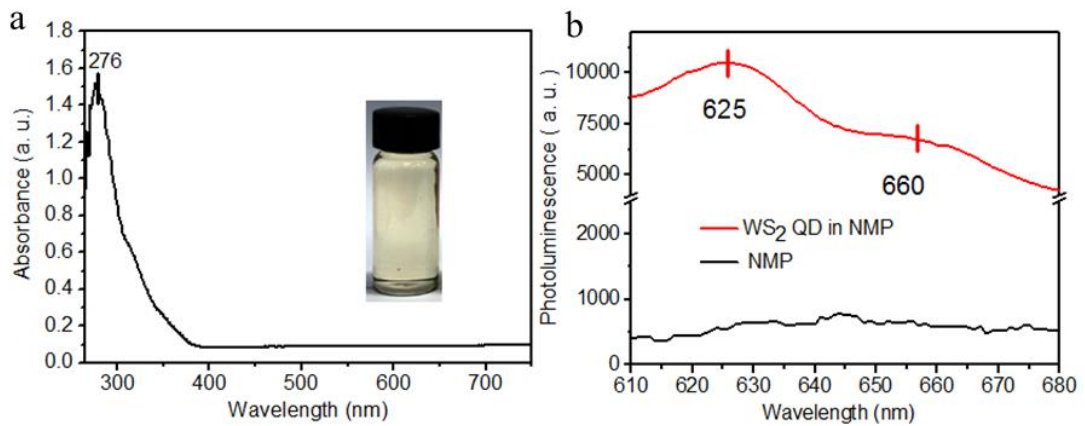


Fig.6.4 (a) Absorption spectrum of the WS₂ QD suspension in NMP; (b) Photoluminescence spectrum of WS₂ QD.

The absorption spectrum of the WS₂ QD suspension in NMP is shown in Fig. 6.4a. It can be observed that one characteristic absorption peaks at 284 nm. As shown in Fig. 6.4a inset, the suspension shows the characteristic bright yellow color of WS₂ QD suspension in NMP, similar to other reports [181]. Fig. 6.4b shows the photoluminescence spectrum of WS₂ QD suspension in NMP under 532 nm excitation. The two emission peaks located at 625 nm and 660 nm are due to the B and A direct excitonic transitions from the lowest conduction band to the highest

spin-split valence band at the K -point of the Brillouin zone, respectively.

6.4 Z-scan measurement of WS₂ QD/PMMA composites

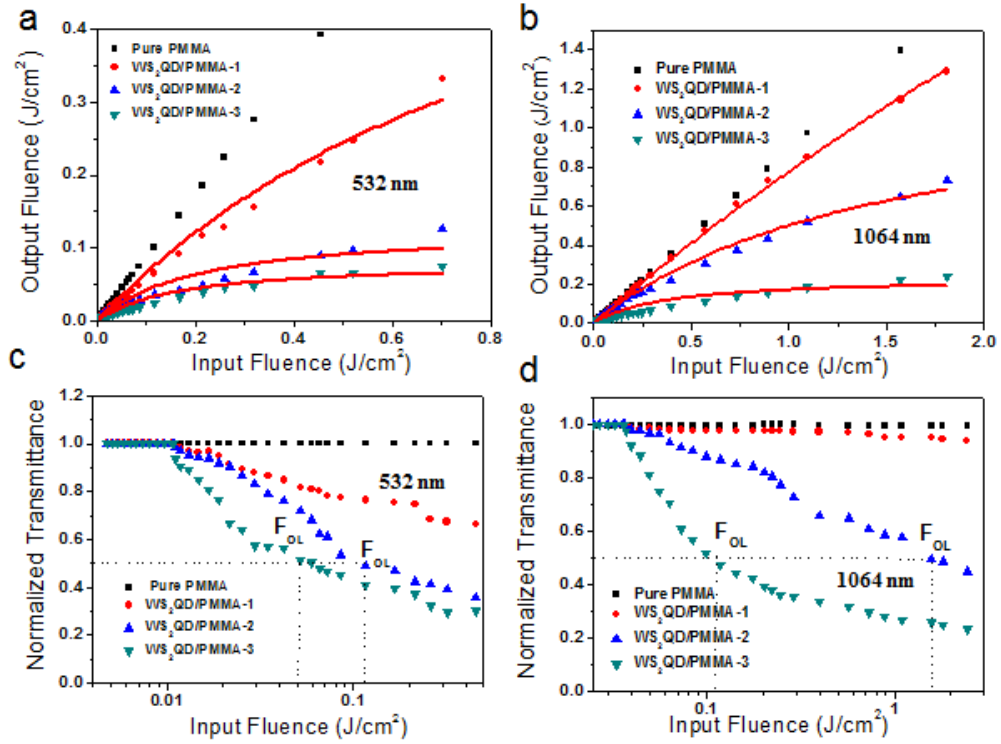


Fig.6.5 Open aperture Z-scan measurement of WS₂ QD/PMMA composites obtained by embedded different WS₂ QD concentration. (a), (b) are the output fluence dependence on the input fluence, the red lines are the fitting curves generated by the TPA calculation; (c) and (d) are the normalized transmittance dependence on the input fluence for 532 and 1064 nm, respectively. The concentrations of WS₂ QD in WS₂ QD/PMMA-1, WS₂ QD/PMMA-2, and WS₂ QD/PMMA-3 are 0.008 mg cm⁻³, 0.016 mg cm⁻³ and 0.027 mg cm⁻³.

Nonlinear optical (NLO) characteristics were measured using an open-aperture Z-scan technique and an 8 nanosecond pulsed Q-switched laser operating at 1064 nm or 532 nm are used for the Z-scan experiments to measure the nonlinear absorption

(NOA) properties of WS₂ quantum dots incorporated into PMMA. The experimental details were described in our former report [178]. The transmittance of the samples was characterized as a function of the incident laser fluence by moving the sample through the focal plane along its propagation Z axis.

Fig. 6.5 shows the NOA response of the three different WS₂ QD embedded in PMMA samples with concentration ranged from 0.008 mg cm⁻³ to 0.027 mg cm⁻³. At lower input fluence (F_{in}), the output fluence (F_{out}) of pure PMMA and WS₂ QD/PMMA composites exhibit linear transmittance (T_L), the exact values are presented in Table 6-1. However, T_L shows a decreasing tendency for both 532 and 1064 nm with the increase in the concentration of WS₂ quantum dots. Higher WS₂ quantum dot concentration leads to more sensitive NLO response for both excitation wavelengths. Then F_{out} decreases with the increasing input fluence for all WS₂ QD/PMMA composites. However, for pure PMMA, it exhibits linear transmittance at any input fluence revealing the PMMA matrix has no contribution to the observed NOA properties. These results demonstrated strong and broadband optical limiting property of the WS₂QD.

Fig. 6.5a and 6.5b present plots of F_{out} versus F_{in} for the WS₂ QD/PMMA composites at 532 and 1064 nm, respectively. The ratio F_{out}/F_{in} in the limit of zero fluence gives the linear transmittance (T_L). Fig. 6.5c and 6.5d show the variation of normalized transmittance as a function of input fluence for different WS₂ QD/PMMA samples under excitation wavelengths of 532 and 1064 nm. Two important parameters, named NLO onset threshold (F_{ON}) - the turning point of the transmittance from linear to nonlinear and the optical threshold (F_{OL}) - the input fluence at which the normalized transmittance drops to 50% are generally used to

quantify the optical limiting performance of a material. Herein F_{ON} and F_{OL} values are presented in Table 6-1. F_{ON} and F_{OL} exhibit the similar tendency with T_L , decreasing with the increasing concentration of embedded WS₂ QD. For a specific material, the lower F_{ON} and F_{OL} values predict the more sensitive optical limiting effects, with the sample WS₂ QD/PMMA-3 with highest concentration of 0.027 mg cm⁻³, F_{ON} are 0.011 J cm⁻² and 0.07 J cm⁻², F_{OL} are 0.04 J cm⁻² and 0.14 J cm⁻² at 532 nm and 1064 nm as excitation wavelength, respectively. These thresholds are comparable to the single-layer graphene dispersion and much lower when compared with metal nanostructure, carbon nanotubes, graphene oxide, etc [34]. Therefore, those results suggest the WS₂ QD/PMMA composite also possesses superior optical limiting property.

Two dominant mechanisms are used to explain the NLO properties, nonlinear scattering (NLS) and two photo absorption (TPA), resulting from the bubbles formation within the solution based nonlinear materials. Therefore, we can assume that TPA process makes the main contribution to the NLO performance of solid-state WS₂ QD/PMMA composite bulk and the TPA coefficient (β) can be obtained by equation 6-1 [112] :

$$I_0 = \frac{I_i e^{-\alpha L}}{1 + (1 - e^{-\alpha L}) \beta I_i / 2\sqrt{2}\alpha} \quad (6-1)$$

Where I_i and I_o are the input and output laser power respectively, L is the path length, and α is the linear absorption coefficient. The β values given in Table 6-1 are larger than or compatible to the other carbon materials, indicating efficient TPA process in such WS₂ QD/PMMA composite bulk at both wavelength of 532 and 1064

nm and resulting in excellent NLO properties for optical limiting application.

Table 6-1 Optical parameters of linear transmittance (T_L), two-photon absorption coefficient (β), NOL onset thresholds (F_{ON}) and optical limiting thresholds (F_{OL}) for WS₂ QD/PMMA composites

Samples	532 nm				1064 nm			
	T_L	β_{TPA}	F_{ON}	F_{OL}	T_L	β_{TPA}	F_{ON}	F_{OL}
WS ₂ QD/PMMA-1	72.51	7.93	0.018	—	85.96	0.833	0.12	—
WS ₂ QD/PMMA-2	62.55	43.41	0.013	0.117	82.71	5.11	0.05	1.2
WS ₂ QD/PMMA-3	49.85	145.5	0.01	0.062	65.22	73.80	0.03	0.1
S7000	44	44.46	0.011	0.245	65	21.87	0.036	0.48

Note: The units of T_L , TPA, F_{ON} and F_{OL} are %, cm GW⁻¹, J cm⁻² and J cm⁻², respectively. The concentration of WS₂QD in WS₂QD/PMMA-1, WS₂QD /PMMA-2 and WS₂QD/PMMA-3 are 0.008 mg/cm³, 0.016 mg/cm³ and 0.027 mg/cm³, respectively.

These fabricated WS₂ QDs are also incorporated in PMMA for NOA response measurement, and the results are shown in Fig. 6.6. Compared with S7000, WS₂ QDs exhibits much lower F_{ON} and F_{OL} at 532 nm and 1064 nm as shown in Table 6-1. These threshold values are comparable to the lowest demonstrated record of single-layer graphene which is considered as one of the best NOA materials, [34] and lower than all the demonstrated records of the traditional metal nanoparticles, carbon nanotube, graphene oxide. We attribute the excellent NOA performance of WS₂ QDs to the edge and quantum confinement effects. Assuming the WS₂ sheet of S7000 as

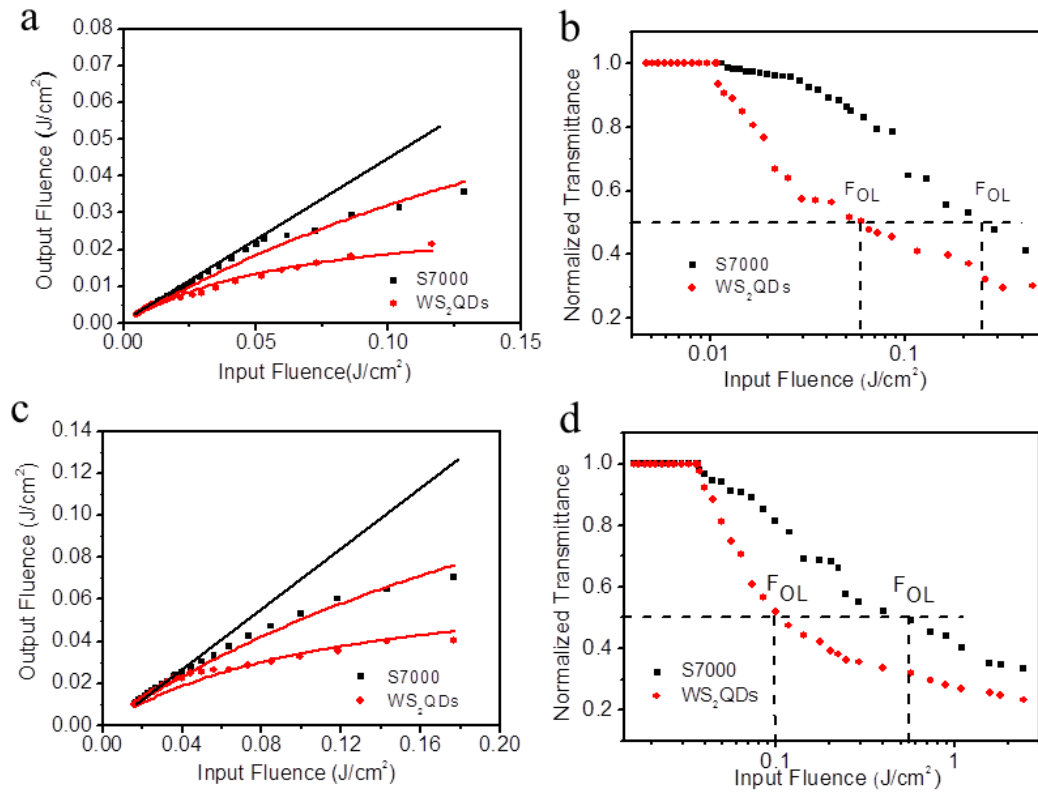


Fig.6.6 The comparison of NOA response of S7000 and WS₂ QDs at (a) 532 nm and (b) 1064 nm, respectively. Insets are the corresponding normalized transmittance dependence on the input fluence.

cylinder and QDs as sphere, the active surface area to volume ratio of WS₂ QDs is about 25 times higher than that of sample S7000. Therefore, WS₂ QDs has much more active surface and edges. The active edges of WS₂ lead to sub-bandgap absorption and further enhance the NOA performance [132], SA or RSA, depending on the value of the laser input fluence [34, 160]. Moreover, WS₂ QDs has stronger quantum confinement effect because of their ultrasmall size. Active edges and quantum confinement effect can further enhance NOA behavior due to the enhanced two-photon and three-photon absorption, which is a commonly acknowledged theory [189, 190]. Table 6-2 presents the onset thresholds (F_{ON}) and optical limiting

thresholds (F_{OL}) of different materials for the nanosecond laser operating at 532 and 1064 nm. These thresholds of sample S7000 are close to the 2D single-layer graphene embedded polycarbonate (PC) matrix [34], and much lower than other existent nonlinear optical materials including metal nanostructures [106, 111], carbon nanotubes [106], graphene oxide[104, 87], graphene nanosheet and nanoribbon [53].

Table 6-2 The nonlinear optical property onset thresholds (F_{ON}) and optical limiting thresholds (F_{OL}) of different materials for the nanosecond laser operating at 532 and 1064 nm, respectively.

Materials	532 nm			1064 nm		
	T _L (%)	F _{ON} (J/cm ²)	F _{OL} (J/cm ²)	T _L (%)	F _{ON} (J/cm ²)	F _{OL} (J/cm ²)
Pd NW [110]	80	0.09	0.90	80	0.30	8.00
Au NP [162]	70	0.07	0.60	77	0.60	7.50
MWCNTs [163]	70	0.04	0.68	70	0.13	9.69
CNTs-PTh-CdS[163]	70	0.03	0.47	70	0.09	6.66
GO [164]	70	0.19	1.19	75	1.36	10.32
GO NRs [165]	70	0.10	1.00	70	0.20	4.00
PNP ⁺ GO ⁻ [166]	63	0.21	1.55	74	2.00	8.10
PEG-OPE-rGO[164]	70	0.07	0.31	75	0.54	3.50

Graphene NSs [165]	70	0.10	0.50	70	0.20	6.30
Graphene NRs [165]	70	0.10	0.70	70	0.20	3.40
Graphene [167]	73	0.01	0.08	85	0.01	0.1
MoS ₂ /PMMA [168]	44	0.01	0.40	53	0.04	1.30
S7000*	44	0.011	0.245	65	0.036	0.48
WS ₂ QD	48	0.010	0.062	63	0.030	0.10

6.5 Summary

In conclusion, a simple and effective liquid phase exfoliation method has been successfully employed to fabricate ultra-small WS₂ quantum dots with diameter of 2.4 nm. We have also found that it is better to fabricate the WS₂ quantum dots within the NMP solution compared with water and alcohol mixture due to surface energy matching. Excellent NLO property of the WS₂ quantum dots embedded into solid state matrix PMMA have been reported for both 532 and 1064 nm. The z-scan results of the WS₂ QD/PMMA confirmed that the lower onset thresholds (F_{ON}), lower optical limiting thresholds (F_{OL}), and higher two-photon absorption coefficient (β) are obtained for the higher concentration of embedded WS₂ quantum dots for both excitation wavelengths 532 and 1064 nm. The demonstrated WS₂ QD/PMMA NLO performance is excellent compared with some common NLO materials e.g. metal nanostructure, carbon nanotubes, graphene oxide, etc.

CHAPTER 7

Conclusions and Future Work

7.1 Conclusions

In this thesis, various types of novel two dimensional transition metal dichalcogenide materials have been prepared through ultrasonication exfoliation method. Then those two dimensional nanosheets are embedded into solid stat matrix PMMA for nonlinear optical measurement. Their optical properties and related mechanism are investigated. All key results and conclusions of these research works are summarized in this thesis.

Two dimensional (2D) materials and laser interaction is a very important research topic due to the unique properties of 2D materials, making them a promising candidate for high power applications such as optical limiter and saturable absorber for mode locking laser generation. Micron size MoS_2 are prepared using hydrothermal method through chemical reaction between Na_2MoO_4 and $\text{CS}(\text{NH}_2)_2$. Then, few-layer MoS_2 nanosheets are successfully prepared by further ultrasonic exfoliation treatment in NMP solution due to the relatively weak van der Waals (VDW) force between interlayers. The size, thickness and atomic structure of MoS_2 nanosheets have been characterized by transmission electron microscopy (TEM) and atomic force microscopy (AFM). The interesting dependence of interlayer separation with respect to the layer number of MoS_2 has been successfully

quantified. The average interlayer separation of the MoS₂ nanosheets increases and deviates much from the theoretical value of 0.31 nm with reducing the layer number. That is primarily due to the weaker van de Waals force and increased interlayer repulsive force resulted from the active edge effect of the smaller nanosheets. Such few-layer MoS₂ nanosheets have been homogeneously incorporated into solid-state PMMA. The good nonlinear optical (NLO) property of the MoS₂/PMMA composite for the nanosecond pulsed laser at both 532 and 1064 nm has been reported. Z-scan results of MoS₂/PMMA composite bulk further demonstrate the low NLO onset threshold F_{ON} , low optical limiting threshold F_{OL} , low optical limiting differential transmittance T_C , and high two-phonon absorption coefficient β at both 532 and 1064 nm, confirming the good NLO property of these fabricated materials. The MoS₂/PMMA composites show low optical limiting thresholds, 0.4 and 1.3 J/cm², low limiting differential transmittance (T_C), 2% and 3% for the nanosecond laser operating at 532 nm and 1064 nm, respectively. Therefore, the few-layer MoS₂ nanosheets incorporated PMMA bulk can be a kind of novel NLO material with great potential for optical limiting applications.

The morphology and optical property changes of few layers MoS₂ nanosheet in NMP solution under the illumination of Q-switched laser with operational wavelength of 532 and 1064 nm with respect to various laser energy densities have also been studied. MoS₂ suspension in NMP will reduce in size under laser excitation. The experimental results show significant changes caused by the oxidization of molybdenum disulfide (MoS₂) into molybdenum oxide (MoO₃). Due to its stronger absorption in visible range, the illumination wavelength of 532 nm has relatively stronger effect on MoS₂ suspension compared to 1064 nm because of its higher

optical absorption at 532 nm. Thus, 532 nm laser can oxidize MoS₂ to MoO₃ easily with even lower laser intensity compared with 1064 nm, which leads to the changes in optical properties including absorption, photoluminescence and nonlinear optical absorption properties after laser illumination. The nonlinear optical absorption properties of the MoS₂ in liquid NMP and in solid PMMA have been studied by using z-scan technique and their results are compared. It has been shown experimentally that the nonlinear optical absorption properties of MoS₂ in NMP disappeared but without changes in MoS₂/PMMA composites after laser illumination. It confirms that the MoS₂ is relatively much more stable within PMMA for preserving nonlinear absorption properties under high intensity laser illumination. Compared with the samples of MoS₂ in NMP, we have found that the initial transmittance and nonlinear optical absorption property of MoS₂ nanosheet in PMMA do not change much after laser illumination. Therefore, it can be concluded that the stability of MoS₂ can be greatly enhanced when it is incorporated into PMMA solid state matrix.

To control the optical properties of two-dimensional (2D) materials is a long-standing goal, being of both fundamental and technological significance. Tuning nonlinear optical absorption (NOA) properties of 2D transition metal dichalcogenides in a cost effective way has emerged as an important research topic because of its possibility to costume design NOA properties, implying enormous applications including optical computer, communications, bioimaging, and so on. In chapter 4, WS₂ with different size and thickness distribution have been successfully fabricated using simple and effective liquid phase exfoliation technique. The NOA property of WS₂ sheet incorporated in PMMA show a close dependence on

both size and thickness. Results demonstrate that both NOA onset threshold, F_{ON} , and optical limiting threshold, F_{OL} , of WS_2 under the excitation of nanosecond pulsed laser can be tuned over a wide range by controlling its size and thickness. The F_{ON} and F_{OL} show a rapid decline with the decrease of size and thickness. It has been confirmed that the smaller and thinner WS_2 contributes to a remarkably enhanced NOA performance (lower F_{ON} and F_{OL}). The tunable NOA properties have been achieved through a control of size and thickness.

Due to the matching surface energy, a simple and effective method has been successfully employed to fabricate ultra-small WS_2 quantum dots with diameter of 2.4 nm through the direct liquid exfoliation in NMP rather than ethanol and water mixture. Ultra-small WS_2 quantum dots are fabricated by ultrasound method followed by high speed centrifugation up to 10000 rpm. Excellent nonlinear optical (NLO) property of the WS_2 QD/ PMMA composite for the nanosecond pulsed laser at both 532 and 1064 nm has been measured. The z-scan results illustrate the lower onset thresholds (F_{ON}), lower optical limiting thresholds (F_{OL}), and higher two-photon absorption coefficient (β) with respect to higher concentration of embedded WS_2 quantum dots into PMMA solid state matrix for both 532 and 1064 nm. The demonstrated WS_2 QD/PMMA NLO performance is excellent compared with some common NLO materials e.g. metal nanostructure, carbon nanotubes, graphene oxide, etc.

7.2 Future work

The present thesis focused on the preparation of two dimensional transition metal dichalcogenide through the simple and effective ultrasonication exfoliation and their nonlinear optical measurement in liquid NMP and solid state matrix PMMA.

The future works suggested in this section will make these two dimensional transition metal dichalcogenide embedded into solid state matrix a step forward for their practical applications.

Since hydrothermal reaction have been used to prepare MoS₂ bulk in small size, many other two dimensional materials can also be prepared through this simple method. The future research work can be focused on the preparation of two-dimensional materials, eg, WS₂, Sb₂Te₃, MoSe₂. Therefore, it is necessary to improve the crystallinity and quality of the two dimensional transition metal dichalcogenide bulk materials through composition optimization.

Ultrasonication exfoliation method can be used to exfoliate two dimensional bulk materials effectively and efficiently. More appropriate solution with similar surface energy to various bulk 2D materials should be found. In order to tune the size and thickness of two dimensional nanosheet effectively, ultrasonic power and time can be further optimized.

Solid-state two dimensional nanosheets, e.g. MoS₂, WS₂, homogeneously incorporated PMMA organic glasses were fabricated and the good nonlinear optical (NLO) response shown indicates its high potential to be the optical limiting material for protecting detectors and human eyes from high power lasers. However, thermal and mechanical properties are not as good as the glasses obtained by traditional melt-quenching method. Therefore, it is necessary to improve the thermal and mechanical quality of the organic glasses.

References

- [1] K. S. Novoselov, V. I. Fal'ko, L. Colombo, P. R. Gellert, M. G. Schwab, and K. Kim, "A roadmap for graphene," *Nature*, vol. 490, p. 192, 2012.
- [2] M. Lukas, V. Meded, A. Vijayaraghavan, L. Song, P. M. Ajayan, K. Fink, W. Wenzel, and R. Krupke, "Catalytic subsurface etching of nanoscale channels in graphite," *Nat. Commun.*, vol. 4, p. 1379, 2013.
- [3] P. Y. Huang, C. S. Ruiz-vargas, A. M. Van Der Zande, W. S. Whitney, M. P. Levendorf, J. W. Kevek, S. Garg, J. S. Alden, C. J. Hustedt, Y. Zhu, J. Park, P. L. Mceuen, and D. A. Muller, "Grains and grain boundaries in single-layer graphene atomic patchwork quilts," *Nature*, vol. 469, p. 389, 2011.
- [4] J. Zang, S. Ryu, N. Pugno, Q. Wang, Q. Tu, M. J. Buehler, and Z. Xuanhe, "Multifunctionality and control of the crumpling and unfolding of large-area graphene," *Nat. Mater.*, vol. 12, p. 321, 2013.
- [5] A. K. Geim and I. V Grigorieva, "Van der waals heterostructures," *Nature*, vol. 499, p. 419, 2013.
- [6] D. Voiry, H. Yamaguchi, J. Li, R. Silva, D. C. B. Alves, T. Fujita, M. Chen, T. Asefa, V. B. Shenoy, G. Eda, and M. Chhowalla, "Enhanced catalytic activity in strained chemically exfoliated WS₂ nanosheets for hydrogen evolution.,"

- Nat. Mater.*, vol. 12, p. 850, 2013.
- [7] L. Alexey, S. Pankaj, G. Alexei, and Sinitskii Alexander, “Optoelectrical molybdenum disulfide MoS₂ ferroelectric memories,” *ACS Nano*, vol. 9, p. 8089, 2015.
- [8] R. Bhandavat, L. David, and G. Singh, “Synthesis of surface-functionalized WS₂ nanosheets and performance as Li-ion battery anodes.,” *J. Phys. Chem. Lett.*, vol. 3, p. 1523, 2012.
- [9] K. S. Novoselov, D. Jiang, F. Schedin, T. J. Booth, V. V Khotkevich, S. V Morozov, and A. K. Geim, “Two-dimensional atomic crystals,” *Proc. Natl. Acad. Sci. U. S. A.*, vol. 102, p. 10451, 2005.
- [10] Z. Zeng, T. Sun, J. Zhu, X. Huang, Z. Yin, G. Lu, Z. Fan, Q. Yan, H. H. Hng, and H. Zhang, “An effective method for the fabrication of few-layer-thick inorganic nanosheets,” *Angew. Chem. Int. Ed.*, vol. 51, p. 9052, 2012.
- [11] K. Zhou, N. Mao, H. Wang, Y. Peng, and H. Zhang, “A mixed-solvent strategy for efficient exfoliation of inorganic graphene analogues,” *Angew. Chem. Int. Ed.*, vol. 50, p. 10839, 2011.
- [12] G. C. A, M. Barkelid, A. M. Goossens, V. E. Calado, H. S. J. Van Der Zant, and G. A. Steele, “Laser-thinning of MoS₂: on demand generation of a

- single-layer semiconductor,” *Nano Lett.*, vol. 12, p. 3187, 2012.
- [13] R. F. Frindt, “Single crystals of MoS₂ several molecular layers thick,” *J. Appl. Phys.*, vol. 1928, p. 37, 1966.
- [14] B. Radisavljevic, a Radenovic, J. Brivio, V. Giacometti, and a Kis, “Single-layer MoS₂ transistors.,” *Nat. Nanotechnol.*, vol. 6, p. 147, 2011.
- [15] C. Lee, H. Yan, L. E. Brus, T. F. Heinz, K. J. Hone, and S. Ryu, “Anomalous lattice vibrations of single- and few layer MoS₂,” *ACS Nano*, vol. 4, p. 2695, 2010.
- [16] N. S. K, K. A. Geim, V. . Morozov, Jiang.D, Z. Y, D. V. S, V. I. Grigorieva, and A. A. Firsov, “Electric field effect in atomically thin carbon films,” *Science*, vol. 306, p. 666, 2004.
- [17] F. G. L, R. J. Kieran, and F. H. Richard, “Novel electrodes from solution-processed layer-structure materials,” *Adv. Mater.*, vol. 14, p. 265, 2002.
- [18] C. Liu, S. P. Joensen, A. E. Curzon, and R. F. Frindt, “X-Ray and electron microscope studies of single-layer TaS₂ and NbS₂,” *Thin Solid Films*, vol. 113, p. 165, 1984.
- [19] J. N. Coleman, M. Lotya, A. O’Neill, S. D. Bergin, P. J. King, U. Khan, K.

- Young, A. Gaucher, S. De, R. J. Smith, I. V. Shvets, S. K. Arora, G. Stanton, H.-Y. Kim, K. Lee, G. T. Kim, G. S. Duesberg, T. Hallam, J. J. Boland, J. J. Wang, J. F. Donegan, J. C. Grunlan, G. Moriarty, A. Shmeliov, R. J. Nicholls, J. M. Perkins, E. M. Grieveson, K. Theuwissen, D. W. McComb, P. D. Nellist, and V. Nicolosi, “Two-dimensional nanosheets produced by liquid exfoliation of layered materials,” *Science*, vol. 331, p. 568, 2011.
- [20] K. Lee, H. Kim, M. Lotya, J. N. Coleman, G. Kim, and G. S. Duesberg, “Electrical characteristics of molybdenum disulfide flakes produced by liquid exfoliation,” *Adv. Mater.*, vol. 23, p. 4178, 2011.
- [21] C. Artur and S. Paols, “Graphene via sonication assisted liquid-phase exfoliation,” *Chem. Soc. Rev.*, vol. 43, p. 381, 2014.
- [22] G. Cunningham, M. Lotya, C. S. Cucinotta, S. Sanvito, S. D. Bergin, R. Menzel, M. S. P. Shaffer, and J. N. Coleman, “Solvent exfoliation of transition metal dichalcogenides: dispersibility of exfoliated nanosheets varies only weakly between compounds,” *ACS Nano*, vol. 6, p. 3468, 2012.
- [23] R. J. Smith, P. J. King, M. Lotya, C. Wirtz, U. Khan, S. De, A. O. Neill, G. S. Duesberg, J. C. Grunlan, G. Moriarty, J. Chen, J. Wang, A. I. Minett, V. Nicolosi, and J. N. Coleman, “Large-scale exfoliation of inorganic layered

- compounds in aqueous surfactant solutions,” *Adv. Mater.*, vol. 23, p. 3944, 2011.
- [24] Y. Yu, C. Li, Y. Liu, L. Su, Y. Zhang, and L. Cao, “Controlled scalable synthesis of uniform, high-quality monolayer and few-layer MoS₂ films.,” *Sci. Rep.*, vol. 3, p. 1866, 2013.
- [25] L. Y. Chuan, Z. Wenjing, J. K. Huang, L. K. Ku, Y. H. Lee, C. Te Liang, C. W. Chu, and L. L. Jong, “Wafer scale MoS₂ thin layers prepared by MoO₃ sulfurization,” *Nanoscale*, vol. 4, p. 6637, 2012.
- [26] C. Cong, J. Shang, X. Wu, B. Cao, N. Peimyoo, C. Qiu, S. Litao, and T. Yu, “Synthesis and optical properties of large-area single-crystalline 2D semiconductor WS₂ monolayer from chemical vapor deposition,” *Adv. Opt. Mater.*, vol. 2, p. 131, 2014.
- [27] Y. H. Lee, X. Q. Zhang, W. Zhang, M. T. Chang, C. Te Lin, K. Di Chang, Y. C. Yu, J. T. W. Wang, C. S. Chang, L. J. Li, and T. W. Lin, “Synthesis of large-area MoS₂ atomic layers with chemical vapor deposition,” *Adv. Mater.*, vol. 24, p. 2320, 2012.
- [28] S. Tongay, W. Fan, J. Kang, J. Park, U. Koldemir, J. Suh, D. S. Narang, K. Liu, J. Ji, J. Li, R. Sinclair, and J. Wu, “Tuning interlayer coupling in

- large-area heterostructures with CVD- grown MoS₂ and WS₂ monolayers,” *Nano Lett.*, vol. 14, p. 3185, 2014.
- [29] M. Chhowalla, H. S. Shin, G. Eda, L.-J. Li, K. P. Loh, and H. Zhang, “The chemistry of two-dimensional layered transition metal dichalcogenide nanosheets,” *Nat. Chem.*, vol. 5, p. 263, 2013.
- [30] L. Tao, H. Long, B. Zhou, S. F. Yu, S. P. Lau, Y. Chai, K. H. Fung, Y. H. Tsang, J. Yao, and D. Xu, “Preparation and characterization of few-layer MoS₂ nanosheets and their good nonlinear optical responses in the PMMA matrix,” *Nanoscale*, vol. 6, p. 9713, 2014.
- [31] M. Zelisko, Y. Hanlummyuang, S. Yang, Y. Liu, C. Lei, J. Li, P. M. Ajayan, and P. Sharma, “Anomalous piezoelectricity in two-dimensional graphene nitride nanosheets,” *Nat. Commun.*, vol. 5, p. 4284, 2014.
- [32] S. Ghatak, A. N. Pal, and A. Ghosh, “Nature of electronic states in atomically thin MoS₂ field effect transistors,” *ACS Nano*, vol. 5, p. 7707, 2011.
- [33] F. Bonaccorso, Z. Sun, T. Hasan, and A. C. Ferrari, “Graphene photonics and optoelectronics,” *Nat. Photonics*, vol. 4, p. 611, 2010.
- [34] G.-K. Lim, Z.-L. Chen, J. Clark, R. G. S. Goh, W.-H. Ng, H.-W. Tan, R. H. Friend, P. K. H. Ho, and L.-L. Chua, “Giant broadband nonlinear optical

- absorption response in dispersed graphene single sheets,” *Nat. Photonics*, vol. 5, p. 554, 2011.
- [35] K. Kieu, R. J. Jones, and N. Peyghambarian, “High power femtosecond source near 1 micron based on an all-fiber Er-doped mode-locked laser,” *Opt. Express*, vol. 18, p. 21350, 2010.
- [36] V. R. Supradeepa, J. W. Nicholson, C. E. Headley, M. F. Yan, B. Palsdottir, and D. Jakobsen, “A high efficiency cascaded raman fiber lasers,” *Opt. Express*, vol. 21, p. 7148, 2013.
- [37] Q. H. Wang, K. Kalantar-Zadeh, A. Kis, J. N. Coleman, and M. S. Strano, “Electronics and optoelectronics of two-dimensional transition metal dichalcogenides,” *Nat. Nanotechnol.*, vol. 7, p. 699, 2012.
- [38] X. Huang, Z. Zeng, and H. Zhang, “Metal dichalcogenide nanosheets: preparation, properties and applications,” *Chem. Soc. Rev.*, vol. 42, p. 1934, 2013.
- [39] K. Wang, J. Wang, J. Fan, M. Lotya, A. O. Neill, D. Fox, Y. Feng, X. Zhang, B. Jiang, Q. Zhao, H. Zhang, and J. N. Coleman, “Ultrafast saturable absorption of two dimensional MoS₂ nanosheets,” *ACS Nano*, vol. 7, p. 9260, 2013.

- [40] A. H. Reshak and S. Auluck, "The linear and nonlinear optical properties of WS_xSe_{2-x} ($x=0.5, 1.5,$ and 2.0)," *Phys. B Condens. Matter*, vol. 393, p. 88, 2007.
- [41] R. I. Woodward, R. C. T. Howe, G. Hu, F. Torrisi, M. Zhang, T. Hasan, and E. J. R. Kelleher, "Few-layer MoS_2 saturable absorbers for short-pulse laser technology: current status and future perspectives," *Phot. Res*, vol. 3, p. 30, 2015.
- [42] D. Mao, Y. Wang, C. Ma, L. Han, B. Jiang, X. Gan, S. Hua, W. Zhang, T. Mei, and J. Zhao, " WS_2 mode-locked ultrafast fiber laser," *Sci. Rep.*, vol. 5, p. 7965, 2015.
- [43] M. Zhang, R. C. T. Howe, R. I. Woodward, E. J. R. Kelleher, F. Torrisi, G. Hu, S. V. Popov, J. R. Taylor, and T. Hasan, "Solution processed MoS_2 -PVA composite for sub-bandgap mode-locking of a wideband tunable ultrafast Er:fiber laser," *Nano Res.*, vol. 8, p. 1522, 2015.
- [44] X. Zheng, M. Feng, and H. Zhan, "Giant optical limiting effect in ormosil gel glasses doped with graphene oxide materials," *J. Mater. Chem. C*, vol. 1, p. 6759, 2013.
- [45] N. Dong, Y. Li, Y. Feng, S. Zhang, X. Zhang, C. Chang, J. Fan, L. Zhang, and

- J. Wang, "Optical limiting and theoretical modelling of layered transition metal dichalcogenide nanosheets," *Sci. Rep.*, vol. 5, p. 14646, 2015.
- [46] Z. Sun, A. Martinez, and F. Wang, "Optical modulators with two-dimensional layered materials," *Nat. Photonics*, vol. 10, p. 227, 2016.
- [47] M. Yi, S. Yang, Z. Peng, C. Liu, J. Li, W. Zhong, R. Yang, and W. Tan, "Two-photon graphene oxide / aptamer nanosensing conjugate for in vitro or in vivo molecular probing," *Anal. Chem.*, vol. 86, p. 3548, 2014.
- [48] M. Wang, G. Li, H. Xu, Y. Qian, and J. Yang, "Enhanced lithium storage performances of hierarchical hollow MoS₂ nanoparticles assembled from nanosheets," vol. 5, p. 1003, 2013.
- [49] L. David, R. Bhandavat, U. Barrera, and G. Singh, "Polymer-derived ceramic functionalized MoS₂ composite paper as a stable lithium-ion battery electrode," *Sci. Rep.*, vol. 5, p. 9792, 2015.
- [50] H. Jiang, D. Ren, H. Wang, Y. Hu, S. Guo, H. Yuan, P. Hu, L. Zhang, and C. Li, "2D Monolayer MoS₂-carbon interoverlapped superstructure: engineering ideal atomic interface for lithium ion storage," *Adv. Mater.*, vol. 27, p. 3687, 2015.
- [51] Y. Wang, X. Chen, Y. Zhong, F. Zhu, and K. P. Loh, "Large area, continuous,

- few-layered graphene as anodes in organic photovoltaic devices,” *Appl. Phys. Lett.*, vol. 95, p. 63302, 2009.
- [52] H. Li, Z. Yin, Q. He, H. Li, X. Huang, G. Lu, D. W. H. Fam, A. I. Y. Tok, Q. Zhang, and H. Zhang, “Fabrication of single- and multilayer MoS₂ film-based field-effect transistors for sensing NO at room temperature,” *Small*, vol. 8, p. 63, 2012.
- [53] M. Feng, H. Zhan, and Y. Chen, “Nonlinear optical and optical limiting properties of graphene families,” *Appl. Phys. Lett.*, vol. 96, p. 33107, 2010.
- [54] B. Zhao, B. Cao, W. Zhou, D. Li, and W. Zhao, “Nonlinear optical transmission of nanographene and its composites,” *J. Phys. Chem. C*, vol. 114, p. 12517, 2010.
- [55] P. L. Huang, S.-C. Lin, C.-Y. Yeh, H.-H. Kuo, S.-H. Huang, G.-R. Lin, L.-J. Li, C.-Y. Su, and W.-H. Cheng, “Stable mode-locked fiber laser based on CVD fabricated graphene saturable absorber,” *Opt. Express*, vol. 20, p. 2460, 2012.
- [56] G. Eda, Y. Y. Lin, C. Mattevi, H. Yamaguchi, H. A. Chen, I. S. Chen, C. W. Chen, and M. Chhowalla, “Blue photoluminescence from chemically derived graphene oxide,” *Adv. Mater.*, vol. 22, p. 505, 2010.

- [57] G. Eda, H. Yamaguchi, D. Voiry, T. Fujita, M. Chen, and M. Chhowalla, "Photoluminescence from chemically exfoliated MoS₂," *Nano Lett.*, vol. 11, p. 5111, 2011.
- [58] G. Delmas, D. Patterson, and T. Somecynsky, "Thermodynamics of polyisobutylene-alkane systems," *J. Polym. Sci.*, vol. 57, p. 79, 1962.
- [59] L. P. McMaster, "Aspects of polymer-polymer thermodynamics," *Macromolecules*, vol. 6, p. 760, 1973.
- [60] T. Hiemstra, "Formation, stability, and solubility of metal oxide nanoparticles: surface entropy, enthalpy, and free energy of ferrihydrite," *Geochim. Cosmochim. Acta*, vol. 158, p. 179, 2015.
- [61] G. Vazquez, E. Alvarez, and J. M. Navaza, "Surface tension of Alcohol + water from 20 to 50 C," *J. Chem. Eng. Data*, vol. 40, p. 611, 1995.
- [62] A. García-Abuín, D. Gómez-Díaz, J. M. Navaza, and I. Vidal-Tato, "Surface tension of aqueous solutions of short N -Alkyl-2-pyrrolidinones," *J. Chem. Eng. Data*, vol. 53, p. 2671, 2008.
- [63] R. Lv, Q. Li, A. R. Botello-Méndez, T. Hayashi, B. Wang, A. Berkdemir, Q. Hao, A. L. Elías, R. Cruz-Silva, H. R. Gutiérrez, Y. A. Kim, H. Muramatsu, J. Zhu, M. Endo, H. Terrones, J.-C. Charlier, M. Pan, and M. Terrones,

- “Nitrogen-doped graphene: beyond single substitution and enhanced molecular sensing,” *Sci. Rep.*, vol. 2, p. 586, 2012.
- [64] Q. Bao, H. Zhang, Y. Wang, Z. Ni, Y. Yan, Z. X. Shen, K. P. Loh, and D. Y. Tang, “Atomic-layer graphene as a saturable absorber for ultrafast pulsed lasers,” *Adv. Funct. Mater.*, vol. 19, p. 3077, 2009.
- [65] Z. Liu, L. Ma, G. Shi, W. Zhou, Y. Gong, S. Lei, X. Yang, J. Zhang, J. Yu, K. P. Hackenberg, A. Babakhani, J.-C. Idrobo, R. Vajtai, J. Lou, and P. M. Ajayan, “In-plane heterostructures of graphene and hexagonal boron nitride with controlled domain sizes,” *Nat. Nanotechnol.*, vol. 8, p. 119, 2013.
- [66] I. Jo, M. T. Pettes, J. Kim, K. Watanabe, T. Taniguchi, Z. Yao, and L. Shi, “Thermal conductivity and phonon transport in suspended few-layer hexagonal boron nitride,” *Nano Lett.*, vol. 13, p. 550, 2013.
- [67] Y. Shi, J.-K. Huang, L. Jin, Y.-T. Hsu, S. F. Yu, L.-J. Li, and H. Y. Yang, “Selective decoration of Au nanoparticles on monolayer MoS₂ single crystals,” *Sci. Rep.*, vol. 3, p. 1839, 2013.
- [68] K. F. Mak, K. He, C. Lee, G. H. Lee, J. Hone, T. F. Heinz, and J. Shan, “Tightly bound trions in monolayer MoS₂,” *Nat. Mater.*, vol. 12, p. 207, Mar. 2013.

- [69] H. Li, J. Wu, X. Huang, G. Lu, J. Yang, X. Lu, Q. Xiong, and H. Zhang, “Rapid and reliable thickness identification of two-dimensional nanosheets using optical microscopy,” *ACS Nano*, vol. 7, p. 10344, 2013.
- [70] D. J. Late, B. Liu, H. S. S. R. Matte, C. N. R. Rao, and V. P. Dravid, “Rapid characterization of ultrathin layers of chalcogenides on SiO₂/Si substrates,” *Adv. Funct. Mater.*, vol. 22, p. 1894, 2012.
- [71] G. Eda, G. Fanchini, and M. Chhowalla, “Large-area ultrathin films of reduced graphene oxide as a transparent and flexible electronic material,” *Nat. Nanotechnol.*, vol. 3, p. 270, 2008.
- [72] J. Wu, H. Li, Z. Yin, H. Li, J. Liu, X. Cao, Q. Zhang, and H. Zhang, “Layer thinning and etching of mechanically exfoliated MoS₂ nanosheets by thermal annealing in air,” *Small*, vol. 9, p. 3314, 2013.
- [73] H. Li, X. Qi, J. Wu, Z. Zeng, J. Wei, and H. Zhang, “Investigation of MoS₂ and graphene nanosheets by magnetic force microscopy,” *ACS Nano*, vol. 7, p. 2842, 2013.
- [74] A. Splendiani, L. Sun, Y. Zhang, T. Li, J. Kim, C. Y. Chim, G. Galli, and F. Wang, “Emerging photoluminescence in monolayer MoS₂,” *Nano Lett.*, vol. 10, p. 1271, 2010.

- [75] C. Zhu, Z. Zeng, H. Li, F. Li, C. Fan, and H. Zhang, "Single-layer MoS₂-based nanoprobe for homogeneous detection of biomolecules," *J. Am. Chem. Soc.*, vol. 135, p. 5998, 2013.
- [76] A. O. Neill, U. Khan, and J. N. Coleman, "Preparation of high concentration dispersions of exfoliated MoS₂ with increased flake size," *Chem. Mater.*, vol. 24, p. 2414, 2012.
- [77] K. F. Mak, C. Lee, J. Hone, J. Shan, and T. F. Heinz, "Atomically thin MoS₂: A new direct-gap semiconductor," *Phys. Rev. Lett.*, vol. 105, p. 136805, 2010.
- [78] S. Tongay, J. Zhou, C. Ataca, K. Lo, T. S. Matthews, J. Li, J. C. Grossman, and J. Wu, "Thermally driven crossover from indirect toward direct bandgap in 2D semiconductors: MoSe₂ versus MoS₂," *Nano Lett.*, vol. 12, p. 5576, 2012.
- [79] K. Liu, W. Zhang, Y. Lee, Y. Lin, M.-T. Chang, C.-Y. Su, C.-S. Chang, and H. Li, "Growth of large-area and highly crystalline MoS₂ thin layers on insulating substrates," *Nano Lett.*, vol. 12, p. 1538, 2012.
- [80] Y. Y. Hui, X. Liu, W. Jie, N. Y. Chan, J. Hao, Y.-T. Hsu, L.-J. Li, W. Guo, and S. P. Lau, "Exceptional tunability of band energy in a compressively strained trilayer MoS₂ sheet," *ACS Nano*, vol. 7, p. 7126, 2013.

- [81] Q. Ouyang, H. Yu, H. Wu, Z. Lei, L. Qi, and Y. Chen, "Graphene/MoS₂ organic glasses: fabrication and enhanced reverse saturable absorption properties," *Opt. Mater.*, vol. 35, p. 2352, 2013.
- [82] D. Xu, Y. Wang, H. Li, J. Yao, and Y. H. Tsang, "104 W high stability green laser generation by using diode laser pumped intracavity frequency-doubling Q-switched composite ceramic Nd:YAG laser," *Opt. Express*, vol. 15, p. 3991, 2007.
- [83] Y. H. Tsang, T. A. King, D. K. Ko, and J. Lee, "Output dynamics and stabilisation of a multi-mode double-clad Yb-doped silica fibre laser," *Opt. Commun.*, vol. 259, p. 236, 2006.
- [84] Y. H. Tsang, T. A. King, T. Thomas, C. Udell, and M. C. Pierce, "Efficient high power Yb³⁺-silica fibre laser cladding-pumped at 1064 nm," *Opt. Commun.*, vol. 215, p. 381, 2003.
- [85] Y. Wang, Z. Qu, J. Liu, and Y. H. Tsang, "Graphene oxide absorbers for Watt-level high power passive mode-locked Nd: GdVO₄ laser operating at 1 μ m," *J. Light. Technol.*, vol. 30, p. 3259, 2012.
- [86] L. Zhang, Y. G. Wang, H. J. Yu, W. Sun, Y. Y. Yang, Z. H. Han, Y. Qu, W. Hou, J. M. Li, X. C. Lin, and Y. H. Tsang, "20W high-power picosecond

- single-walled carbon nanotube based MOPA laser system,” *J. Light. Technol.*, vol. 30, p. 2713, 2012.
- [87] J. Balapanuru, J.-X. Yang, S. Xiao, Q. Bao, M. Jahan, L. Polavarapu, J. Wei, Q.-H. Xu, and K. P. Loh, “A Graphene oxide-organic dye ionic complex with DNA-sensing and optical-limiting properties,” *Angew.Chem.*, vol. 122, p. 6699, 2010.
- [88] A. Midya, V. Mamidala, J. X. Yang, P. K. L. Ang, Z. K. Chen, W. Ji, and K. P. Loh, “Synthesis and superior optical-limiting properties of fluorene-thiophene- benzothiadazole polymer-functionalized graphene sheets,” *Small*, vol. 6, p. 2292, 2010.
- [89] Q. Bao, H. Zhang, J. X. Yang, S. Wang, D. Y. Tang, R. Jose, S. Ramakrishna, C. T. Lim, and K. P. Loh, “Graphene-polymer nanofiber membrane for ultrafast photonics,” *Adv. Funct. Mater.*, vol. 20, p. 782, 2010.
- [90] J. Zhu, Y. Li, Y. Chen, J. Wang, B. Zhang, J. Zhang, and W. J. Blau, “Graphene oxide covalently functionalized with zinc phthalocyanine for broadband optical limiting,” *Carbon.*, vol. 49, p. 1900, 2011.
- [91] X. Xu, D. Ou, X. Luo, J. Chen, J. Lu, H. Zhan, Y. Dong, J. Qin, and Z. Li, “Water-soluble graphene sheets with large optical limiting response via

- non-covalent functionalization with polyacetylenes,” *J. Mater. Chem.*, vol. 22, p. 22624, 2012.
- [92] T. Ramanathan, A. A. Abdala, S. Stankovich, D. A. Dikin, M. Herrera-Alonso, R. D. Piner, D. H. Adamson, H. C. Schniepp, X. Chen, R. S. Ruoff, S. T. Nguyen, I. A. Aksay, R. K. Prud’Homme, and L. C. Brinson, “Functionalized graphene sheets for polymer nanocomposites,” *Nat. Nanotechnol.*, vol. 3, p. 327, 2008.
- [93] Y. Hernandez, V. Nicolosi, M. Lotya, F. M. Blighe, Z. Sun, S. De, and I. T. McGovern, “High-yield production of graphene by liquid-phase exfoliation of graphite,” *Nat. Nanotechnol.*, vol. 3, p. 563, 2008.
- [94] Y. Li, H. Wang, L. Xie, Y. Liang, G. Hong, and H. Dai, “MoS₂ nanoparticles grown on graphene : an advanced catalyst for the hydrogen evolution reaction,” *J. Am. Chem. Soc.*, vol. 133, p. 7296, 2011.
- [95] L. Ci, L. Song, C. Jin, D. Jariwala, D. Wu, Y. Li, A. Srivastava, Z. F. Wang, K. Storr, L. Balicas, F. Liu, and P. M. Ajayan, “Atomic layers of hybridized boron nitride and graphene domains,” *Nat. Mater.*, vol. 9, p. 430, 2010.
- [96] A. Reina, X. Jia, J. Ho, D. Nezich, H. Son, V. Bulovic, M. Dresselhaus, K. Jing, and J. Kong, “Large area, few-layer graphene films on arbitrary

- substrates by chemical vapor deposition,” *Nano Lett.*, vol. 9, p. 30, 2008.
- [97] Y. Ni, Y. Chalopin, and S. Volz, “Significant thickness dependence of the thermal resistance between few-layer graphenes,” *Appl. Phys. Lett.*, vol. 103, p. 61906, 2013.
- [98] M. R. Karim, K. Hatakeyama, T. Matsui, H. Takehira, T. Taniguchi, M. Koinuma, Y. Matsumoto, and T. Akutagawa, “Graphene oxide nanosheet with high proton conductivity,” *J. Am. Chem. Soc.*, vol. 135, p. 8097, 2013.
- [99] J. Xie, H. Zhang, S. Li, R. Wang, X. Sun, M. Zhou, J. Zhou, X. W. Lou, and Y. Xie, “Defect-rich MoS₂ ultrathin nanosheets with additional active edge sites for enhanced electrocatalytic hydrogen evolution,” *Adv. Mater.*, vol. 25, p. 5807, 2013.
- [100] J. Brivio, D. T. L. Alexander, and A. Kis, “Ripples and layers in ultrathin MoS₂ membranes,” *Nano Lett.*, vol. 11, p. 5148, 2011.
- [101] S. Najmaei, Z. Liu, P. M. Ajayan, and J. Lou, “Thermal effects on the characteristic Raman spectrum of molybdenum disulfide (MoS₂) of varying thicknesses,” *Appl. Phys. Lett.*, vol. 100, p. 13106, 2012.
- [102] Y. Zhan, Z. Liu, S. Najmaei, P. M. Ajayan, and J. Lou, “Large-area vapor-phase growth and characterization of MoS₂ atomic layers on a SiO₂

- substrate,” *Small*, vol. 8, p. 966, 2012.
- [103] M. Feng, R. Sun, H. Zhan, and Y. Chen, “Lossless synthesis of graphene nanosheets decorated with tiny cadmium sulfide quantum dots with excellent nonlinear optical properties,” *Nanotechnology*, vol. 21, p. 75601, 2010.
- [104] L. Tao, B. Zhou, G. Bai, Y. Wang, S. F. Yu, S. P. Lau, Y. H. Tsang, J. Yao, and D. Xu, “Fabrication of covalently functionalized graphene oxide incorporated solid-state hybrid silica gel glasses and their improved nonlinear optical response,” *J. Phys. Chem. C*, vol. 117, p. 23108, 2013.
- [105] T. He, X. Qi, R. Chen, J. Wei, H. Zhang, and H. Sun, “Enhanced optical nonlinearity in noncovalently functionalized amphiphilic graphene composites,” *Chempluschem*, vol. 77, p. 688, 2012.
- [106] M. Feng, R. Sun, H. Zhan, and Y. Chen, “Decoration of carbon nanotubes with CdS nanoparticles by polythiophene interlinking for optical limiting enhancement,” *Carbon*, vol. 48, p. 1177, 2010.
- [107] X. Sun, R. Q. Yu, G. Q. Xu, T. S. A. Hor, and W. Ji, “Broadband optical limiting with multiwalled carbon nanotubes,” *Appl. Phys. Lett.*, vol. 73, p. 3632, 1998.
- [108] P. Chen, X. Wu, X. Sun, J. Lin, W. Ji, and K. L. Tan, “Electronic structure and

- optical limiting behavior of carbon nanotubes,” *Phys. Rev. Lett.*, vol. 82, p. 2548, 1999.
- [109] R. West, Y. Wang, T. Goodson, and T. G. Iii, “Nonlinear absorption properties in novel gold nanostructured topologies,” *J. Phys. Chem. B*, vol. 107, p. 3419, 2003.
- [110] H. Pan, W. Chen, Y. P. Feng, W. Ji, and J. Lin, “Optical limiting properties of metal nanowires,” *Appl. Phys. Lett.*, vol. 88, p. 223106, 2006.
- [111] L. Polavarapu, N. Venkatram, W. Ji, and Q. H. Xu, “Optical-limiting properties of oleylamine-capped gold nanoparticles for both femtosecond and nanosecond laser pulses,” *ACS Appl. Mater. Interfaces*, vol. 1, p. 2298, 2009.
- [112] K. M. Bohnert, K. Mansour, and A. L. Smirl, “Simultaneous measurement of the two-photon coefficient and free carrier cross section above the bandgap of crystalline silicon,” *IEEE J. Quantum Electron.*, vol. 22, p. 360, 1986.
- [113] S. Husaini, J. E. Slagle, J. M. Murray, S. Guha, L. P. Gonzalez, and R. G. Bedford, “Broadband saturable absorption and optical limiting in graphene-polymer composites,” *Appl. Phys. Lett.*, vol. 102, p. 191112, 2013.
- [114] Z. Liu, Y. Wang, X. Zhang, Y. Xu, Y. Chen, and J. Tian, “Nonlinear optical properties of graphene oxide in nanosecond and picosecond regimes,” *Appl.*

Phys. Lett., vol. 94, p. 21902, 2009.

- [115] X.-L. Zhang, X. Zhao, Z.-B. Liu, S. Shi, W.-Y. Zhou, J.-G. Tian, Y.-F. Xu, and Y.-S. Chen, “Nonlinear optical and optical limiting properties of graphene oxide–Fe₃O₄ hybrid material,” *J. Opt.*, vol. 13, p. 75202, 2011.
- [116] X. Huang, C. Tan, Z. Yin, and H. Zhang, “25th anniversary article: hybrid nanostructures based on two-dimensional nanomaterials,” *Adv. Mater.*, vol. 26, p. 2185, 2014.
- [117] H. Li, J. Wu, Z. Yin, and H. Zhang, “Preparation and applications of mechanically exfoliated single-layer and multilayer MoS₂ and WSe₂ Nanosheets,” *Acc. Chem. Res.*, vol. 47, p. 1067, 2014.
- [118] C. Tan and H. Zhang, “Two-dimensional transition metal dichalcogenide nanosheet-based composites,” *Chem. Soc. Rev.*, vol. 44, p. 2713, 2015.
- [119] H. Zhang, “Ultrathin two-dimensional nanomaterials,” *ACS Nano*, vol. 9, p. 9451, 2015.
- [120] H. Li, Z. Yin, Q. He, H. Li, X. Huang, G. Lu, D. W. H. Fam, A. I. Y. Tok, Q. Zhang, and H. Zhang, “Fabrication of single- and multilayer MoS₂ film-based field-effect transistors for sensing NO at room temperature,” *Small*, vol. 8, p. 63, 2012.

- [121] H. Wang, L. Yu, Y.-H. Lee, Y. Shi, A. Hsu, M. L. Chin, L.-J. Li, M. Dubey, J. Kong, and T. Palacios, “Integrated circuits based on bilayer MoS₂ transistors,” *Nano Lett.*, vol. 12, p. 4674, 2012.
- [122] Z. Sun and H. Chang, “Graphene and graphene-like two-dimensional materials in photodetection : mechanisms and methodology,” *ACS Nano*, vol. 8, p. 4133, 2014.
- [123] X. Peng, L. Peng, C. Wu, and Y. Xie, “Two dimensional nanomaterials for flexible supercapacitors,” *Chem. Soc. Rev.*, vol. 43, p. 3303, 2014.
- [124] X. Huang, Z. Zeng, S. Bao, M. Wang, X. Qi, Z. Fan, and H. Zhang, “Solution-phase epitaxial growth of noble metal nanostructures on dispersible single-layer molybdenum disulfide nanosheets,” *Nat. Commun.*, vol. 4, p. 1444, 2013.
- [125] Z. Zeng, C. Tan, X. Huang, S. Bao, and H. Zhang, “Growth of noble metal nanoparticles on single-layer TiS₂ and TaS₂ nanosheets for hydrogen evolution reaction,” *Energy Environ. Sci.*, vol. 7, p. 797, 2014.
- [126] Z. Yin, H. Li, H. Li, L. Jiang, Y. Shi, Y. Sun, G. Lu, Q. Zhang, X. Chen, and H. Zhang, “Single-layer MoS₂ phototransistors,” *ACS Nano*, vol. 6, p. 74, 2012.

- [127] J. Chen, X. J. Wu, L. Yin, B. Li, X. Hong, Z. Fan, B. Chen, C. Xue, and H. Zhang, "One-pot synthesis of CdS nanocrystals hybridized with single-layer transition-metal dichalcogenide nanosheets for efficient photocatalytic hydrogen evolution," *Angew. Chemi. Int. Ed.*, vol. 54, p. 1210, 2015.
- [128] Q. He, Z. Zeng, Z. Yin, H. Li, S. Wu, X. Huang, and H. Zhang, "Fabrication of flexible MoS₂ thin-film transistor arrays for practical gas-sensing applications," *Small*, vol. 8, p. 2994, 2012.
- [129] C. Feng, Y. Wang, J. Liu, Y. H. Tsang, Y. Song, and Z. Yu, "3W high-power laser passively mode-locked by graphene oxide saturable absorber," *Opt. Commun.*, vol. 298, p. 168, 2013.
- [130] Y. Wang, H. Chen, W. Hsieh, and Y. Tsang, "Mode-locked Nd: GdVO₄ laser with graphene oxide/polyvinyl alcohol composite material absorber as well as an output coupler," *Opt. Commun.*, vol. 289, p. 119, 2013.
- [131] Y. Wang, Z. Qu, J. Liu, and Y. H. Tsang, "Graphene oxide absorbers for watt-level high-power passive mode-locked Nd : GdVO laser operating at 1 μ m," *J. Light. Technol.*, vol. 30, p. 3259, 2012.
- [132] R. I. Woodward, E. J. R. Kelleher, R. C. T. Howe, G. Hu, F. Torrisi, T. Hasan, S. V Popov, and J. R. Taylor, "Tunable Q-switched fiber laser based on

- saturable edge-state absorption in few-layer molybdenum disulfide (MoS₂),” *Opt. Express*, vol. 22, p. 31113, 2014.
- [133] S. Zhang, N. Dong, N. McEvoy, M. O’Brien, S. Winters, N. C. Berner, C. Yim, Y. Li, X. Zhang, Z. Chen, L. Zhang, G. S. Duesberg, and J. Wang, “Direct observation of degenerate two-photon absorption and its saturation in WS₂ and MoS₂,” *ACS Nano*, vol. 9, p. 7142, 2015.
- [134] Y. He, L. Zhang, X. Wang, Y. Wu, H. Lin, L. Zhao, W. Weng, H. Wan, and M. Fan, “Enhanced photodegradation activity of methyl orange over Z-scheme type MoO₃-g-C₃N₄ composite under visible light irradiation,” *RSC Adv.*, vol. 4, p. 13610, 2014.
- [135] H. Yang, X. Li, A. Wang, Y. Wang, and Y. Chen, “Photocatalytic degradation of methylene blue by MoO₃ modified TiO₂ under visible light,” *Chinese J. Catal.*, vol. 35, p. 140, 2014.
- [136] B. L. Li, H. L. Zou, L. Lu, Y. Yang, J. L. Lei, H. Q. Luo, and N. B. Li, “Size-dependent optical absorption of layered MoS₂ and DNA oligonucleotides induced dispersion behavior for label-free detection of single-nucleotide polymorphism,” *Adv. Funct. Mater.*, vol. 25, p. 3541, 2015.
- [137] J. Wang, Y. Hernandez, M. Lotya, J. N. Coleman, and W. J. Blau, “Broadband

- nonlinear optical response of graphene dispersions,” *Adv. Mater.*, vol. 21, p. 2430, 2009.
- [138] L. Tao, H. Long, B. Zhou, S. F. Yu, S. P. Lau, Y. Chai, K. H. Fung, Y. H. Tsang, J. Yao, and D. Xu, “Preparation and characterization of few-layer MoS₂ nanosheets and their good nonlinear optical responses in the PMMA matrix.,” *Nanoscale*, vol. 6, p. 9713, 2014.
- [139] R. R. Nair, M. Sepioni, I.-L. Tsai, O. Lehtinen, J. Keinonen, a. V. Krasheninnikov, T. Thomson, a. K. Geim, and I. V. Grigorieva, “Spin-half paramagnetism in graphene induced by point defects,” *Nat. Phys.*, vol. 8, p. 199, 2012.
- [140] M. Liu, X. Yin, E. Ulin-Avila, B. Geng, T. Zentgraf, L. Ju, F. Wang, and X. Zhang, “A graphene-based broadband optical modulator,” *Nature*, vol. 474, p. 64, 2011.
- [141] Y. Zhao, Z. Liu, T. Sun, L. Zhang, W. Jie, X. Wang, Y. Xie, Y. H. Tsang, H. Long, and Y. Chai, “Mass transport mechanism of Cu species at the metal/dielectric interfaces with a graphene barrier,” *ACS Nano*, vol. 8, p. 12601, 2014.
- [142] F. Yavari, C. Kritzinger, C. Gaire, L. Song, H. Gulapalli, T. Borca-Tasciuc, P.

- M. Ajayan, and N. Koratkar, “Tunable bandgap in graphene by the controlled adsorption of water molecules,” *Small*, vol. 6, p. 2535, 2010.
- [143] W. Wu, L. Wang, Y. Li, F. Zhang, L. Lin, S. Niu, D. Chenet, X. Zhang, Y. Hao, T. F. Heinz, J. Hone, and Z. L. Wang, “Piezoelectricity of single-atomic-layer MoS₂ for energy conversion and piezotronics,” *Nature*, vol. 514, p. 470, 2014.
- [144] T. Georgiou, R. Jalil, B. D. Belle, L. Britnell, R. V Gorbachev, S. V Morozov, Y.-J. Kim, A. Gholinia, S. J. Haigh, O. Makarovskiy, L. Eaves, L. a Ponomarenko, A. K. Geim, K. S. Novoselov, and A. Mishchenko, “Vertical field-effect transistor based on graphene-WS₂ heterostructures for flexible and transparent electronics,” *Nat. Nanotechnol.*, vol. 8, p. 100, 2013.
- [145] X. Hong, J. Kim, S.-F. Shi, Y. Zhang, C. Jin, Y. Sun, S. Tongay, J. Wu, Y. Zhang, and F. Wang, “Ultrafast charge transfer in atomically thin MoS₂/WS₂ heterostructures,” *Nat. Nanotechnol.*, vol. 9, p. 682, 2014.
- [146] A. L. Elias, N. P. Lopez, A. C. Beltran, A. Berkdemir, H. Terrones, and M. Terrones, “Controlled synthesis and transfer of large-area WS₂ sheets : from single layer to few layers,” *ACS Nano*, vol. 7, p. 5235, 2013.
- [147] L. W. Tutt and T. F. Boggess, “A review of optical limiting mechanisms and

- devices using organics, fullerenes, semiconductors and other materials,” vol. 17, p. 299, 1993.
- [148] L. Cao, X. Wang, M. J. Mezziani, F. Lu, H. Wang, P. G. Luo, B. A. Harruff, L. M. Veca, D. Murray, S. Xie, Y. Sun, and Y. Lin, “Carbon dots for multiphoton bioimaging carbon dots for multiphoton bioimaging,” *J.AM.CHEM.SOC*, vol. 129, p. 11318, 2007.
- [149] M. O. Senge, M. Fazekas, E. G. A. Notaras, W. J. Blau, M. Zawadzka, O. B. Locos, and E. M. N. Mhuircheartaigh, “Nonlinear optical properties of porphyrins,” *Adv. Mater.*, vol. 19, p. 2737, 2007.
- [150] G. Zhou, W. Y. Wong, S. Y. Poon, C. Ye, and Z. Lin, “Symmetric versus unsymmetric platinum(II) bis(aryleneethynylene)s with distinct electronic structures for optical power limiting/optical transparency trade-off optimization,” *Adv. Funct. Mater.*, vol. 19, p. 531, 2009.
- [151] K. G. Zhou, M. Zhao, M. J. Chang, Q. Wang, X. Z. Wu, Y. Song, and H. L. Zhang, “Size-dependent nonlinear optical properties of atomically thin transition metal dichalcogenide nanosheets,” *Small*, vol. 11, p. 694, 2015.
- [152] K. Wang, Y. Feng, C. Chang, J. Zhan, C. Wang, Q. Zhao, J. N. Coleman, L. Zhang, W. Blau, and J. Wang, “Broadband ultrafast nonlinear absorption and

- nonlinear refraction of layered molybdenum dichalcogenide semiconductors,”
Nanoscale, vol. 6, p. 10530, 2014.
- [153] B. Chakraborty, H. S. S. R. Matte, A. K. Sood, and C. N. R. Rao,
“Layer-dependent resonant Raman scattering of a few layer MoS₂,” *J. Raman
Spectrosc.*, vol. 44, p. 92, 2013.
- [154] H. Zeng, G.-B. Liu, J. Dai, Y. Yan, B. Zhu, R. He, L. Xie, S. Xu, X. Chen, W.
Yao, and X. Cui, “Optical signature of symmetry variations and spin-valley
coupling in atomically thin tungsten dichalcogenides,” *Sci. Rep.*, vol. 3, p.
1608, 2013.
- [155] W. Zhao, Z. Ghorannevis, K. K. Amara, J. R. Pang, M. Toh, X. Zhang, C.
Kloc, P. H. Tan, and G. Eda, “Lattice dynamics in mono- and few-layer sheets
of WS₂ and WSe₂,” *Nanoscale*, vol. 5, p. 9677, 2013.
- [156] X. Xue, W. Ji, Z. Mao, H. Mao, Y. Wang, X. Wang, W. Ruan, B. Zhao, and J.
R. Lombardi, “Raman investigation of nanosized TiO₂: effect of crystallite
size and quantum confinement,” *J. Phys. Chem. C*, vol. 116, p. 8792, 2012.
- [157] L. K. Pan, C. Q. Sun, and C. M. Li, “Elucidating Si–Si dimer vibration from
the size-dependent raman shift of nanosolid Si,” *J. Phys. Chem. B*, vol. 108, p.
3404, 2004.

- [158] C. Backes, R. J. Smith, N. McEvoy, N. C. Berner, D. McCloskey, H. C. Nerl, and A. O'Neill, "Edge and confinement effects allow in situ measurement of size and thickness of liquid-exfoliated nanosheets.," *Nat. Commun.*, vol. 5, p. 4576, 2014.
- [159] W. Zhao, Z. Ghorannevis, L. Chu, M. TOh, C. Kloc, P. H. Tan, and G. Eda, "Evolution of electronic structure in atomically thin sheets of WS₂ and WSe₂," *ACS Nano*, vol. 7, p. 791, 2013.
- [160] B. Qu, Q. Ouyang, X. Yu, W. Luo, L. Qi, and Y. Chen, "Nonlinear absorption, nonlinear scattering, and optical limiting properties of MoS₂-ZnO composite-based organic glasses," *Phys. Chem. Chem. Phys.*, vol. 17, p. 6036, 2015.
- [161] Y. Li, N. Dong, S. Zhang, X. Zhang, Y. Feng, K. Wang, L. Zhang, and J. Wang, "Giant two-photon absorption in monolayer MoS₂," *Laser Photon. Rev.*, vol. 9, p. 427, 2015.
- [162] L. Polavarapu, N. Venkatram, W. Ji, and Q.-H. Xu, "Optical-limiting properties of oleylamine-capped gold nanoparticles for both femtosecond and nanosecond laser pulses.," *ACS Appl. Mater. Interfaces*, vol. 1, p. 2298, 2009.
- [163] M. Feng, R. Sun, H. Zhan, and Y. Chen, "Decoration of carbon nanotubes

- with CdS nanoparticles by polythiophene interlinking for optical limiting enhancement,” *Carbon*, vol. 48, p. 1177, 2010.
- [164] T. He, X. Qi, R. Chen, J. Wei, H. Zhang, and H. Sun, “Enhanced optical nonlinearity in noncovalently functionalized amphiphilic graphene composites,” *Chempluschem*, vol. 77, p. 688, 2012.
- [165] M. Feng, H. Zhan, and Y. Chen, “Nonlinear optical and optical limiting properties of graphene families,” *Appl. Phys. Lett.*, vol. 96, p. 2008, 2010.
- [166] J. Balapanuru, J.-X. Yang, S. Xiao, Q. Bao, M. Jahan, L. Polavarapu, J. Wei, Q.-H. Xu, and K. P. Loh, “A graphene oxide-organic dye ionic complex with DNA-sensing and optical-limiting properties,” *Angew. Chemie*, vol. 122, p. 6699, 2010.
- [167] G.-K. Lim, Z.-L. Chen, J. Clark, R. G. S. Goh, W.-H. Ng, H.-W. Tan, R. H. Friend, P. K. H. Ho, and L.-L. Chua, “Giant broadband nonlinear optical absorption response in dispersed graphene single sheets,” *Nat. Photonics*, vol. 5, p. 554, 2011.
- [168] L. Tao, H. Long, B. Zhou, S. F. Yu, S. P. Lau, Y. Chai, K. H. Fung, Y. H. Tsang, J. Yao, and D. Xu, “Preparation and characterization of few-layer MoS₂ nanosheets and their good nonlinear optical responses in the PMMA

- matrix.," *Nanoscale*, vol. 6, p. 9713, 2014.
- [169] L. Dou, F. Cui, Y. Yu, G. Khanarian, S. W. Eaton, Q. Yang, J. Resasco, C. Schildknecht, K. Schierle-Arndt, and P. Yang, "Solution-processed copper/reduced-graphene-oxide core/shell nanowire transparent conductors," *ACS Nano*, vol. 10, p. 2600, 2016.
- [170] H. Tan, Y. Fan, Y. Rong, B. Porter, C. S. Lau, Y. Zhou, Z. He, S. Wang, H. Bhaskaran, and J. H. Warner, "Doping graphene transistors using vertical stacked monolayer WS₂ heterostructures grown by chemical vapor deposition.," *ACS Appl. Mater. Interfaces*, vol. 8, p. 1644, 2016.
- [171] L. Zeng, C. Xie, L. Tao, H. Long, C. Tang, Y. H. Tsang, and J. Jie, "Bilayer graphene based surface passivation enhanced nano structured self-powered near-infrared photodetector," *Opt. Express*, vol. 23, p. 4839, 2015.
- [172] L. Zeng, L. Tao, C. Tang, B. Zhou, H. Long, Y. Chai, S. P. Lau, and Y. H. Tsang, "High-responsivity UV-Vis photodetector based on transferable WS₂ film deposited by magnetron sputtering," *Sci. Rep.*, vol. 6, p. 20343, 2016.
- [173] D.-S. Tsai, K.-K. Liu, D.-H. Lien, M.-L. Tsai, C.-F. Kang, C.-A. Lin, L.-J. Li, and J.-H. He, "Few layer MoS₂ with broadband high photogain and fast optical switching for use in harsh environments.," *ACS Nano*, vol. 7, p. 3905,

2013.

- [174] H. Zhang, S. B. Lu, J. Zheng, J. Du, S. C. Wen, D. Y. Tang, and K. P. Loh, “Molybdenum disulfide (MoS_2) as a broadband saturable absorber for ultra-fast photonics,” *Opt. Express*, vol. 22, p. 7249, 2014.
- [175] R. Khazaeinezhad, S. Hosseinzadeh Kassani, T. Nazari, H. Jeong, J. Kim, K. Choi, J. U. Lee, J. H. Kim, H. Cheong, D. Il Yeom, and K. Oh, “Saturable optical absorption in MoS_2 nano-sheet optically deposited on the optical fiber facet,” *Opt. Commun.*, vol. 335, p. 224, 2015.
- [176] J.-Q. Zhao, Y.-G. Wang, P.-G. Yan, S.-C. Ruan, J.-Q. Cheng, G.-G. Du, Y.-Q. Yu, G.-L. Zhang, H.-F. Wei, J. Luo, and Y. H. Tsang, “Graphene-oxide-based Q-switched fiber laser with stable five-wavelength operation,” *Chinese Phys. Lett.*, vol. 29, p. 114206, 2012.
- [177] J. Q. Zhao, Y. G. Wang, P. G. Yan, S. C. Ruan, G. L. Zhang, H. Q. Li, and Y. H. Tsang, “An L-band graphene-oxide mode-locked fiber laser delivering bright and dark pulses,” *Laser Phys.*, vol. 23, p. 75105, 2013.
- [178] H. Long, L. Tao, C. Y. Tang, B. Zhou, Y. Zhao, L. Zeng, S. F. Yu, S. P. Lau, Y. Chai, and Y. H. Tsang, “Tuning nonlinear optical absorption properties of WS_2 nanosheets,” *Nanoscale*, vol. 7, p. 17771, 2015.

- [179] B. Ullrich and J. S. Wang, "All-optical tuning of the Stokes shift in PbS quantum dots," *Appl. Phys. Lett.*, vol. 102, p. 71905, 2013.
- [180] H. S. Kim and K. B. Yoon, "Increase of third-order nonlinear optical activity of PbS quantum dots in zeolite Y by increasing cation size.," *J. Am. Chem. Soc.*, vol. 134, p. 2539, 2012.
- [181] L. Lin, Y. Xu, S. Zhang, I. M. Ross, A. C. M. Ong, and D. A. Allwood, "Fabrication of luminescent monolayered tungsten dichalcogenides quantum dots with giant spin-valley coupling," *ACS Nano*, vol. 7, p. 8214, 2013.
- [182] X. Zhang, Z. Lai, Z. Liu, C. Tan, Y. Huang, B. Li, M. Zhao, L. Xie, W. Huang, and H. Zhang, "A facile and universal top-down method for preparation of monodisperse transition-metal dichalcogenide nanodots," *Angew. Chemie - Int. Ed.*, vol. 127, p. 5515, 2015.
- [183] E. M. Nanosheets, D. Gopalakrishnan, D. Damien, and M. M. Shaijumon, "MoS₂ quantum dot-interspersed exfoliated MoS₂ nanosheets," *ACS Nano*, vol. 8, p. 5297, 2014.
- [184] H. Long, L. Tao, C. Y. Tang, H. Y. Tam, Q. Wen, and Y. Hong, "Effect of laser illumination on the morphology and optical property of few-layer MoS₂ nanosheet in NMP and PMMA," *J. Mater. Chem. C*, vol. 4, p. 678, 2016.

- [185] J. Gliński, G. Chavepeyer, J. K. Platten, and P. Smet, “Surface properties of diluted aqueous solutions of normal short-chained alcohols,” *J. Chem. Phys.*, vol. 109, p. 5050, 1998.
- [186] Y. Maham and A. E. Mather, “Surface thermodynamics of aqueous solutions of alkylethanolamines,” *Fluid Phase Equilib.*, vol. 182, p. 325, 2001.
- [187] T. A. Pascal and W. A. Goddard, “Interfacial thermodynamics of water and six other liquid solvents,” *J. Phys. Chem. B*, vol. 118, p. 5943, 2014.
- [188] J. Gliski, G. Chavepeyer, and J. K. Platten, “Surface properties of diluted aqueous solutions of tert-butyl alcohol,” *J. Chem. Phys.*, vol. 102, p. 2113, 1995.
- [189] A. W. Achtstein, J. Hennig, A. Prudnikau, M. V Artemyev, and U. Woggon, “Linear and two-photon absorption in zero- and one-dimensional CdS nanocrystals: influence of size and shape,” *J. Phys. Chem. C*, vol. 117, p. 25756, 2013.
- [190] Q. Liu, B. Guo, Z. Rao, B. Zhang, and J. R. Gong, “Strong two-photon-induced fluorescence from photostable, biocompatible nitrogen-doped graphene quantum dots for cellular and deep-tissue imaging,” *Nano Lett.*, vol. 13, p. 2436, Jun. 2013.